EXPERIMENTAL CHARACTERIZATION OF FEMTOSECOND LASER MICROMACHINING FOR SILICON MOLD FABRICATION AND HOT EMBOSSING FOR POLYMER MICROREPLICATION

by

SUNIL RANGANATH BELLIGUNDU

Presented to the Faculty of the Graduate School of

The University of Texas at Arlington in Partial Fulfillment

of the Requirements

for the Degree of

DOCTOR OF PHILOSOPHY

THE UNIVERSITY OF TEXAS AT ARLINGTON

December 2005

ACKNOWLEDGEMENTS

I express my gratitude towards my supervising professor Dr. Panos Shiakolas for his invaluable advice, guidance and support throughout the course of my research work. I would also like to thank the professors in my dissertation committee – Dr. Lawrence, Dr. Aswath, Dr. Eberhart and Dr. Dennis, for taking time to serve the committee and showing interest in my research. I reserve my special thanks to Mr. Tom Leeds and Mr. Mike Baker of the Mechanical Engineering Machine Shop for their invaluable advice during this research especially during the fabrication and assembly of the hot embossing and laser microfabrication systems.

Rajkumar Thanu, Dipanjan Ghosh and Aditya Deshmukh helped in designing and assembling the hot embossing system while Gaurav Keswani, Arvind Ramachandran and Vikram Patil helped in setting up the femtosecond laser system. I would like to also thank Nitin Uppal for his assistance with the laser micromachining experiments and Puneet Saggar for his help with bond strength measurement experiments. Dr. Aswath and Anurag Pandey provided the PLLA samples used in this research. Finally, I also appreciate the support of my colleagues in the MARS lab – Tony Chang, Desiree Bennett and Mohammad Mayyas.

Part of the material presented in this dissertation is based upon the work performed under Texas Advanced Technology Program Grant No. 003656-0034-2001.

November 16, 2005

ABSTRACT

EXPERIMENTAL CHARACTERIZATION OF FEMTOSECOND LASER MICROMACHINING FOR SILICON MOLD FABRICATION AND HOT EMBOSSING FOR POLYMER MICROREPLICATION

Publication No. ______

Sunil Ranganath Belligundu, PhD.

The University of Texas at Arlington, 2005

Supervising Professor: Panayiotis S. Shiakolas

Hot embossing is a fabrication technique employed for replicating microfeatures on a polymer surface that was primarily developed to fabricate MEMS devices for microfluidic applications. This manuscript deals with characterization of the femtosecond laser micromachining (FLM) and hot embossing (HEMM) processes for master mold fabrication on silicon and polymer replication respectively. Given the required size of the features to be fabricated or replicated, process parameters for FLM can be determined using the derived empirical equations, process parameters for the HEMM process can be established using the characteristic plots. A novel two-stage

embossing process is developed and introduced that employs polymer molds during the second stage. Validation experiments along with results focusing on mold quality with respect to the embossing cycles of the secondary polymer mold and the embossing quality of the substrate as compared to the primary silicon mold have been presented. Micromachining of a biodegradable polymer, PLLA, with potential drug delivery applications have been performed using hot embossing and laser micromachining. The comparison of flow rate of PLLA into the mold during single and two stage embossing has been studied. Threshold fluence values of different number of pulses for PLLA during femtosecond laser micromachining have been determined. Finally, process parameters for thermal bonding using the HEMM system of two PMMA substrates are established along with their effects on feature quality after bonding.

TABLE OF CONTENTS

ACKNOWLEDGEMENTS ii

ABSTRACT iii

LIST OF ILLUSTRATIONS x

LIST OF TABLES xvi

Chapter

1. INTRODUCTION 1

1.1 Introduction to Microelectromechanical Systems 1

1.2 MEMS Microfabrication Techniques 3

1.2.1 Bulk Micromachining 5

1.2.2 Surface Micromachining 5

1.2.3 High Aspect Ratio Micromachining 6

1.3 Need to Use Polymers as Substrates 7

1.4 Polymer Microfabrication Techniques 8

1.4.1 Microinjection Molding 8

1.4.2 Hot Embossing 10

1.4.3 Injection Compression Molding 11

1.4.4 Polymer Casting 12

1.5 Laser Based Microfabrication 13

1.6 Scope of this Research 15

1.7 Report Layout ……... 15

2. MOLD FABRICATION USING FEMTOSECOND LASER MICROMACHINING 17

2.1 Micromachining with Ultra-short Pulses 17

2.2 FLM Micromachining Parameters 19

2.2.1 Laser Beam Machining Parameters 19

2.2.2 Machining Setup Parameters 20

2.3 FLM System at UTA 21

2.4 Feature Measurements 23

2.5 Mold Fabrication Steps Using FLM 24

2.5.1 Finishing Passes 26

2.5.2 Jet of Air…. 28

2.5.3 Treatment with Acetone 28

2.6 Characterization of FLM Process 29

2.6.1 Determination of Machining Parameters 29

2.7 Experimental Results and Discussion 36

2.7.1 Characterization of Channels 36

2.7.2 Characterization of Reservoirs 47

2.8 Conclusions…..…. 56

3. HOT EMBOSSING PROCESS CHARACTERIZATION 57

3.1 Hot Embossing Process 57

3.2 Basic Configuration and Subsystems of HEMM System 61

3.3 Advantages of HEMM 62

3.4 Applications of HEMM 63

3.5 Commercial Hot Embossing Systems 64

3.6 HEMM System at UTA 65

3.7 Embossing Process Parameters 67

3.8 Embossing Process on the HEMM System 68

3.9 De-embossing System 71

3.10 Feature Measurements 72

3.11 Polymer Characterization 72

3.12 Experimental Results and Discussion 74

3.12.1 Poly Carbonate (PC) 74

3.12.2 Poly Methyl Meth Acrylate (PMMA) 79

3.12.3 Poly L-Lactic Acid (PLLA) 82

3.13 Normalization of Embossing Temperatures 86

3.14 Conclusions 90

4. TWO STAGE EMBOSSING 91

4.1 Need for Two-Stage Embossing 91

4.2 Two-Stage Embossing Process 93

4.3 Advantages and Limitations 94

4.4 Experiments and Results 95

4.4.1 Experiment # 1: Wet Etched Silicon Mold 96

4.4.2 Experiment # 2: FLM Silicon Mold with Channels 97

4.4.3 Experiment # 3: FLM Silicon Mold with Reservoirs 100

4.5 Discussions…..…….. 103

4.6 Conclusions…..…….. 104

5. MICROMACHINING OF POLY L-LACTIC ACID 106

5.1 Introduction…..……... 106

5.2 Hot Embossing on PLLA.. 109

5.3 FLM on PLLA …….. 116

5.4 Conclusions…..…….. 120

6. POLYMER BONDING USING HEMM SYSTEM 122

6.1 Different Polymer Bonding Techniques.. 122

6.1.1 Adhesives or Tapes.. 122

6.1.2 Solvent Assisted Bonding... 123

6.1.3 Laser/plastic Welding... 123

6.1.4 Deep X-Ray Irradiation 123

6.1.5 Lamination 124

6.1.6 Thermal Bonding... 124

6.2 Preliminary Experiments Using HEMM System 125

6.2.1 Measurement of Bonding Strength
Stack Thickness Difference 126

6.3 Bonding Experiments and Discussion.. 130

6.4 Conclusions…..……... 133

7. CONCLUSIONS AND RECOMMENDATIONS...................................... 134

7.1 Conclusions……….. 134

7.1.1 Characterization of FLM 134

7.1.2 Characterization of HEMM 135

7.1.3 Two-Stage Embossing Process.. 135

7.1.4 Micromachining of PLLA 136

7.1.5 Thermal Bonding of PMMA 136

7.2 Recommendations for Future Research.. 136

7.2.1 Characterization of FLM for Different Lenses......................... 136

7.2.2 Finite Element Analysis of Hot Embossing............................. 137

7.2.3 Temperature Control of the HEMM System 138

7.2.4 Nanoimprinting... 138

7.2.5 Other Suggestions.. 138

Appendix

A. CNC CODE FOR CHANNEL FABRICATION ON FLM 140

B. CHANNEL DEPTH AND WIDTH DATA 143

C. CNC CODE FOR RESERVOIR FABRICATION ON FLM 146

D. RESERVOIR DEPTH DATA 150

E. HEMM CHARACTERIZATION DATA 152

REFERENCES 155

BIOGRAPHICAL INFORMATION.. 166

LIST OF ILLUSTRATIONS

Figure Page

1.1 Microchemical reactor chips 2

1.2 Deep cavity etched in silicon 5

1.3 Microengine gear meshing with another gear 6

1.4 Microtrajectory sensing device 6

1.5 Schematic of injection molding machine 9

1.6 Microinjection molding device 9

1.7 Hot embossed device 11

1.8 Polymer cast device 12

1.9 Laser micromachining of a channel 14

2.1 Machining due to ultra short pulsed laser 18

2.2 FLM system at BioMEMS laboratory 22

2.3 Feature measurement 23

2.4 Mold rapid prototyping procedure 24

2.5 Focusing of the laser beam on silicon wafer 25

2.6 Steps for FLM machining 27

2.7 Visual comparison of edge quality of feature 28

2.8 Acetone treatment on features 29

2.9 Feature dimensions vs. power levels 31

2.10 Channels fabricated at different power levels 31

2.11 Plots for # of passes 33

2.12 Channels fabricated at different passes 33

2.13 Feature cross-sections at different passes 34

2.14 *zDist* values 35

2.15 Different Z-Down levels 36

2.16 Channels at different power levels 37

2.17 Determination of constants k_1 and k_2 39

2.18 Comparison between measured and calculated depths – 25 mW 40

2.19 Comparison between measured and calculated depths – 50 mW 41

2.20 Comparison between measured and calculated depths – 75 mW 41

2.21 Comparison between measured and calculated depths – 100 mW 42

2.22 Comparison between measured and calculated depths – 150 mW 42

2.23 Determination of constants k_4 and k_5 43

2.24 Comparison between measured and calculated widths – Passes = 1 44

2.25 Comparison between measured and calculated widths – Passes = 2 45

2.26 Comparison between measured and calculated widths – Passes = 3 45

2.27 Reservoirs at different power levels 49

2.28 Determination of constants k_1 and k_2 50

2.29 Values of constant k_3 51

2.30 Comparisons between measured and calculated depths – 5 mW 52

2.31 Comparisons between measured and calculated depths – 10 mW 52

2.32 Comparisons between measured and calculated depths – 20 mW 53

2.33 Comparisons between measured and calculated depths – 30 mW 53

2.34 Comparisons between measured and calculated depths – 40 mW 54

3.1 Traditional hot embossing microreplication process 58

3.2 Young's modulus variation with temperature 59

3.3 Temperature and pressure plot for hot embossing process 60

3.4 Basic schematic representation of hot embossing equipment 61

3.5 PMMA embossed features 63

3.6 Different embossing systems 64

3.7 HEMM system at UTA 66

3.8 HEMM control interface 67

3.9 Force control LabVIEW interface 69

3.10 Setup of mold and substrate on the HEMM system 70

3.11 Representative temperature and pressure plot 70

3.12 De-embossing system 72

3.13 Mold used for characterization experiments 74

3.14 Embossing results on PC (function of temperatures)
– Row 1 75

3.15 Embossing results on PC (function of temperatures)
– Row 2 76

3.16 Embossing results on PC (function of temperatures)
– Row 3 76

3.17 Embossing characteristic plots for PC (function of rows)
Holding time = 30 seconds 78

3.18 Embossing characteristic plots for PC (function of rows)
Holding time = 90 seconds 78

3.19 Embossing results on PMMA (function of temperatures)
– Row 1 80

3.20 Embossing results on PMMA (function of temperatures)
– Row 2 80

3.21 Embossing results on PMMA (function of temperatures)
– Row 3 81

3.22 Embossing characteristic plots for PMMA (function of rows)
Holding time = 30 seconds 81

3.23 Embossing characteristic plots for PMMA (function of rows)
Holding time = 90 seconds 82

3.24 Embossing results on PLLA (function of temperatures)
– Row 1 83

3.25 Embossing results on PLLA (function of temperatures)
– Row 2 84

3.26 Embossing results on PLLA (function of temperatures)
– Row 3 84

3.27 Embossing characteristic plots for PLLA (function of rows)
Holding time = 30 seconds 85

3.28 Embossing characteristic plots for PLLA (function of rows)
Holding time = 90 seconds 85

3.29 Comparison of behavior of the three polymers – Row 2 88

3.30 Comparison of behavior of the three polymers – Row 3 89

4.1 Mold making 92

4.2 Male and female molds 92

4.3 Two-stage embossing process 94

4.4 Silicon (primary) mold, PC (secondary) molds and PMMA
substrate at different cycles of embossing 97

4.5 Silicon (primary) mold, PC (secondary) molds and PMMA
substrate at different cycles of embossing 99

4.6 Average channel dimensions 100

4.7 Silicon (primary) mold, PC (secondary) molds and PLLA
substrate at different cycles of embossing 102

4.8 Average reservoir dimensions 103

5.1 Silicon primary mold 109

5.2 Comparison for single-stage embossing 111

5.3 Comparison for two-stage embossing 112

5.4 Average linear filling rate as a function of holding time 115

5.5 Laser micromachining of biodegradable polymers 117

5.6 Threshold fluence value calculation 119

5.7 Features on PLLA using FLM 120

6.1 Bonding test sample 127

6.2 Tensile load vs. extension for expt. # 7 (Set 2) 127

6.3 Bond pressure vs. stack thickness difference ... 129

6.4 PMMA substrate for bonding ... 130

6.5 Channel on PMMA substrate ... 131

6.6 Reservoir on PMMA substrate ... 131

LIST OF TABLES

Table Page

1.1 Summary of polymer microfabrication techniques 13

2.1 Constant values for channel depth 39

2.2 Constant values for channel width 44

2.3 Value of *zdowns* when $h_c = 50$ 46

2.4 Values of channel widths (um) for combinations selected 46

2.5 Constant values for reservoir depth.. 50

2.6 Value of *zdowns* when $h_r = 250$ 55

3.1 Comparison of design specifications 65

3.2 Properties of polymers used for characterization... 73

4.1 Two-stage embossing process parameters – experiment #1 96

4.2 Two-stage embossing process parameters – experiment #2 98

4.3 Two-stage embossing process parameters – experiment #3 101

5.1 Single-stage embossing process parameters 110

5.2 Two-stage embossing process parameters 110

5.3 Threshold fluence values for different pulses 119

6.1 Experiment results for Set 1 128

6.2 Experiment results for Set 2 129

6.3 Bonding parameters.. 130

6.4 Feature changes after bonding... 132

CHAPTER 1

INTRODUCTION

This chapter begins with a brief introduction to Microelectromechanical systems (MEMS) and microfluidics. Common MEMS fabrication technologies are discussed along with their disadvantages. Reasons for using polymers as substrates in a microdevice are explained. Various polymer microfabrication methods are then explained. The scope of this research and organization of the remaining chapters are mentioned.

1.1 Introduction to Microelectromechanical Systems

MEMS deal with the miniaturization of range of devices, from sensors to mechanical actuators to microfluidic devices for a variety of applications. Miniaturization of devices is an obvious trend and has tremendous potential to provide excellent opportunities for technological advances and commercial profit while at the same affecting people's lives in a positive way. For example, MEMS based accelerometers have been used as automobile air-bag deployment sensors for many years.

A microdevice is a device consisting of components with dimensions less than one millimeter. The main factor contributing to the fairly wide use of micro devices in today's world is the technological advancements in the field of microengineering and

microfabrication. Microengineering refers to technologies and practice of designing 3D structures and devices in the order of microns, whereas microfabrication refers to technologies and practice of manufacturing micro sized features. In most cases, integrating microengineering and microfabrication results in a microdevice. Microengineered devices have a wide range of applications in the automotive, aerospace, telecommunications and biomedical industry.

The advantages of microdevices as compared to macro sized devices are:

- Extremely light, small and several of them can be accommodated in the same space occupied by one macrodevice
- Cumbersome electrical components are not required
- Increased performance with less consumption of power
- Lesser materials required for fabrication and batch fabrication at low cost

A microfluidic device is one that has one or more channels with at least one dimension less than 1 mm [1]. Figure 1.1 [2] shows a chemical reactor chip that has the two most common features on a microfluidic device – channels and reservoirs.

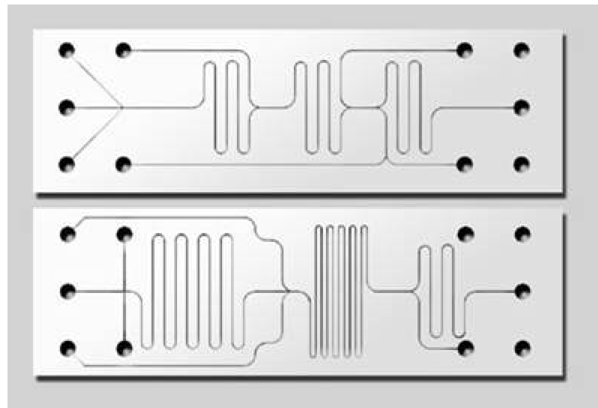

Figure 1.1 Microchemical reactor chips

Some of the applications of microfluidic devices include

- Genomics and proteomics – DNA fingerprinting, gene assays
- Clinical analysis – rapid analysis of blood and bodily fluids
- Chemical/biological warfare – detection and identification of pathogens
- Biomedical devices, implantable devices – drug delivery
- Environmental testing – in situ analysis of environmental contamination

1.2 MEMS Microfabrication Techniques

Microfabricating a device has always been a challenge. This miniaturization process requires suitable microfabrication techniques to fabricate devices in the micro scale while forming a bridge between the conceptual design of a microdevice and a real working device. Initially, microfabrication techniques for MEMS were adopted from the already existing fabrication techniques used robustly in the Integrated Circuit (IC) industry like lithography, patterning etc. Over the years, they have evolved, different from the set of techniques used in the IC industry, and have been used to produce the microstructures and moving parts of microengineered devices. They have incorporated newer materials instead of silicon (building block in the IC world) for fabrication. Introduction of new advanced microfabrication techniques such as LIGA, hot embossing and injection molding has made it possible to incorporate new materials like quartz, glass and a wide range of polymers as substrates for microdevices.

At the micro level, some physical effects that conventional manufacturing techniques rely on become less effective. Traditional metal machining techniques rely

on the bulk of the mass being machined resisting the cutting force, whereas friction and surface tension play a larger role in the micro domain. The mechanical resistance of components is much smaller simply because of the smaller dimensions, which in turn causes traditional cutting techniques to fail. Things behave differently in the micro domain. Forces related to volume like weight and inertia decrease whereas forces related to surface area such as friction tend to become large.

As the field of microdevices expands, and these devices become more popular, production techniques are modified and production volumes are increasing. There is also a need to investigate the use of non-traditional materials for manufacturing. For example, if biocompatible polymers are used, implantable sensors, drug delivery systems and intelligent stents could be manufactured. There is a need for efficient, fast microfabrication techniques that are capable of fabricating devices and components from non-traditional materials.

The microfabrication technique employed contributes significantly towards the cost of the device. This has led to a struggle to find more efficient and cheaper fabrication techniques without compromising performance and the ability to mass produce. Most of the microfabrication or micromachining techniques can be classified into three categories [3]:

- Bulk micromachining
- Surface micromachining
- High aspect ratio micromachining

1.2.1 Bulk Micromachining

Bulk micromachining is a process that removes "bulk" substrate. It is a subtractive process that involves removing selective areas of the substrate material. Some of the features that can be fabricated using this type of process are reservoirs, channels, grooves, cantilevers, etc. Figure 1.2 [4] shows a cavity fabricated using the bulk machining process.

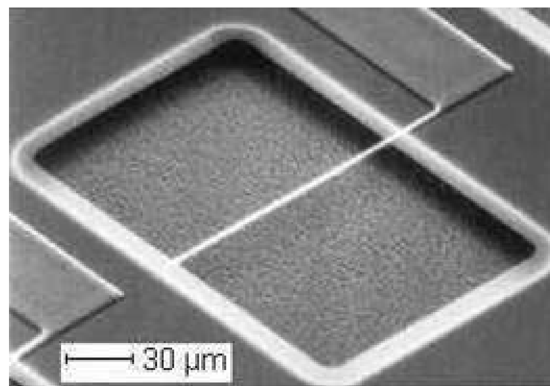

Figure 1.2 Deep cavity etched in silicon

1.2.2 Surface Micromachining

Surface machining is an additive process that refers to processing "above" the substrate. The microstructures are not fabricated in the substrate instead the substrate is used as a base to buildup the microstructures. Released and movable microstructures are fabricated on a single substrate from thin layers of structural materials and sacrificial layers, deposited on the surface of the substrate. Some of the features fabricated using this technique are gears, comb fingers, cantilevers, and membranes. Figure 1.3 [5] shows a microengine gear, that was fabricated using the surface micromachining process, meshing with another gear.

Figure 1.3 Microengine gear meshing with another gear

1.2.3 High Aspect Ratio Micromachining

High Aspect Ratio Micromachining, also called as HARM, involves lithography techniques like LIGA (from the German Lithographie, Galvanoformung, Abformung, meaning lithography, electroplating, and molding). LIGA allows the use of materials other than silicon such as metals, ceramics and polymers, opening the door for many different types of structures and devices. LIGA structures typically have an aspect ratio of greater than 10 to 1, very precise geometries, and smooth, vertical sidewalls. Figure 1.4 shows a microtrajectory sensing device manufactured at Sandia National Laboratories [5].

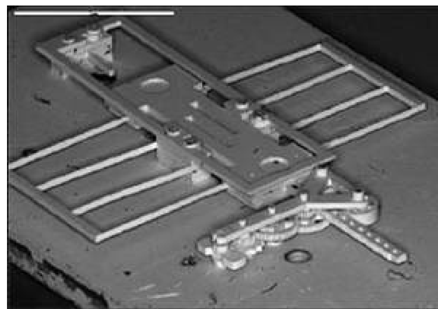

Figure 1.4 Microtrajectory sensing device

1.3 Need to Use Polymers as Substrates

The fabrication techniques mentioned in the previous section have the following disadvantages as it relates to their use for polymer based substrates and microdevices [6]:

- Microfluidic devices tend to be larger in size (several cm^2) with several features on them. Therefore, cost of the substrate is very important. Cost of glass like boro-float glass and photostructurable glass is around 10-40 cents/cm^2 whereas cost of some polymers like PolyMethylMetAcrylate (PMMA) is around 0.2-2 cents//cm^2. Area of a microfluidic chip cannot be decreased without affecting its performance
- Traditional MEMS fabrications techniques tend to require a substantial amount of time, involving lots of chemicals and expensive equipment
- There are limitations in the type of features that can be fabricated, it is difficult to fabricate features of different depths/heights or arbitrary wall angles
- For biomedical or other clinical applications, some biomolecules tend to adhere onto the Si surfaces [6]. Biocompatibility may sometimes be an issue in such cases.

In contrast, many polymers are biocompatible, inexpensive and have faster fabrication times making them an ideal replacement to silicon or glass substrates. They have a wide range of material properties making them suitable for a wide array of medical device applications. These qualities also make it possible to use polymers for high volume fabrication of microfluidic devices.

1.4 Polymer Microfabrication Techniques

Polymer microfabrication techniques mostly rely on replication processes such as microinjection molding, casting, compression molding and hot embossing. The basic principle of these technologies is the replication of a microfabricated master mold tool that represents the negative of the desired feature. The master can be designed and fabricated using any of the common microfabrication methods mentioned in the previous section and can be used multiple times for replication. Limitations of these methods [6] include

- The quality of the finished polymer substrate depends on the quality of the mold and a smoother tool would introduce less frictional forces between the mold and the substrate
- Since demolding between the master and substrate takes place at the end of the cycle, undercuts or overhanging edges cannot be fabricated
- There has to be no chemical interface between the mold and the tool to prevent adhesive forces during demolding

Some of the polymer microfabrication technologies are explained in detail as follows:

1.4.1 Microinjection Molding

Injection molding in the macroscopic world is the most popular and widespread technology used to fabricate plastic parts. A wide variety of feature geometry can be fabricated using this process. Figure 1.5 shows a schematic of a typical injection molding machine [7]. The polymer pellets are fed through the hopper into the barrel

where they start to melt. The melted polymer is then injected under high pressure (typically 60-100 MPa) into the mold cavity that is held at around 60-120°C [6]. The one major difference between the macro and micro injection molding process is that the master mold in microinjection process is also maintained at the polymer melt temperature to allow the polymer to flow into microscopic cavities on the mold. The mold cavity is then cooled to allow for the ejection of the fabricated part. Figure 1.6 [8] shows a typical microdevice fabricated using this process.

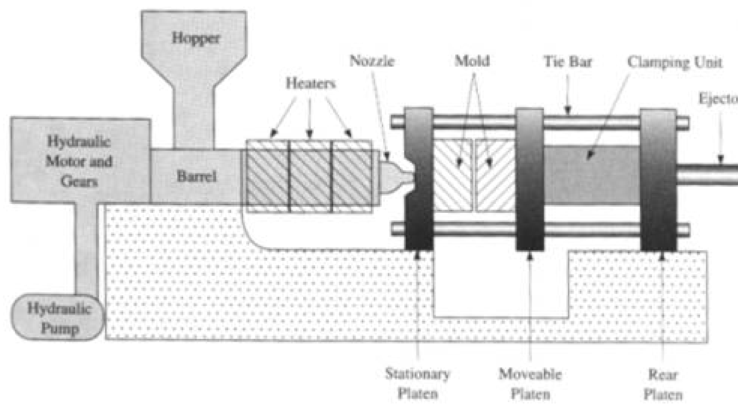

Figure 1.5 Schematic of injection molding machine

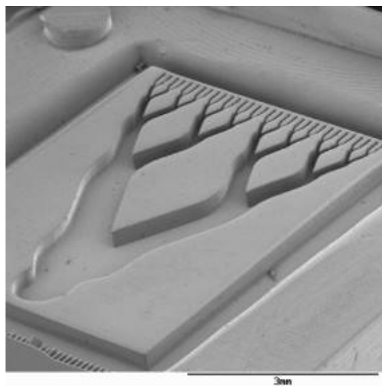

Figure 1.6 Microinjection molding device

The replication accuracy depends on many parameters including the injection flow rate and pressure. Higher flow rates increase the accuracy of the replication process. The cycle time for the injection molding process depends on the aspect ratio of the features to be replicated and the viscosity of the polymer used in the replication process since, the higher the aspect ratio and the viscosity, the longer the cycle time. Since viscosity of a polymer is a function of temperature, injection molding at higher temperatures leads to lower viscosity and hence, lower cycle time. Injection molding is a cost effective process for producing microstructures.

This process is mainly used for low molecular weight thermoplastics. The tooling cost involved is high, and that makes injection molding an efficient process for large volume production, not medium or low volume production.

1.4.2 Hot Embossing

Hot embossing is a relatively new fabrication technique employed for replicating structures on a polymer surface. This technology was primarily developed to fabricate MEMS devices for microfluidic applications. Structures in the order of micro and nanoscale as well as high aspect ratio features have been successfully replicated using this process. Figure 1.7 shows a typical component fabricated using hot embossing.

The polymer used in the hot embossing process is thermoplastic by nature. These types of polymers are characterized by a parameter known as the glass transition temperature (T_g). Beyond this temperature, the mechanical properties of the polymer change substantially, and the polymer becomes soft and rubbery in nature. In the

embossing process, the polymer and the tool are heated just above the T_g (about 10-30 °C) of the polymer and the tool is pressed on to the polymer and held for a pre-determined amount of time. As the polymer behaves like a highly viscous fluid (glassy), the microstructures present on the mold (tool) are easily transferred to the polymer. The most commonly used substrate polymer is PMMA. Other polymers such as Polycarbonate are also used for the embossing process. Typical embossing pressures are about 5-20 MPa depending on the type of the polymer used and the features to be embossed. The hot embossing process is characterized by pressure, strain rate, embossing temperature, holding time and cooling rate as the primary process parameters. The optimum combination of the parameters results in an efficient embossing process. More information on hot embossing is provided in chapter 3.

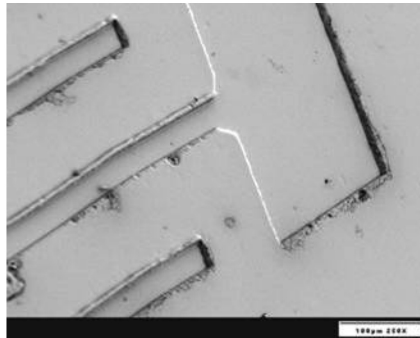

Figure 1.7 Hot embossed device

1.4.3 Injection Compression Molding

Injection compression molding is a combination of injection molding and hot embossing [9]. The plasticized polymer is injected through a screw into a semi-closed mold and then pressed to form microstructures when the mold is closed. Although this

method can be used to fabricate microstructures, only CDs and DVDs have been fabricated using this technique. Since the aspect ratios on CDs are small, demolding is not a problem.

1.4.4 Polymer Casting

Polymer casting is a relatively longer process primarily used for fabrication of elastomers and epoxies [9]. During this process, the prepolymer (for example PDMS) and a curing agent are mixed at a certain ratio, stirred thoroughly and degassed under vacuum [10]. The prepolymer and the curing agent are then poured onto the mold, degassed again and cured for typically several hours. After thoroughly curing the polymer set, it is peeled off from the mold and the microfeatures from the mold are transferred onto the thermosetting polymer. Figure 1.8 [11] shows a drug delivery device fabricated using this process.

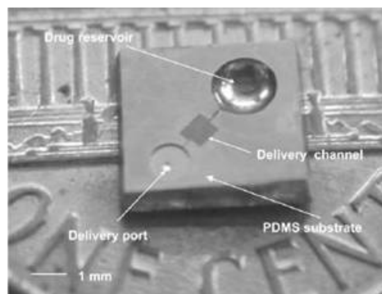

Figure 1.8 Polymer cast device

Table 1.1 [6, 9] summarizes the above mentioned polymer microfabrication processes indicating suitable materials along with process parameters and relative feature sizes expected from each process.

Table 1.1 Summary of polymer microfabrication techniques

Process	Materials	Cycle Time	Forces	Temperature	Feature Dimensions
Injection Molding	Thermoplastics	Short-medium (~3 mins)	High (kN)	Above melting	~ 10 um
Hot Embossing	Thermoplastics, thin Films	Medium (3-8 mins)	High (kN)	Around T_g	nm (nano-imprinting)
Injection Compression Molding	Thermoplastics	Medium (3-8 mins)	High (kN)	Above melting	-
Polymer Casting	Elastomers, epoxies	Long (hours)	No Forces	Room temperature	nm

1.5 Laser Based Microfabrication

Laser microtechnology is a laser assisted technological process for precise treatment, modification and synthesis of materials in the domain of micrometer size [12]. Typical processes in this field include laser micromachining, laser induced heat treatment, laser melting and microwelding, microshaping, micropatterning and pulsed laser plasma deposition.

Laser micromachining, in particular, is very promising and has helped in the development of several novel devices [13, 14]. It is a single stage dry process that is compatible with a wide variety of materials. The process is attractive as it is highly flexible, easy to automate, does not require stringent conditions like clean room facilities, and provides capabilities of rapid prototyping. It also results in fabrication of features of high quality and high accuracy.

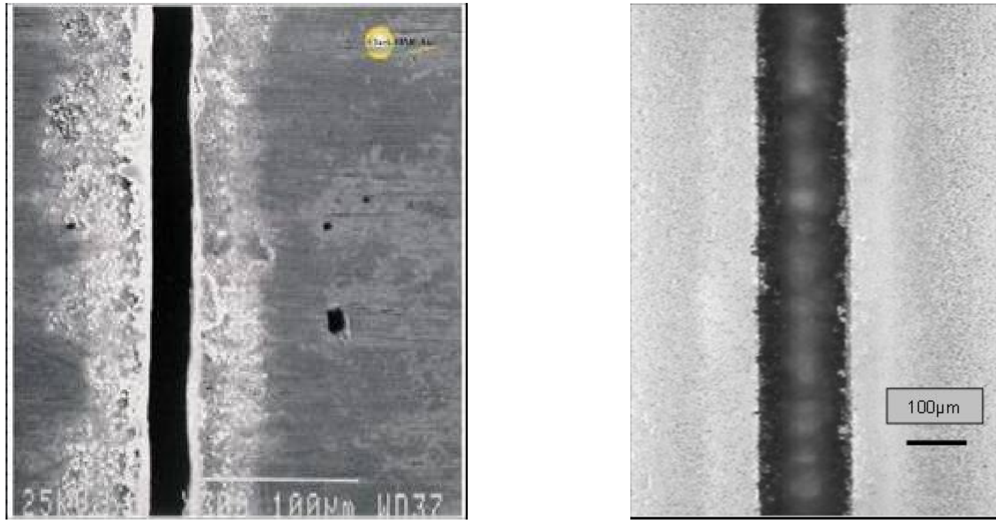

(a) (b)

Figure 1.9 Laser micromachining of a channel (a) Long pulsed laser
(b) Ultra short pulsed laser

The use of ultra short laser pulses, with pulsewidth in the order of 100 femtoseconds, has been shown to provide high quality micromachining with minimal thermal damage as compared to machining quality obtained when using long or continuous laser pulses. Figure 1.9 shows a comparison between machining a channel with a long pulsed laser [15] versus machining a channel with an ultra short pulsed laser [16].

Femtosecond pulsed lasers can be used to improve precision due to efficient energy deposition. This energy deposition, in the case of femtosecond lasers, takes place in time duration smaller than the characteristic heat diffusion time for most materials resulting in a direct transition from solid to dense plasma without the intermediate phases of melting and boiling. This phenomenon occurs due to rapid heating of the solid to temperatures higher than critical point. As plasma formation is

the mode of femtosecond laser pulse ablation, little or no molten material recasts into the machined area. The process of laser ablation occurs through the transfer of optical energy from the photons in the beam to carriers within the material by mechanisms like one photon absorption, multi photon absorption, ionization and avalanche multiplication [17, 18]. More information on femtosecond laser micromachining (FLM) process is given in chapter 2.

1.6 Scope of this Research

This research concentrates on fabrication of polymer substrates using hot embossing and femtosecond laser technologies. As mentioned earlier, a replication process like hot embossing requires a master mold that is replicated on the polymer substrate. It is planned to fabricate this mold using the femtosecond laser. This research characterizes the femtosecond laser micromachining system with the sole aim to fabricate molds for hot embossing. Characterization of the hot embossing process is also performed for three different polymers.

Once a polymer substrate has been fabricated, it is typically covered with another polymer that may or may not have any features on it. Bonding takes place between these two pieces. Thermal bonding that uses the same hot embossing equipment is studied. Finally, microfabrication is performed on a biodegradable polymer using femtosecond laser and hot embossing.

1.7 Report Layout

Chapter 2 discusses the characterization of femtosecond laser micromachining for mold making. Chapter 3 addresses the hot embossing process and characterization

of polymers during hot embossing, and de-embossing/demolding process. Chapter 4 introduces a novel process called two-stage embossing. Chapter 5 presents micromachining of biodegradable polymers for a conceptual drug delivery system. Chapter 6 deals with polymer bonding using the hot embossing machine. Finally, chapter 7 concludes with recommendations for future work.

CHAPTER 2

MOLD FABRICATION USING FEMTOSECOND LASER MICROMACHINING

This chapter provides an introduction to femtosecond laser micromachining technology, and describes the various laser machining parameters. The femtosecond laser micromachining (FLM) system at UTA used for this research is introduced. Finally, characterization experiments and conclusions drawn through these experiments on the FLM process with specific focus on mold fabrication on silicon are described.

2.1 Micromachining with Ultra-short Pulses

Ultra-short laser pulses interact with the material for a time typically of the order of 100 femtoseconds, which is much smaller than the characteristic time for heat diffusion to the lattice. This results in a very small heat affected zone, thereby increasing the efficiency, accuracy and quality of machining process. The physical mechanism of material removal depends upon the intensity of the laser beam. For sufficiently large laser beam intensities, the interaction of the laser beam with the solid material creates dense plasma, which expands due to internal forces. At the end of energy transfer from the beam, part of this plasma condenses and sometimes may recast around the micromachined feature. This redeposition can be avoided by using vacuum during machining or by blowing the plasma away from the site of machining using an

inert gas. As explained later in section 2.5.2, it has also been established experimentally that apart from using vacuum or inert gas, the quality of the channel edge features can also be dramatically improved by blowing a continuous jet of pressurized air over the site of micromachining to remove plasma and prevent it from redepositing itself. The debris can be usually cleaned by treating the silicon wafer with acetone after machining. A pictorial representation [14] of phenomena due to ultra short pulse laser micromachining is shown in figure 2.1.

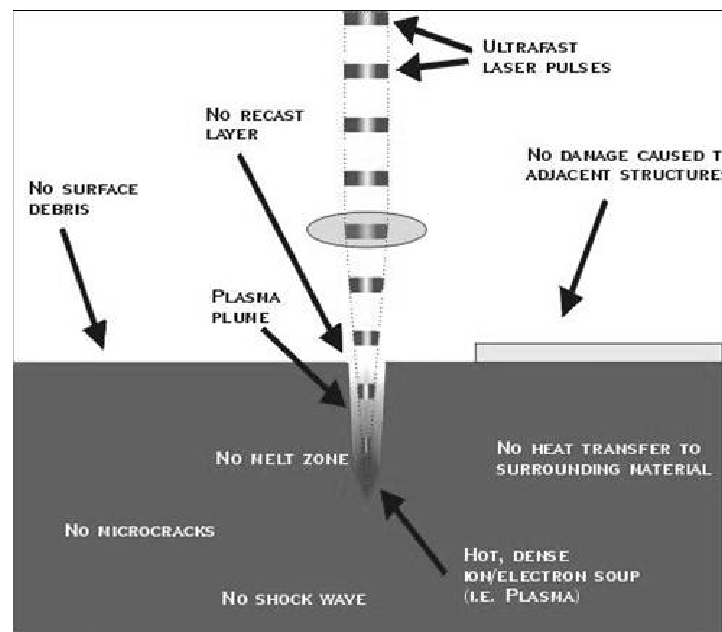

Figure 2.1 Machining due to ultra short pulsed laser

Figure 1.9 shows a channel machined on a silicon wafer with an ultra short pulsewidth laser beam using the setup in the UTA BioMEMS laboratory. There appears to be a very small heat-affected zone and the edges of channel are sharp with no signs of recast material.

2.2 FLM Micromachining Parameters

2.2.1 Laser Beam Machining Parameters

The laser beam parameters that have a decisive influence on the quality of machining and on the topography of machined features [15] are:

- Wavelength: The wavelength of incident radiation determines the coefficient of monochromatic absorption and reflectance of the material. The wavelength has also been shown to affect the size of micromachined features [19].
- Pulsewidth: Briefly, it can be stated that ultrashort pulses have been found to provide high accuracy and improved finish to the micromachined features [20].
- Pulse repetition rate: Pulse repetition rate controls the quality and topology of machining as it determines the allowable time for removal of material and heat since the previous pulse. If beam fluence is in the lower range of damage threshold, repetition rate essentially has the same effect as pulsewidth.
- Laser beam fluence: The laser beam fluence determines the mechanism of heat absorption in the material and the mode of ablation. It has been found that for best micromachining quality of the laser beam fluence should be just above the threshold for laser ablation. At low energy the redeposited melting material reduces significantly [21]. It has been predicted that at energies high above the damage threshold, both plasma and molten phases of material are present whereas at energies just above the threshold value only plasma phase is present thus providing better micromachining results.

2.2.2 Machining Setup Parameters

The following machining parameters [15] were found to affect the topography and quality of machining during experimentation and development of the FLM facility in our laboratory.

- Focusing location effects: Proper identification of focus point in 3D space while micromachining is important to the process. Deviations from focal point cause variations in fluence and spot diameter thereby affecting the ablation process in multiple aspects. Off focus positioning of the workpiece was found to produce fringes on silicon surface.
- Focusing lens: The specifications of the focusing lens used in the process determine the resolution of machining and the intensity of laser beam at the focal spot. The focal spot cannot be made infinitely small and depends upon the divergence of the beam. The beam waist is a small region near the focus within which the intensity of the beam varies up to five percent. The choice of a particular lens for micromachining is a compromise between smaller beam spot for increased intensity and finer resolution, and longer depth of focus for controlling the aspect ratio of feature. A longer focal length lens produces a larger spot size and a larger beam waist than a lens of shorter focal length.
- Type of motion of workpiece relative to laser beam: This parameter has been found to affect quality of continuous features like channels. It includes the number of passes made over the feature with the focused laser beam and the direction of

movement in each pass. Repeated passes over the same feature can either be made in one direction only or in a bi-directional mode.

- Directionality and angle of incident beam: A laser beam incident at an angle other than normal to the surface creates features of distorted shape. For example, a circular beam incident at an angle would machine an ellipse rather than a circular cavity on the surface. It is vital that the beam is incident at a proper angle to the surface to achieve the proper machined feature topography. Inclination of beam to the surface and/or inclination of the plane of the focusing lens to the surface are to be considered for adjusting incident angle of focused beam to the surface.

2.3 FLM System at UTA

The FLM system used in this research work was developed in our laboratory to provide capabilities of rapid prototyping for manufacture of BioMEMS, MEMS and other microdevices.

The main components of the system, shown in figure 2.2, can be classified into the following:

- Femtosecond laser
- Optical components
- Precision motion stages and controllers
- CAD/CAM system

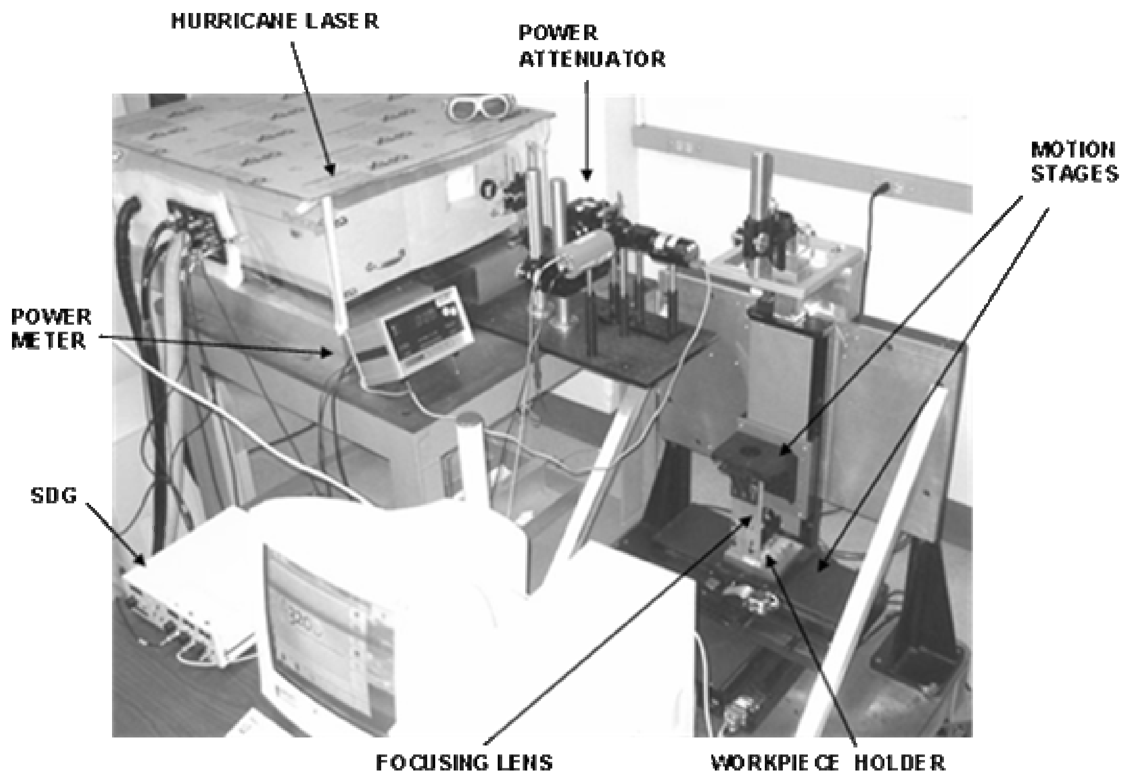

Figure 2.2 FLM system at BioMEMS laboratory

The Hurricane femtosecond laser system, from Spectra-Physics [22], generates a pulsed laser beam of 800 nm wavelength, 120 fs pulsewidth, 1 mJ output with a pulse repetition rate of up to 1 kHz (wavelength 800 nm) and up to 1 mW power per pulse. It uses a diode pumped seed laser called the Mai Tai, a diode pumped Nd:YLF laser, called the Evolution, for pumping the Ti:sapphire regenerative amplifier, and a pulse stretcher and compressor module. The overall system setup is similar to a 3-axis CNC machine with the laser beam acting as the machine tool in a subtractive material removal process. The workpiece is mounted on precision XY-stages from Aerotech Inc. [23] whose motion is computer controlled using the supplied NViewMMI software. The

Z-stage, also by Aerotech Inc., is used to position the focusing lens relative to the workpiece. A series of optical components and lenses guide the laser beam from the laser through the focusing lens to the workpiece. The programming of the system is performed using industry standard G-codes generated from a CAD/CAM system based on the manufacturing module of Pro/ENGINEER [24]. The post processor is customized and amended to include the synchronization of the workpiece stage motion and laser firing based on the requirements of the laser micromachining process [25].

2.4 Feature Measurements

A Nikon Eclipse ME600 optical microscope with CCD camera for image analysis is used to perform feature measurements. The feature depth is measured by focusing at the top surface of the feature and then focusing at the bottom. The difference in the micrometer reading between the top and bottom gives the depth of the feature. Figure 2.3 (a) and (b) shows the top and bottom of a 20 um deep channel machined using a 150 mm lens at 50 mW power and viewed under a lens with 50X magnification.

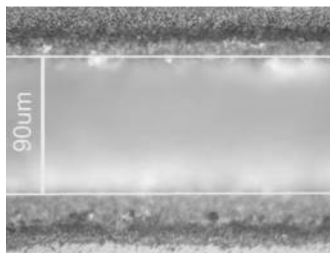

(a)

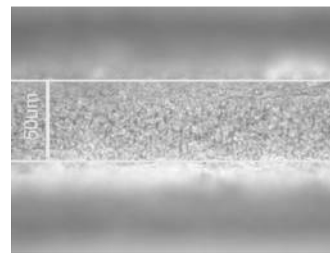

(b)

Figure 2.3 Feature measurement (a) Top surface (b) Bottom surface

The surface features like the width of the channels and diameters of the reservoirs are evaluated using the scale on the pictures taken on the same microscope, with a measurement error of ± 3 um in each case.

2.5 Mold Fabrication Steps Using FLM

One of the goals of this research is the rapid prototyping of the molds using the FLM environment without having to use any traditional MEMS fabrication techniques mentioned in section 1.2. Subsequently, the molds will be used on the HEMM system for replication/fabrication of microfeatures on polymer substrates. The mold rapid prototyping steps describing the procedure employed for replication using the commonly used single stage hot embossing are schematically shown in figure 2.4.

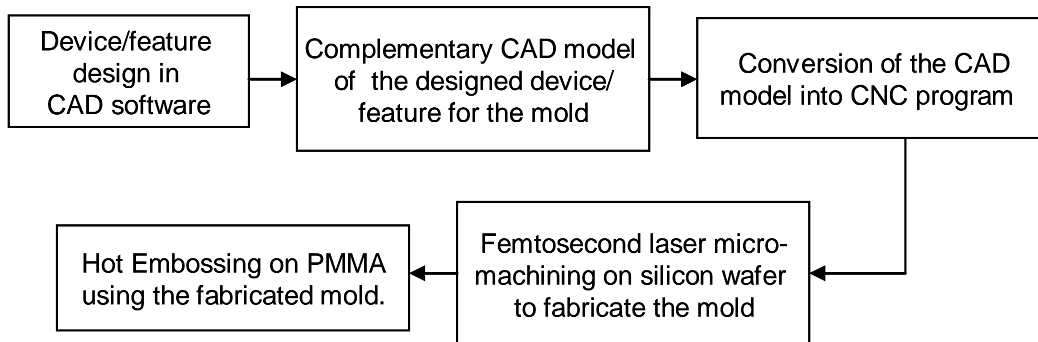

Figure 2.4 Mold rapid prototyping procedure

The device or features to be fabricated are usually modeled and analyzed in a CAD system. Subsequently, the complementary model (to act as the mold) is also modeled. Using industry standard G-codes, a CNC program for the complementary model that plans the motion of the microstages and tool state are generated in the CAD system. The generated G-codes are then automatically parsed to include specific commands relevant to the FLM system such as laser pulse repetition rate and laser

ON/OFF. The parsed G-codes are loaded on the control software for the motion stages, compiled to assure full compatibility, and downloaded to the motion amplifiers/controllers to commence the machining operation. Once the micromachining operation is completed, the result is the desired mold to be used on the HEMM system.

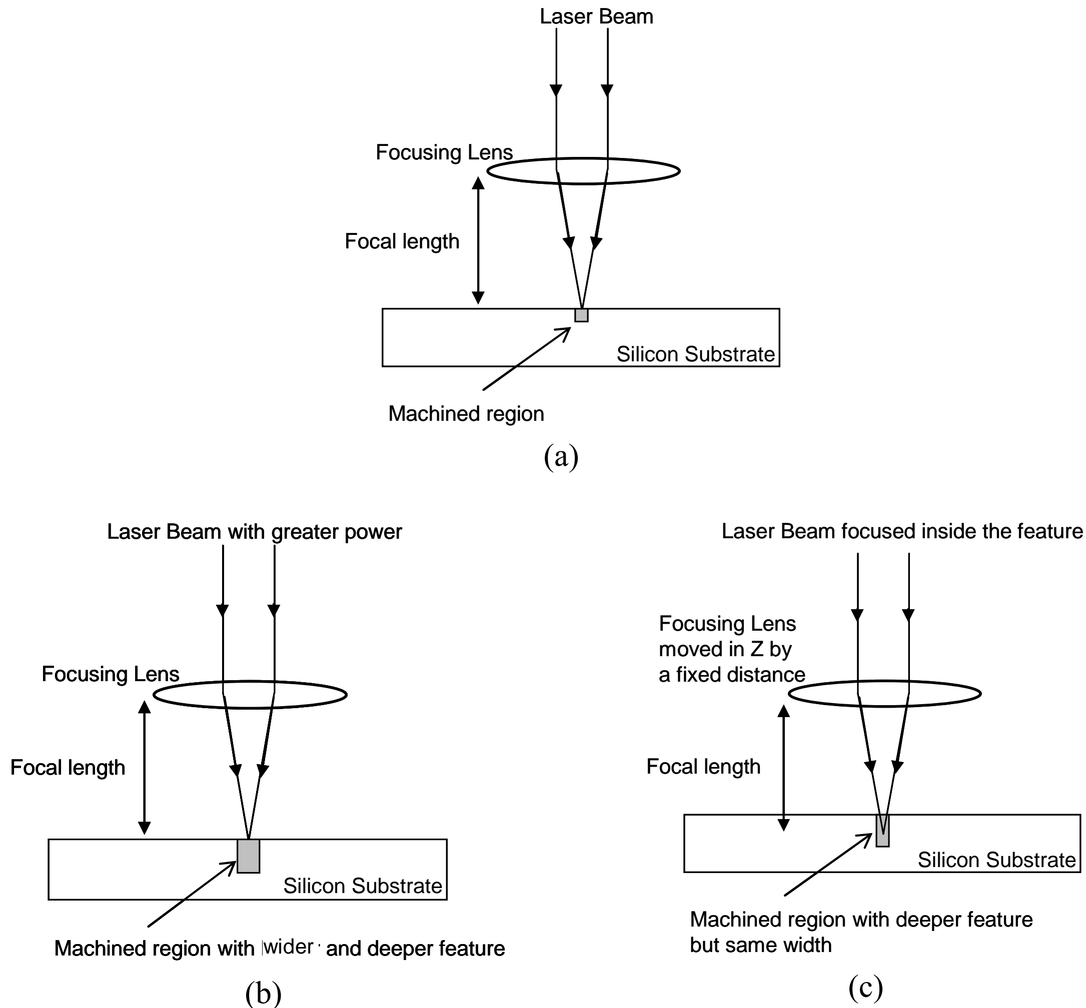

Figure 2.5 Focusing of the laser beam on silicon wafer (a) Laser beam focused on top surface (b) Laser Beam with more power focused on top surface (c) Laser Beam with same power as (a) focused inside wafer

Previous experiments [15] have been performed at a single Z-height of the lens i.e. the laser beam has always been focused on the top surface of the silicon wafer while machining is taking place. One of the disadvantages of this method is that if a deeper feature is to be fabricated, usually the power output of the laser beam has to be increased. Due to this increase in the power level, the feature width cannot be controlled and is dictated by the depth of the feature. This problem can be overcome by dynamically repositioning the lens after a fixed number of passes, so that the laser beam is now focused on the bed of the freshly machined feature instead of the top surface of the silicon wafer as explained in figure 2.5.

Feature quality of the machined silicon substrate can be improved or enhanced by the following three methods:

2.5.1 Finishing Passes

At the lowest Z-level/height, two (2) finishing passes are performed so that the redeposition of ablated material is minimized. Although this increases the depth of the feature by a small amount, there is hardly any redeposition at the bed of the feature. This not only improves the quality of the feature, it also helps in de-embossing when the substrate is used as a mold during hot embossing. A schematic of this process is shown in figure 2.6 and consists of three primary steps.

- Step 1: The focusing lens is positioned such that the laser beam is focused on surface of silicon substrate. Machining takes place at the surface to obtain the desired feature at a particular depth.

- Step 2: Focusing lens moves down by fixed distance thus focusing the laser beam on the freshly machined bed of the feature and machining takes place at this particular depth. This step is repeated until the desired depth of the feature is machined.
- Step 3: Laser beam is now focused at its lowest depth. Two (2) finishing passes are performed to remove the redeposited debris at the bed.

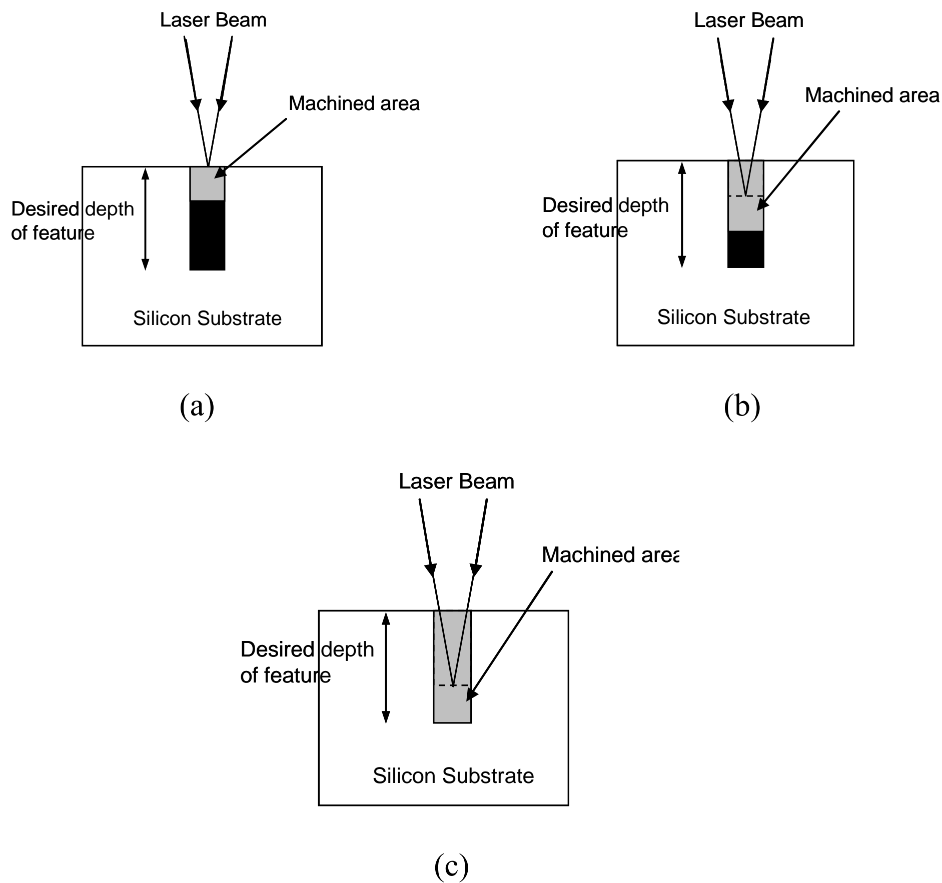

Figure 2.6 Steps for FLM machining (a) Step 1 (b) Step 2 (c) Step 3

2.5.2 Jet of Air

The redeposition of the ablated material can also be minimized by blowing a continuous jet of air at the site of machining. As in the case of finishing passes, this step improves the edge quality of feature as observed in figure 2.7.

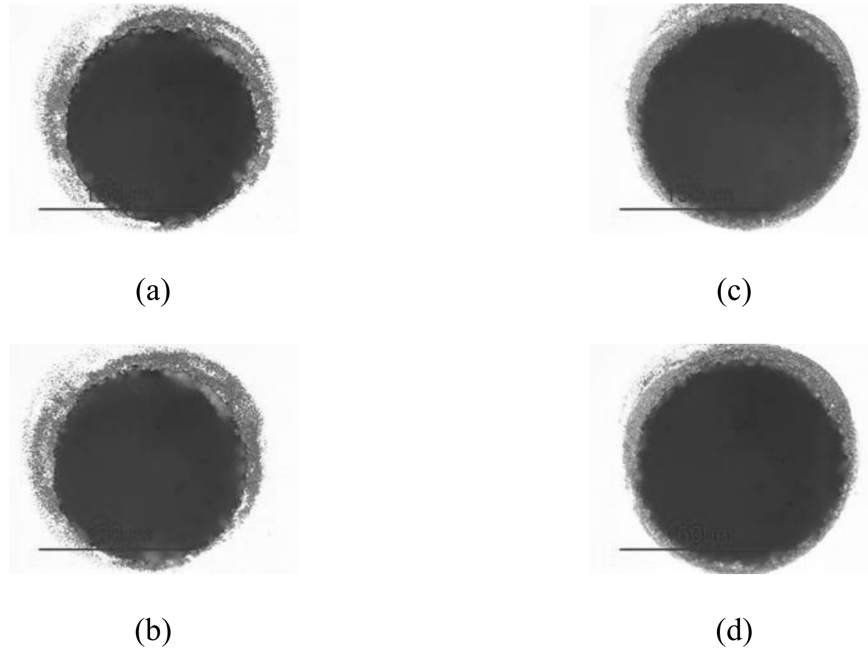

Figure 2.7 Visual comparison of edge quality of feature
(a), (b) without air jet (c), (d) with air jet

2.5.3 Treatment with Acetone

It has been found experimentally that soaking the machined silicon wafer in acetone for about 30 minutes and then drying it improves the aesthetic look of the area surrounding the machined feature. Figure 2.8 shows the difference between the quality of treated and untreated area around a channel.

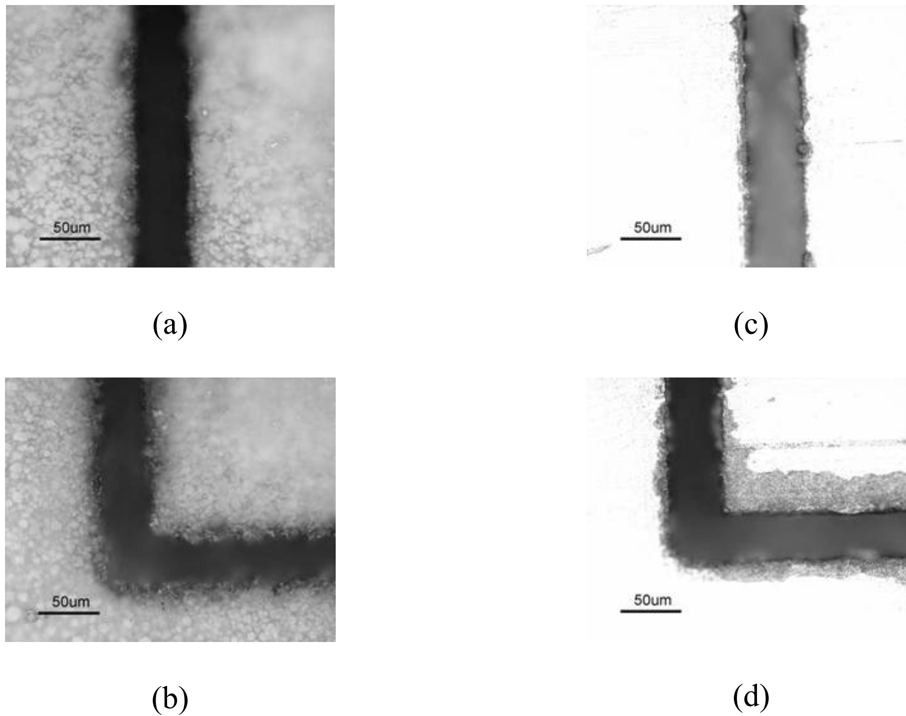

Figure 2.8 Acetone treatment on features (a), (b) channel without acetone treatment (c), (d) channel dipped in acetone for 30 mins

2.6 Characterization of FLM Process

The primary reason for characterizing the FLM process is to estimate the machining parameters when the feature dimensions to be machined are known. The focus of characterization of the FLM process is on mold fabrication. Experiments are performed on silicon wafers with the features machined being reservoirs and channels, the two basic components in microfluidic and other MEMS devices.

2.6.1 Determination of Machining Parameters

All the parameters related to the laser, mentioned in section 2.2.1, except laser beam fluence, which depends on laser power, remain constant for the characterization experiments and have the following values:

- Wavelength = 800 nm
- Pulsewidth = 120 fs
- Pulse repetition rate = 1 kHz

A focusing lens of 25.4 mm focal length is used for all the experiments. The speed of the X and Y stages are kept constant throughout the experiments at 25 mm/min for channels and 10 mm/min for reservoirs. These speeds were determined in [15]. A constant jet of pressured clean air is directed at the machining site at a pressure of around 80 psi. The machined features are soaked in acetone for 30-45 minutes to clean the debris.

The parameters that are varied for each experiment are the discussed next.

2.6.1.1 Power of the Laser (*P*)

The power of the laser beam can be modulated using a manual attenuator and monitored with a power-meter. Increase in the power of the beam increases the depth of cut on the substrate for each machining pass. The optimum value of the laser beam power needs to be calculated for machining so that fast process times are achieved without propagation of heat affected zones (HAZ) in the surrounding of the feature.

Figure 2.9 shows that the width of a channel increase almost linearly with power supplied while the depth tends to reach a plateau at 500 mW. This is possibly due to the generation of plasma and its redeposition that takes place at higher powers. The edge quality of the channels tends to deteriorate at power levels higher than 150 mW as shown in figure 2.10. Therefore, it is not advisable to use power levels more than 150 mW.

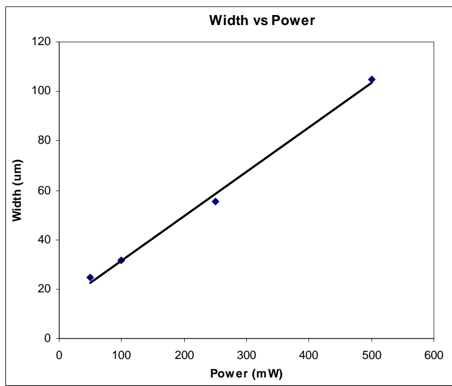

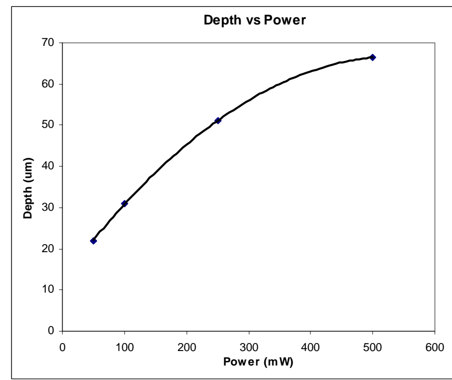

(a) (b)

Figure 2.9 Feature dimensions vs. power levels
(a) Width plot (b) Depth plot

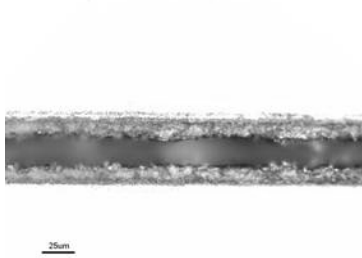

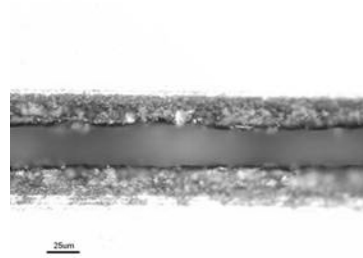

(a) (b)

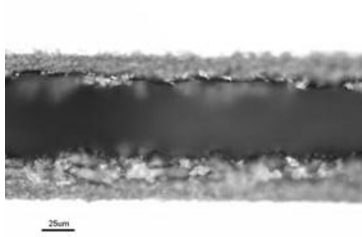

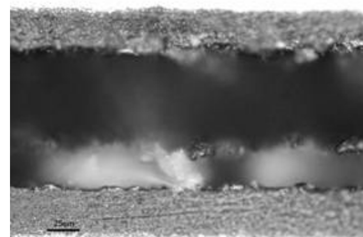

(c) (d)

Figure 2.10 Channels fabricated at different power levels
(a) 50 mW (b) 100 mW (c) 250 mW (d) 500 mW

It has also been observed that higher power is required to fabricate channels than reservoirs of comparable depth. This is due to the fact that the method used to fabricate channels is different than that used for reservoirs. The following power levels are used:

- Channels: 25mW, 50 mW, 75 mW, 100mW, 150 mW
- Reservoirs: 5 mW, 10 mW, 20 mW, 30 mW, 40 mW

2.6.1.2 Number of Passes (*n*)

The number of passes is defined as the number of times the feature geometry is machined without repositioning the focusing lens i.e. at a single Z height. The number of passes also depends on the feature width as increasing the number of passes increases the width of the feature but at the same time improves the edge quality without any propagation of the heat affected zone around the feature.

Figure 2.11 shows that the width and depth of the channel increase almost linearly with an increase in the number of passes. The power used to fabricate these channels is 100 mW. As observed from figure 2.12, the edge quality of the channels after 4 passes is better than the one obtained after 1 and 2 passes. The quality starts degrading again after 6 passes. Since two (2) finishing passes are performed at the lowest Z-depth for reasons mentioned in section 2.5.1, therefore, it is recommended to restrict the number of passes to three (3).

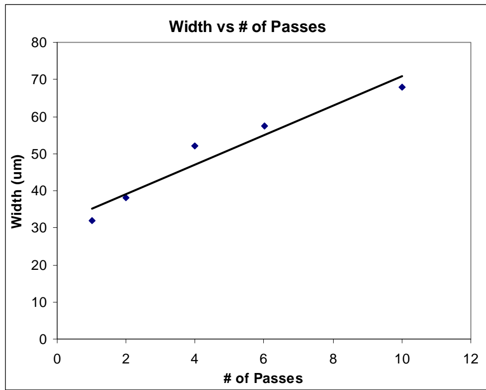

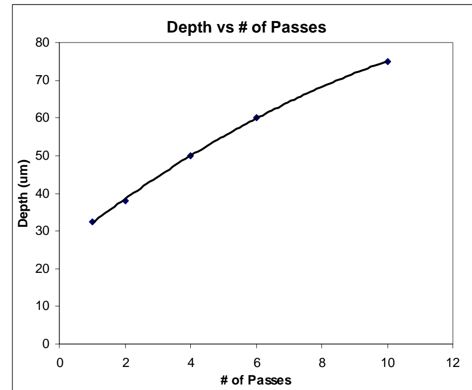

(a) (b)

Figure 2.11 Plots for # of passes (a) Width
(b) Depth

(a) (b) (c)

(d) (e)

Figure 2.12 Channels fabricated at different passes (a) 1 pass
(b) 2 passes (c) 4 passes (d) 6 passes (e) 10 passes

The following numbers of passes, in addition to the finishing passes, are used:

- Channels: 1, 2, 3
- Reservoirs: 1, 2, 3

Figure 2.13 shows the cross section of features machined using different number of passes. It can be seen that vertical walls are obtained using 3 passes. The importance of this observation is explained later in the chapter.

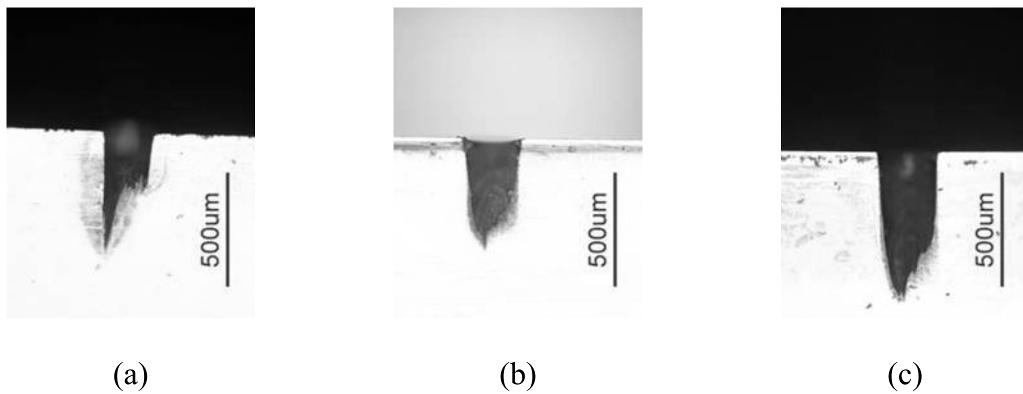

(a) (b) (c)

Figure 2.13 Feature cross-sections at different passes
(a) 1 Pass (b) 2 Passes (c) 3 Passes

2.6.1.3 Depth of Motion (*zDist*)

This is the amount by which the focusing lens has to be repositioned down in the Z-direction after the specified number of passes. This is done to move down the focal spot of the laser to compensate for the depth of the feature machined after the specified number of passes at the previous position. The *zDist* values were determined by performing preliminary experiments at every power level and number of passes. The *zDist* value was taken to be 75 % of the measured depth.

Figure 2.14 presents the plot of the *zDist* values used in the experiment as a function of number of passes for each power level for channels and reservoirs.

2.6.1.4 Number of Z-Downs (*zDowns*)

The number of times the focusing lens is moved down by a value *zDist* determines the final depth of the feature. Preliminary experiments were performed to understand the effect of the number of Z-Downs on the feature dimensions.

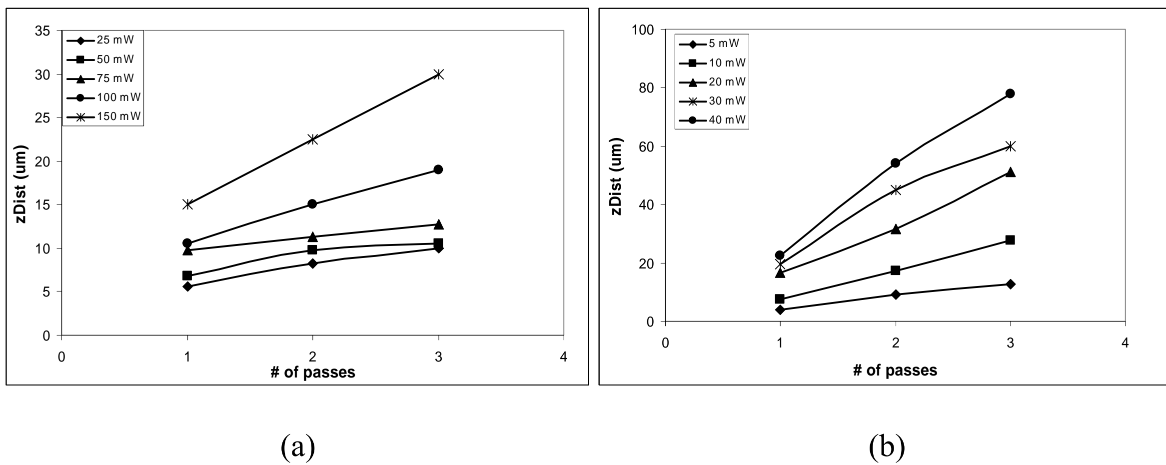

(a) (b)

Figure 2.14 *zDist* values (a) Channels (b) Reservoirs

Figure 2.15 shows that while the depth increases with an increase in number of Z-Downs, the width remains almost constant. The depth of the channels peaks when Z-Down is 3, and starts decreasing from thereon. This is attributed to redeposition of the substrate material. With the increase in the depth, it becomes difficult for the plasma to escape out of the feature. Since the depth of a reservoir is more than the depth of a channel keeping all the parameters constant, it was decided that the maximum number of Z-Downs used was 4 for channels and 3 for reservoirs.

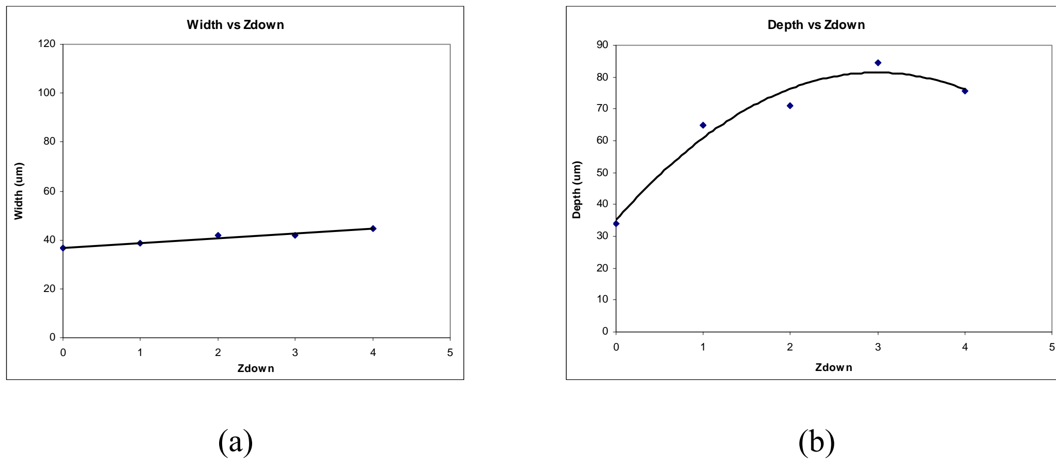

(a) (b)

Figure 2.15 Different Z-Down levels (a) Channel width
(b) Channel depth

2.7 Experimental Results and Discussion

2.7.1 Characterization of Channels

The FLM system is used to machine 10 mm long channels using the parametric values mentioned above. The CNC code used for machining these channels is given in appendix A. The channel depth was measured at three locations and the mean value was considered for the analysis. The measured depth and width values of these channels are given in appendix B. Figure 2.16 shows one channel at every power level. The channel shown has been machined with 2 passes and 1 Z-Downs.

2.7.1.1 Determination of Empirical Equation for Depth of the Channel

The depth of the channels (h_c) is a function of all the machining parameters – power level (*P*), number of passes (*n*) and number of Z-Downs (*zDowns*). Since depth of motion (*zDist*) is a function of P and n, it is not considered for this analysis. In this

section, the channel depth as a function of the process parameters is derived. The depth of the channel is given by

$$h_c = f(P, n, zDowns)$$

For a given power value,

$$h_c\big|_P = g(n, zDowns)$$

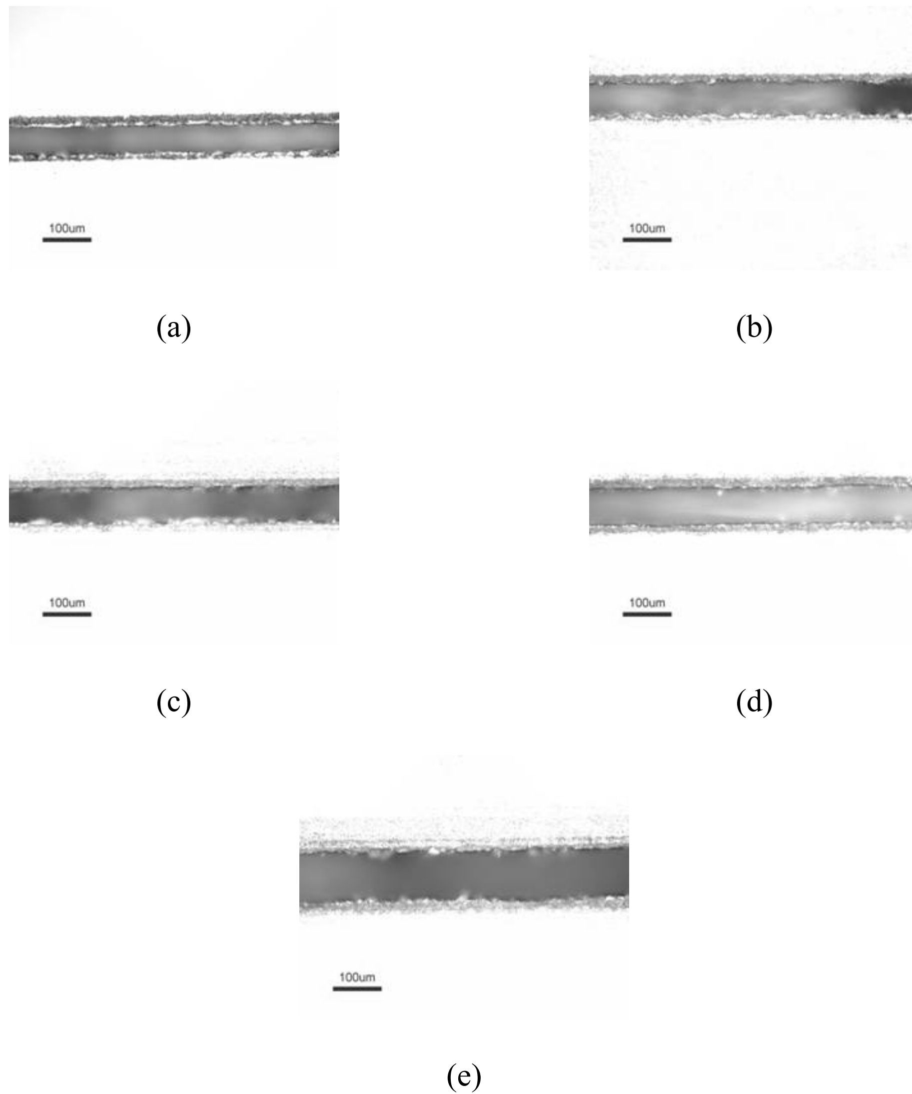

(a) (b) (c) (d) (e)

Figure 2.16 Channels at different power levels (a) 25 mW (b) 50 mW (c) 75 mW (d) 100 mW (e) 150 mW

This leads to the generalized form of the empirical equation for a given power level value

$$h_c\big|_P = k_1 \times zDowns + k_2 \times n + k_3$$

where k_1, k_2 and k_3 are constants having a fixed value for a given power value. A linear relationship was considered between these parameters after examining the data obtained and plotted as shown in figure 2.18 to figure 2.22 for different power levels.

Differentiating the above equation with respect to *zDowns*,

$$\left.\frac{dh_c}{d(zDowns)}\right|_P = k_1\big|_P + k_2 \left.\frac{dn}{d(zDowns)}\right|_P$$

Since the number of passes and Z-Downs are independent of each other,

$$\left.\frac{dn}{d(zDowns)}\right|_P = 0$$

$$\Rightarrow \quad k_1\big|_P = \left.\frac{dh_c}{d(zDowns)}\right|_P$$

Similarly, k_2 can be determined by differentiating the empirical equation with respect to n.

$$k_2\big|_P = \left.\frac{dh_c}{dn}\right|_P$$

The values of k_1 and k_2 are obtained by consulting the plots as shown in figure 2.17. Figure 2.17 (a) shows a plot showing h_c vs. *zDowns* for a power value of 75 mW.

The value of k_1 for 75 mW is evaluated as the average of the slopes of the linear fits for different values of passes; $k_1 = \frac{6.3 + 6.7 + 6.6}{3} = 6.53$

Figure 2.17 (b) shows a plot of h_c vs. n when $zDowns = 0$. The value of k_2 is the slope of the linear fit for each power level.

For $n = 1$ and $zDowns = 0$, $k_3 = h_c - k_2$

The values of the constants (k_1, k_2, k_3) determined by employing the above procedure are given in table 2.1.

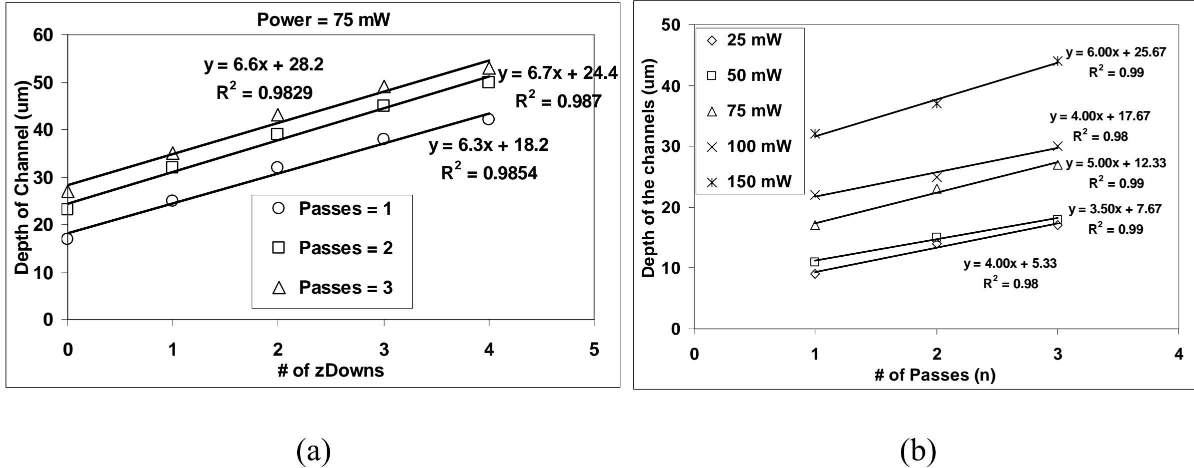

(a) (b)

Figure 2.17 Determination of constants k_1 and k_2
(a) To find k_1 (for 75 mW) (b) To find k_2

Table 2.1 Constant values for channel depth

Power (mW)	25	50	75	100	150
k_1	3.10	5.20	6.53	7.33	11.00
k_2	4.00	3.50	5.00	4.00	6.00
k_3	5.20	6.85	11.80	16.80	22.65

Figures 2.18 to 2.22 show a comparison between experimentally measured and empirically calculated values for the depth of the channels. It is observed that for all

power levels except 150 mW, that the difference between the two is within ± 4 um, which is well within the accuracy of measurement of the features. For the high power level of 150 mW shown in figure 2.22, the maximum difference is as large as 8 um or 10 % indicating that the assumption of linearity might not hold true for higher power levels.

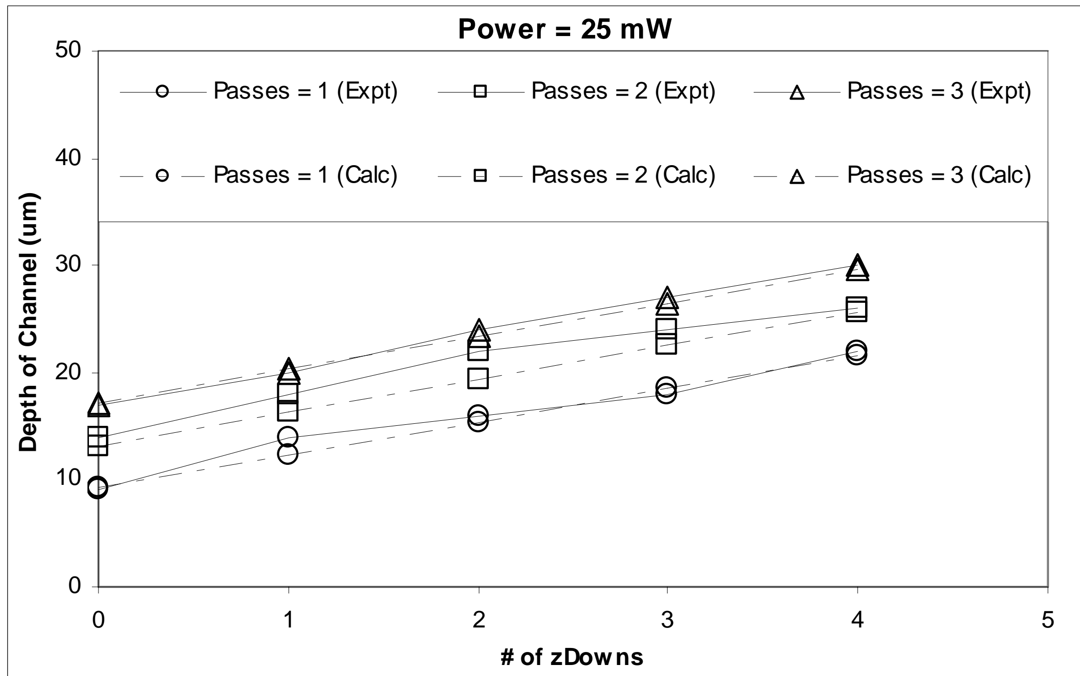

Figure 2.18 Comparison between measured and calculated depths – 25 mW

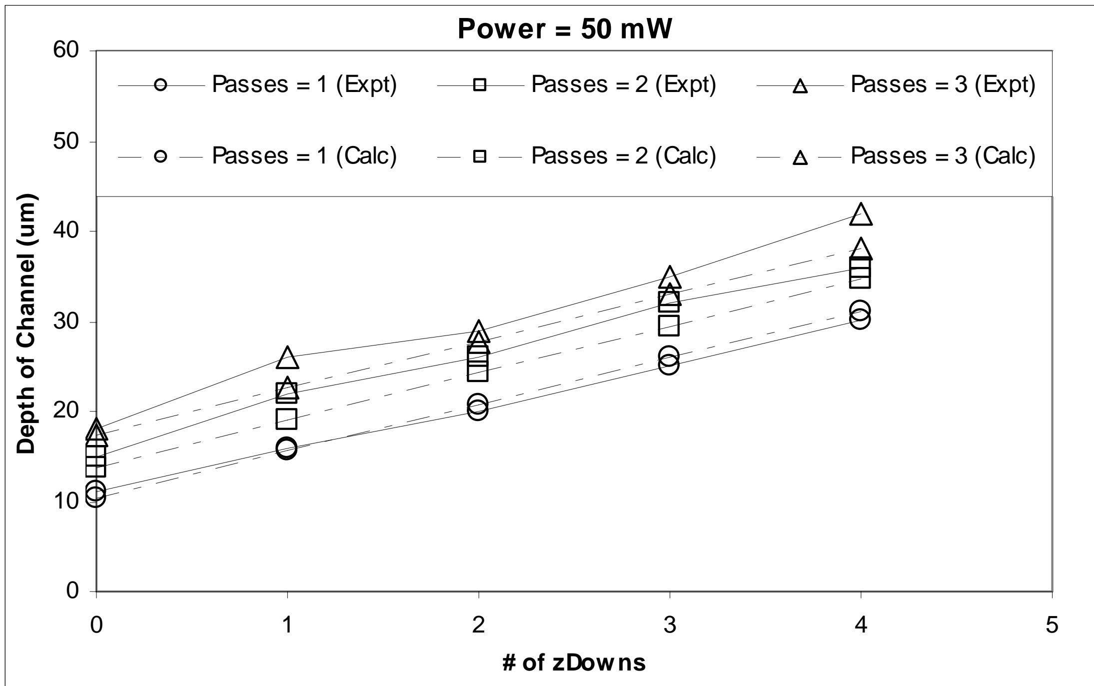

Figure 2.19 Comparison between measured and calculated depths – 50 mW

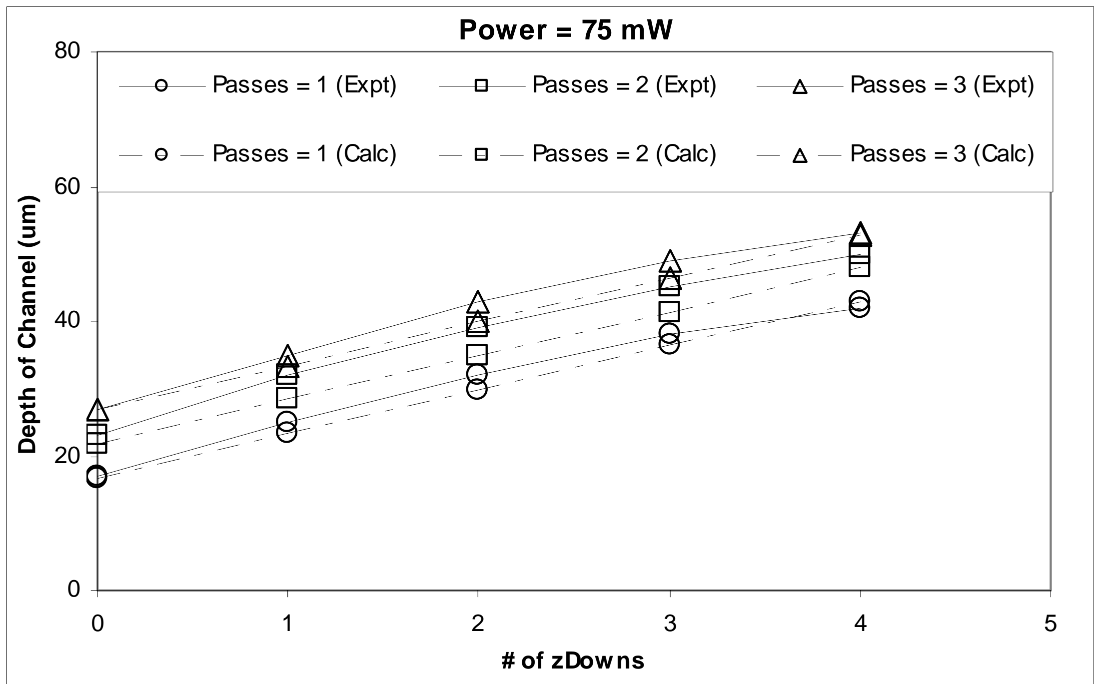

Figure 2.20 Comparison between measured and calculated depths – 75 mW

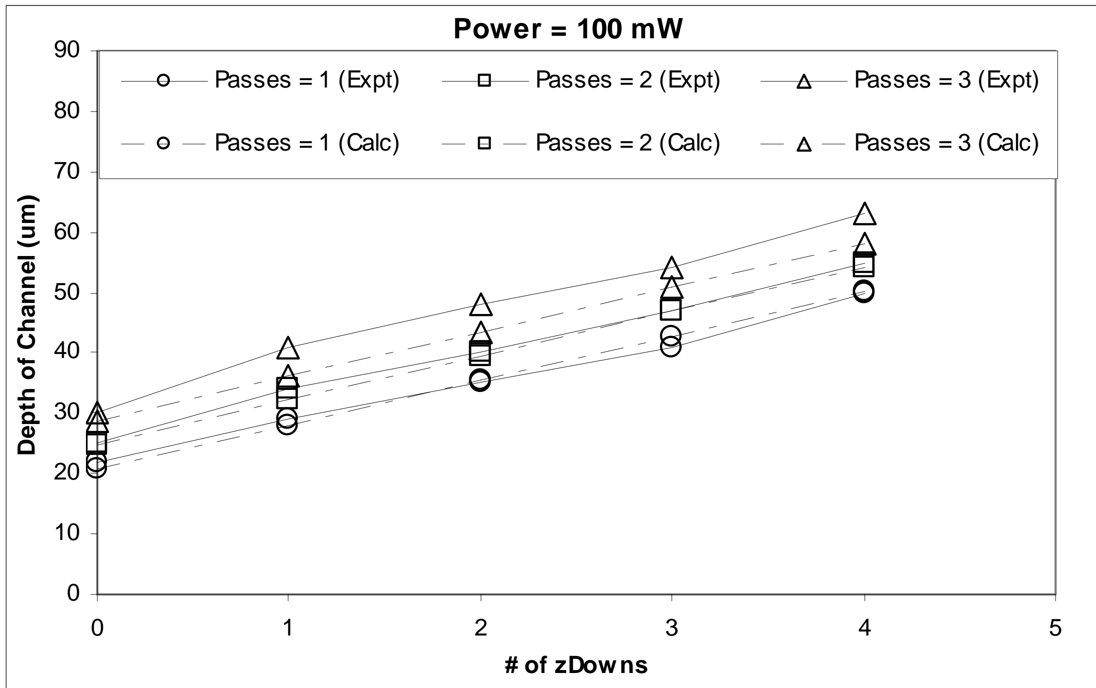

Figure 2.21 Comparison between measured and calculated depths – 100 mW

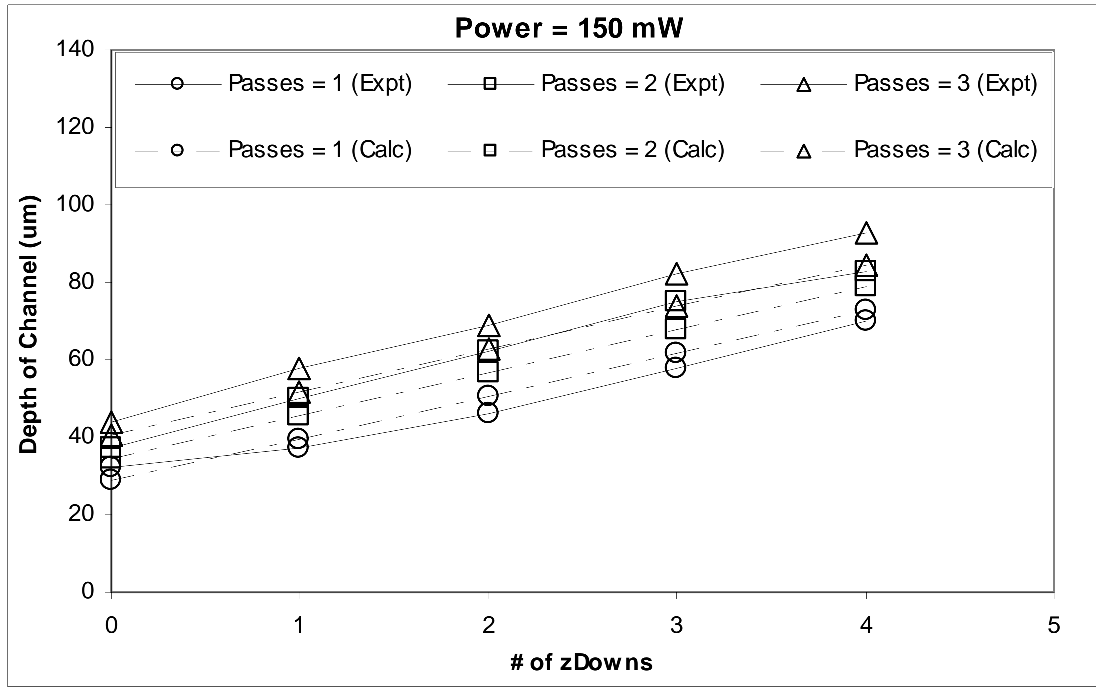

Figure 2.22 Comparison between measured and calculated depths – 150 mW

2.7.1.2 Width of Channels

Measurements of the width of the channels, plotted in figures 2.24 to 2.26, show that although the width increases with an increase in the power level, for all values greater than *zDowns* = 1, it remains almost constant. Therefore, the width of the channels (w_c) is a function of power level (P) and the number of passes (n).

$$w_c = f(P, n)$$

For a given power level, this is reduced to

$$w_c = g(n) = k_4 n + k_5$$

The values of the constants k_4 and k_5 are determined through the linear fit of the plot of average width values vs. number of passes for each power level as shown in figure 2.23 using the same approach presented in section 2.6.1.1 for the depth. Table 2.2 shows the k_4 and k_5 values.

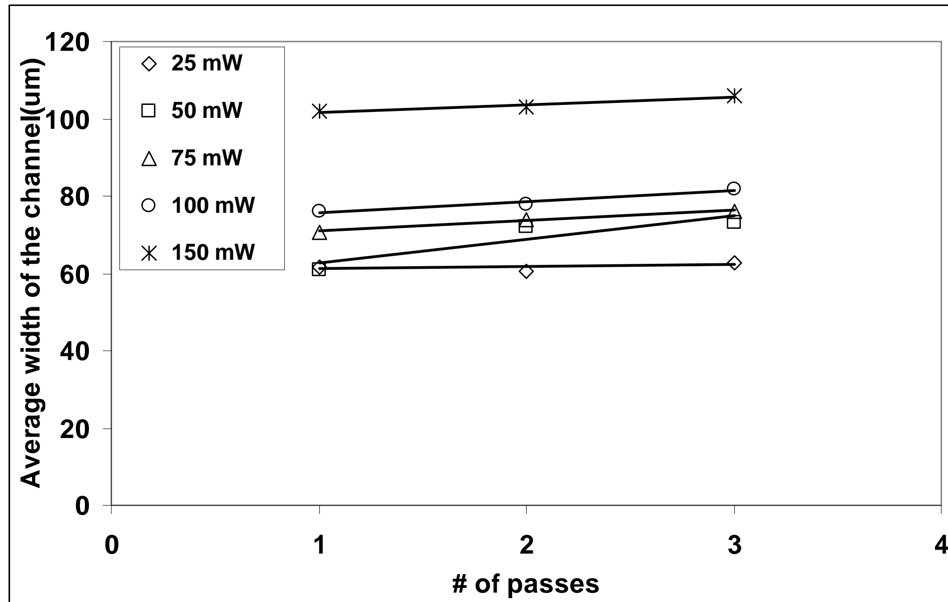

Figure 2.23 Determination of constants k_4 and k_5

Table 2.2 Constant values for channel width

Power (mW)	25	50	75	100	150
k_4	0.50	6.17	2.67	2.83	2.00
k_5	60.77	56.44	68.22	72.78	99.67

Using the values of k_4 and k_5, the values of the width can be calculated. The comparison between the calculated and measured width values for a set of experimentally obtained channels are shown in figures 2.24 to 2.26. The difference between the two is within ± 5 um. It should be noted that the derived empirical equation holds true only for *zDowns* >0. For *zDowns* = 0, experimental values need to be used.

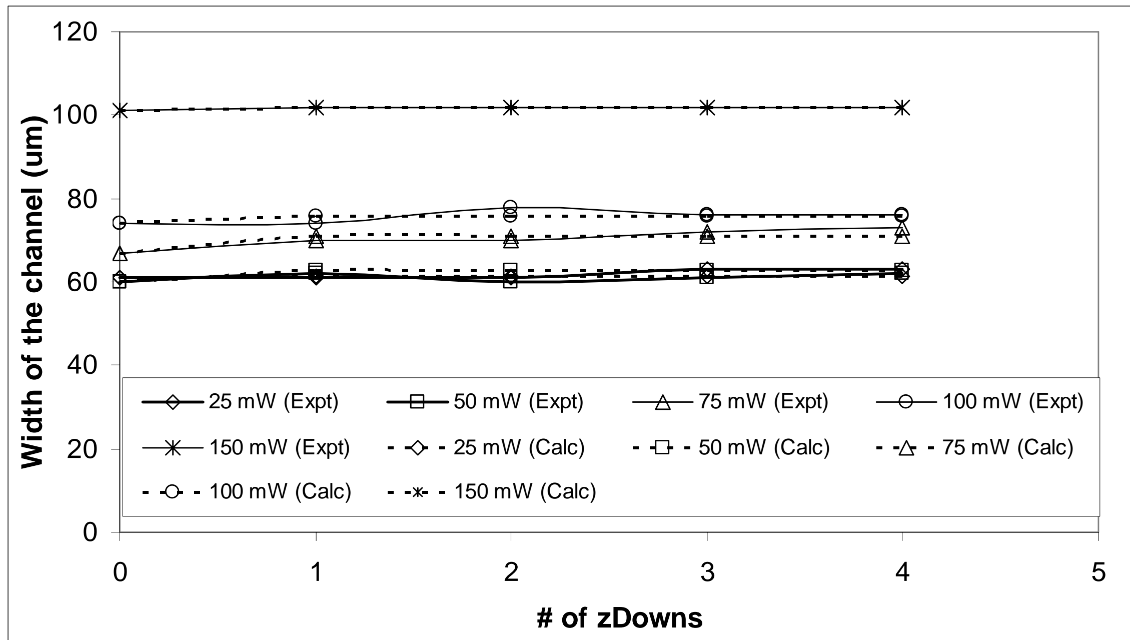

Figure 2.24 Comparison between measured and calculated widths – Passes = 1

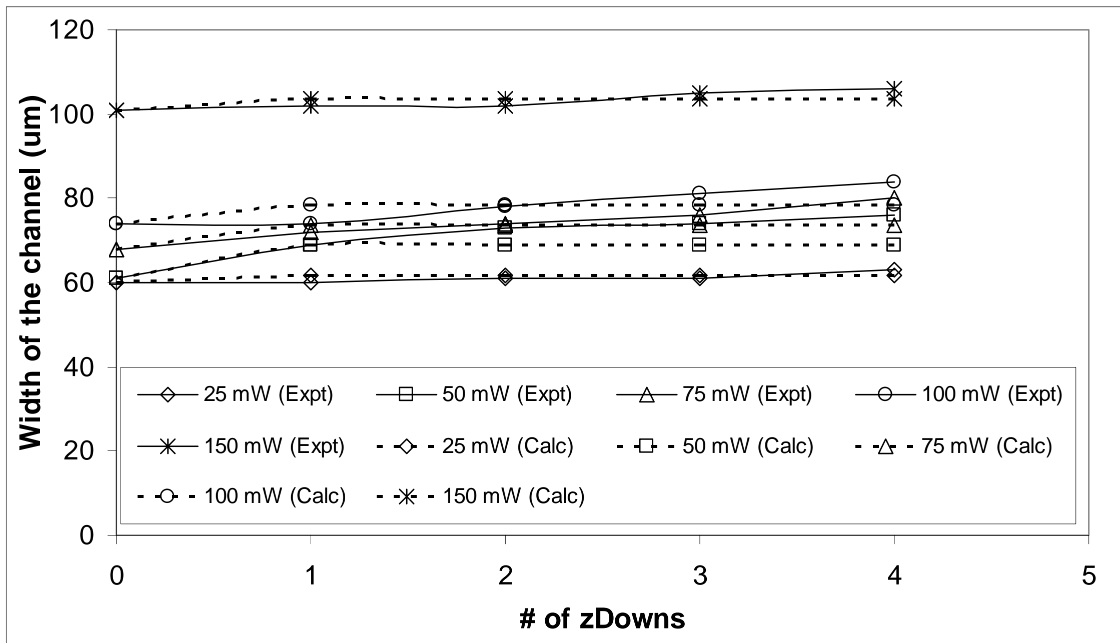

Figure 2.25 Comparison between measured and calculated widths – Passes = 2

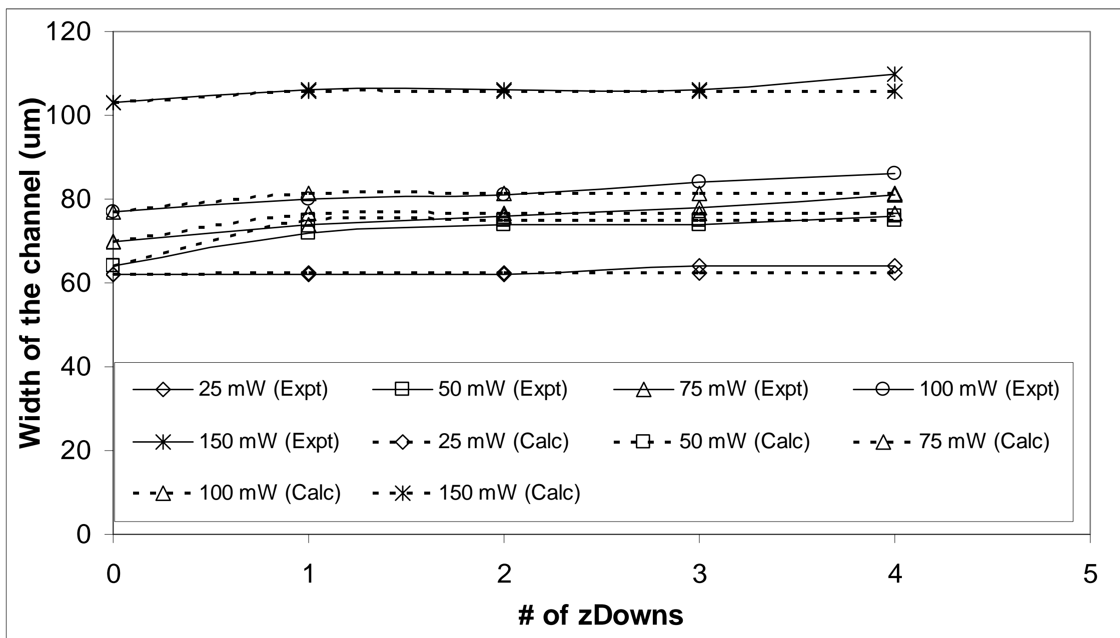

Figure 2.26 Comparison between measured and calculated widths – Passes = 3

2.7.1.3 Application of the Empirical Equations

This example is included to demonstrate the use of the empirical equations in determining the FLM process parameters (viz. the power level, number of passes and number of Z-downs) given the depth and the width of the channel.

Example: Given the desired h_c = 50 um and w_c = 75 um, find P, n and $zDowns$.

For a given P, the $zDowns$ for different n can be obtained from the equation,

$$zDowns = \frac{h_c - k_2 n - k_3}{k_1} = \frac{50 - k_2 n - k_3}{k_1}$$

The number of Z-downs (rounded off to the nearest whole number) required for different power levels and passes are shown in table 2.3.

Table 2.3 Value of $zDowns$ when h_c = 50

Passes (n)	Power (P) (mW)				
	25	50	75	100	150
1	***13***	***8***	***5***	4	2
2	***12***	***7***	4	3	1
3	***11***	***6***	4	3	1

Since the number of Z-downs should not exceed 4, as discussed in section 2.6.1.4, the power levels and passes combination in bold italics can be eliminated. For the remaining combinations, the width of the channel can be found by its empirical equation. The width values calculated for the allowable combinations are shown in table 2.4.

Table 2.4 Values of channel widths (um) for combinations selected

	Power (P) (mW)		
Passes (n)	75	100	150
1	-	75.61	101.67
2	73.78	78.44	103.67
3	76.45	81.27	105.67

Referencing table 2.4, for a channel width of 75 um, a power level of 100 mW with 1 pass can be selected. Therefore, the required machining parameters are P = 100 mW, n = 1 and *zDowns* = 4.

If there is more than one combination that can be used, then it is suggested to use the combination having more number of passes as it has been observed that the channel profile improves with the increase in the number of passes as shown in figure 2.13. The channels have straighter walls when 3 passes are used.

Therefore, in the above example, if an error in the width of about 2 um is permissible, the combination of P = 75 mW, n = 3 and *zDowns* = 4 should be used in order to obtain a better channel profile. A validation experiment was performed using these process parameters and resulted in a channel with width 72 um and an average depth of 49 um.

2.7.2 Characterization of Reservoirs

Three reservoirs with a nominal diameter of 250 um were machined using the FLM system for each combination of the process parameter values mentioned in section 2.6. The CNC code used for machining these reservoirs is given in appendix C. The mean value of all three reservoir depths was considered for the analysis. The measured depth and diameter values of these reservoirs are given in appendix D. Figure 2.27 shows one reservoir at every power level. The reservoirs shown are machined with 2 passes and 1 Z-Downs.

2.6.2.1 Determination of Empirical Equation for Depth of the Reservoir

The depth of the reservoir (h_r) is a function of all the machining parameters – power level (P), number of passes (n) and number of Z-Downs (*zDowns*). In this section, the reservoir depth as a function of the process parameters is derived. The depth of the reservoir is given by

$$h_r = f(P, n, zDowns)$$

For a given power value this reduces to

$$h_r\big|_P = g(n, zDowns)$$

This leads to the generalized form of the empirical equation for a given power value

$$h_r\big|_P = k_1 \times n \times zDowns + k_2 \times zDowns + k_3$$

where k_1, k_2 and k_3 are constants with a fixed value for a given power level. The non-linear equation was considered between these parameters after examining the data obtained and plotted as shown in figures 2.30 to 2.34.

Differentiating the empirical equation with respect to *zDowns*, we get,

$$\left.\frac{dh_r}{d(zDowns)}\right|_P = k_1 \times n + k_2$$

The values of k_1 and k_2 are obtained by linearly fitting the plot between $\left.\frac{dh_r}{d(zDowns)}\right|_P$ and n as shown in figure 2.28 and are tabulated in table 2.5.

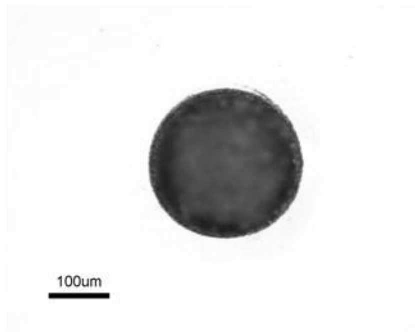

(a)

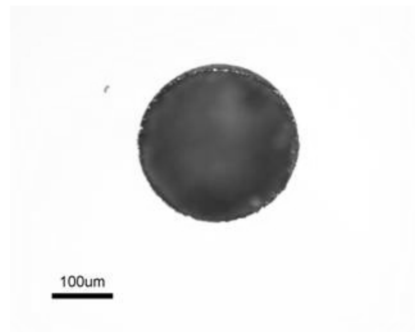

(b)

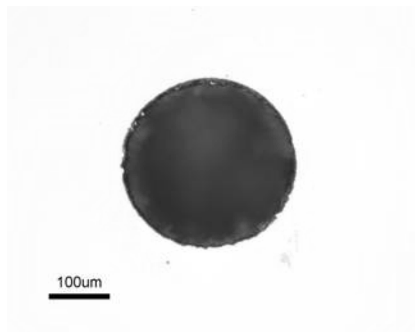

(c)

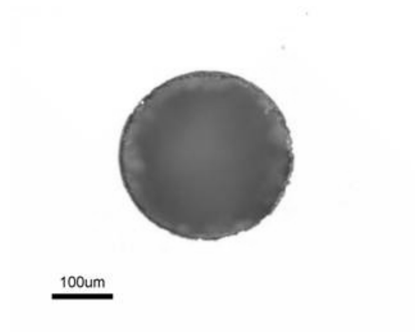

(d)

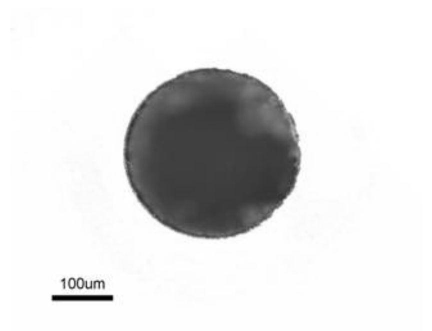

(e)

Figure 2.27 Reservoirs at different power levels
(a) 5 mW (b) 10 mW (c) 20 mW (d) 30 mW (e) 40 mW

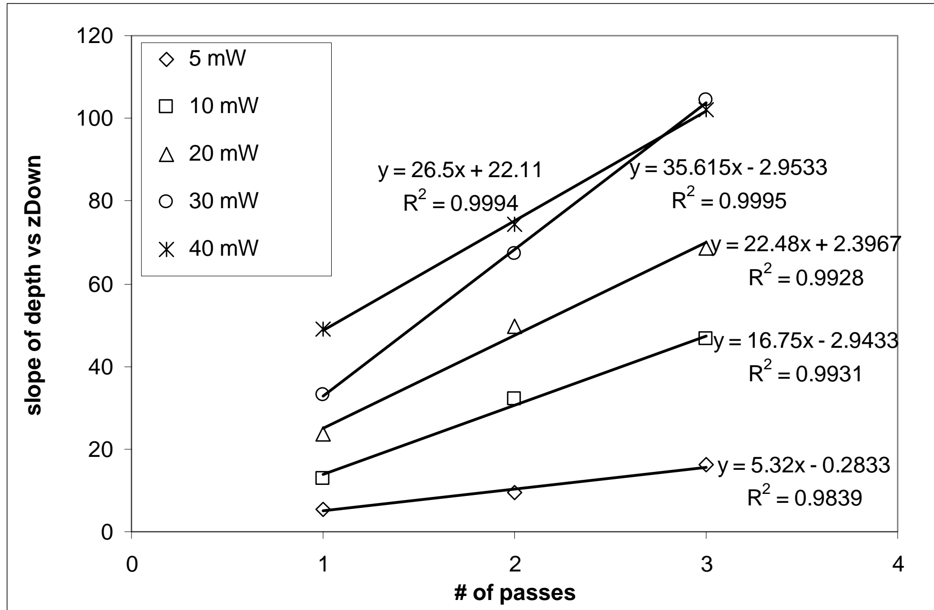

Figure 2.28 Determination of constants k_1 and k_2 for reservoir depth

Table 2.5 Constant values for reservoir depth

Power (mW)	5	10	20	30	40
k_1	5.32	16.75	22.48	35.62	26.5
k_2	-0.28	-2.94	2.40	-2.95	22.11

When *zDowns = 0*, the empirical equation becomes

$$k_3 = h_r \big|_{P,\, n,\, zDowns=0}$$

This k_3 value is the value of the depth of the reservoir when *zDowns* = 0 for all passes and power levels, i.e. $k_3 = f_1(P, n)$ and will have a unique value for all the combinations of *P* and *n*. The k_3 values obtained experimentally are shown in figure 2.29.

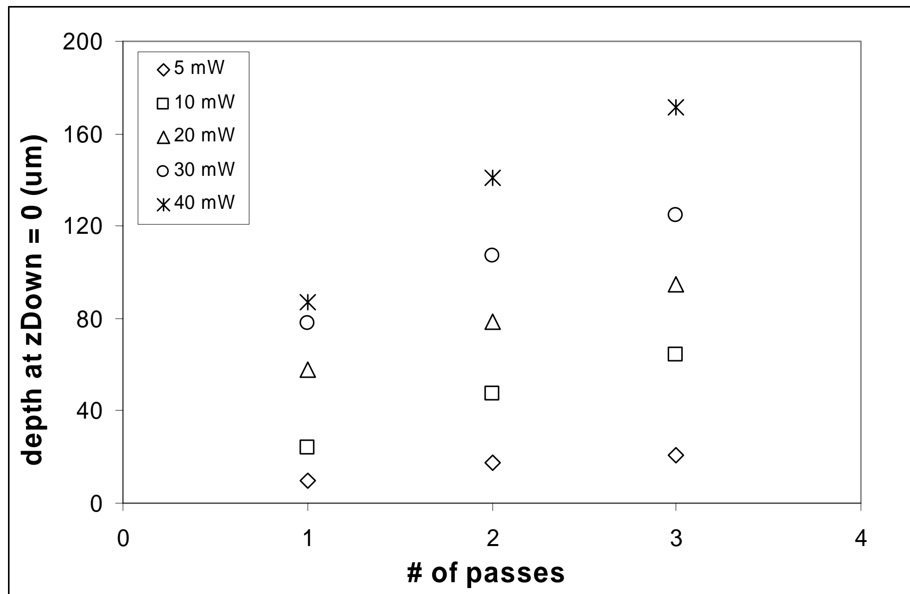

Figure 2.29 Values of constant k_3 for reservoir depth

The comparison between the experimentally obtained values for the depth and the values calculated using the empirically determined equation is shown in figures 2.30 to 2.34. The plots indicate that both the values are within ± 7 % of each other, except for the higher power of 40 mW where the error increases to 10 %.

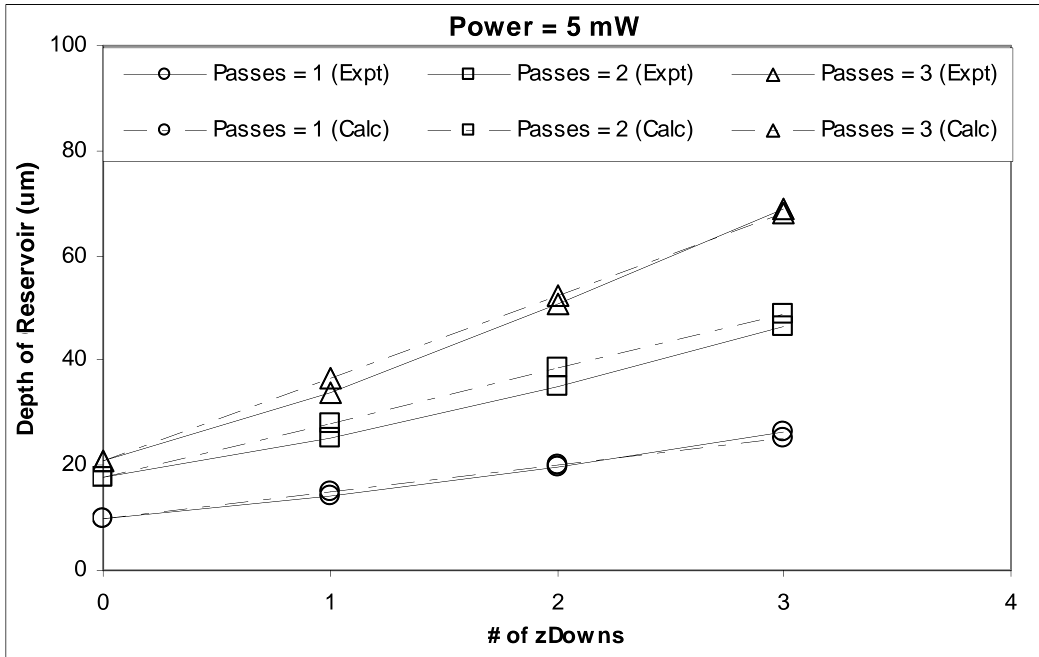

Figure 2.30 Comparisons between measured and calculated depths – 5 mW

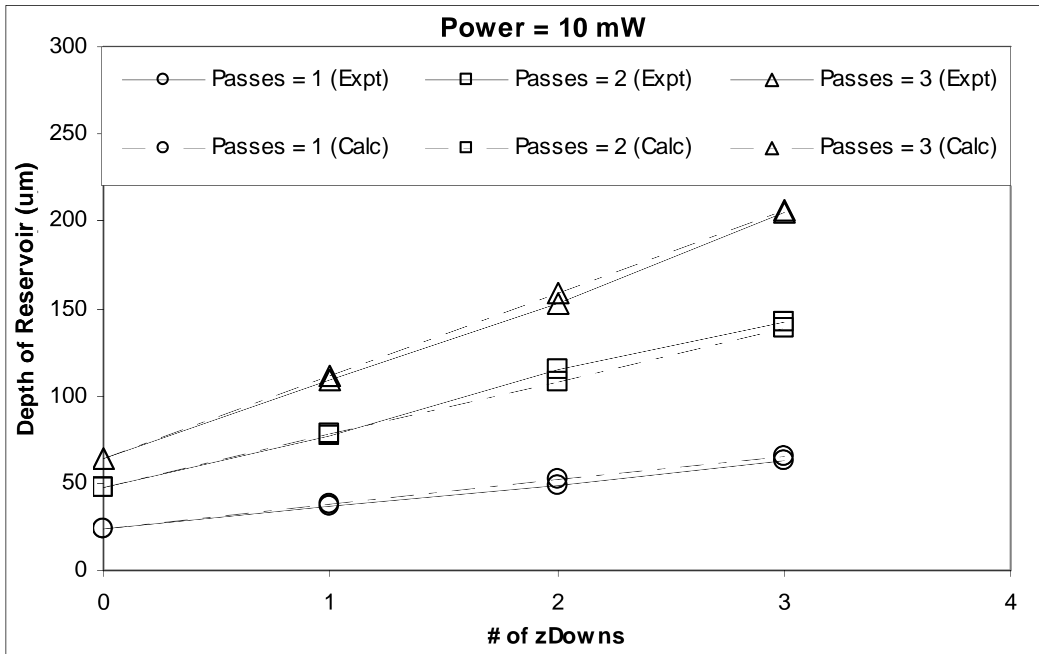

Figure 2.31 Comparisons between measured and calculated depths – 10 mW

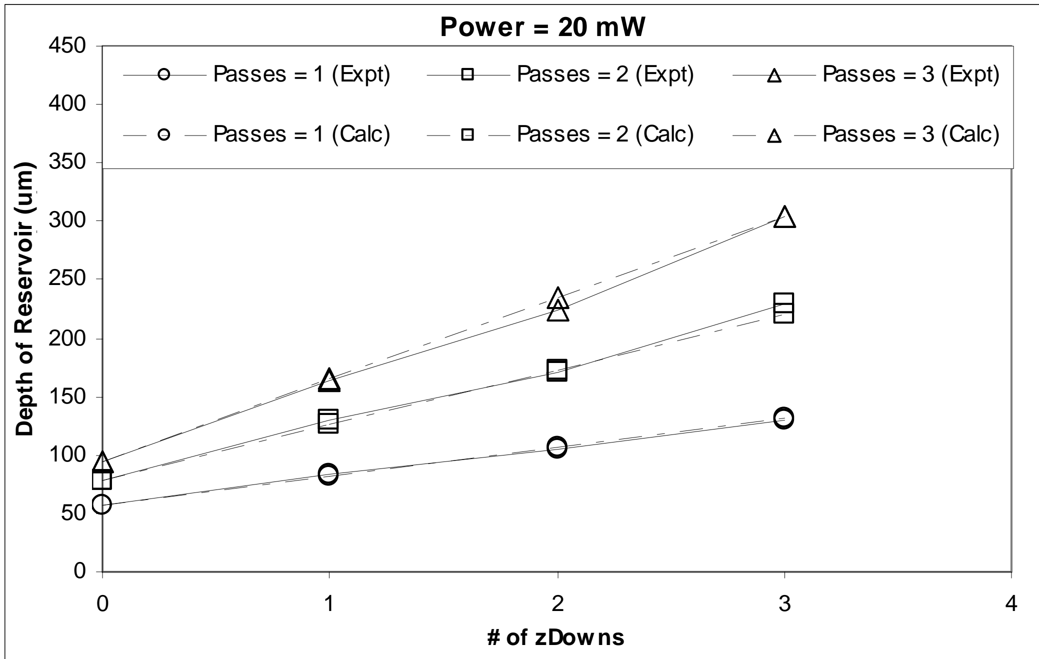

Figure 2.32 Comparisons between measured and calculated depths – 20 mW

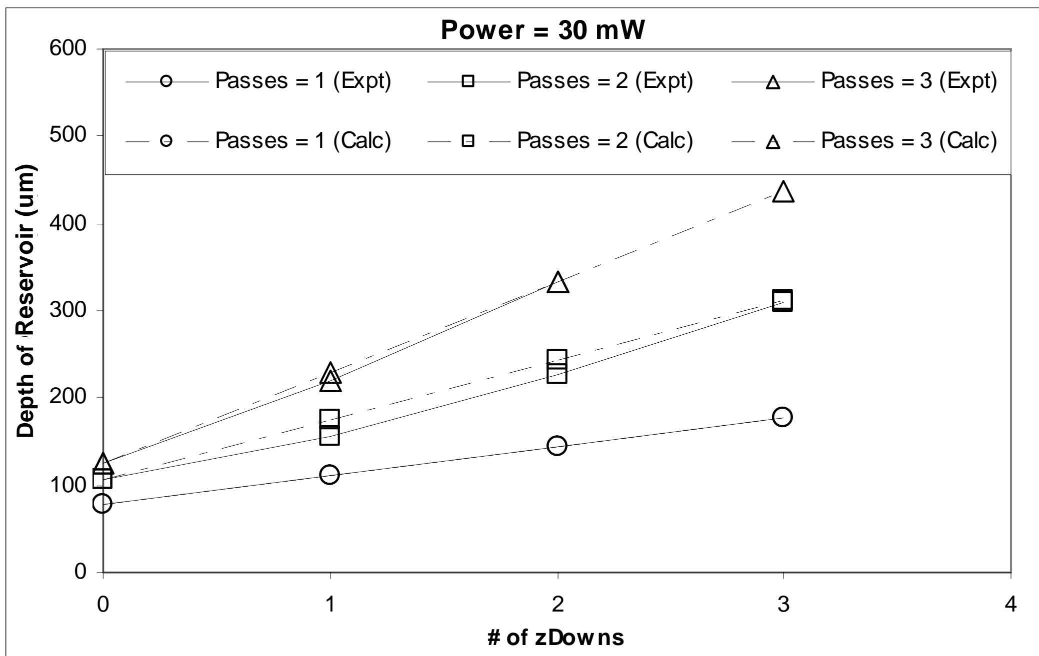

Figure 2.33 Comparisons between measured and calculated depths – 30 mW

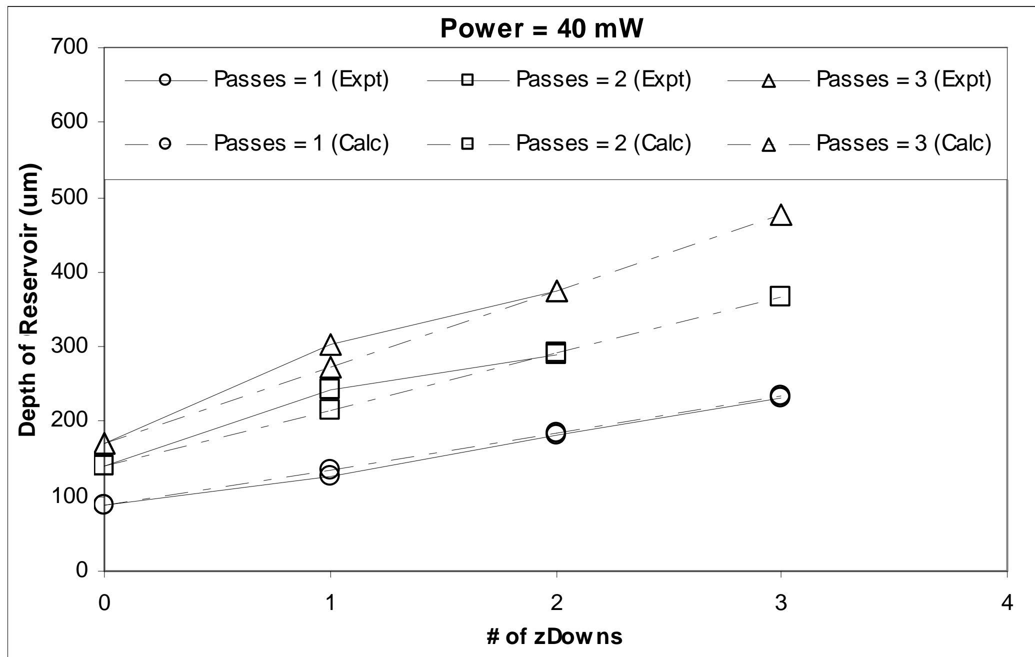

Figure 2.34 Comparisons between measured and calculated depths – 40 mW

Unlike fabrication of channels where the width varies with number of passes and power levels, the diameter of the reservoirs increases by only 5 % as the power is increased. This is attributed to the fact that the diameter of the reservoir is one of the parameters that are used in writing the CNC code for FLM and is a function of the spot diameter of the laser beam. Therefore, no empirical equation for the diameter is evaluated.

2.7.2.2 Application of the Empirical Equation

Similar to the example in section 2.6.1.3 for the channels, this example is included to demonstrate the use of the empirical equations in determining the FLM process parameters (viz. the power level, number of passes and number of Z-downs) given the depth of the reservoir.

Example: Desired h_r = 200 um and diameter = 250 um, find *P*, *n* and *zDowns*.

For a given *P*, the *zDowns* for different *n* can be obtained by the equation

$$zDowns = \frac{h_r - k_3}{k_1 \times n + k_2} = \frac{200 - k_3}{k_1 \times n + k_2}$$

The number of Z-downs (rounded off to the nearest whole number) required for different power levels and passes are shown in table 2.6.

Table 2.6 Value of *zDowns* when h_r = 250

Passes	Power (mW)				
	5	10	20	30	40
1	***38***	***13***	***6***	***4***	2
2	***18***	***5***	3	1	1
3	***11***	3	2	1	0

Since the number of Z-downs should not exceed 3, as reasoned in section 2.6.1.4, the power level and passes combinations in bold italics can be eliminated. For the remaining combinations, it is suggested to use the combination having more number of passes, as in the case of channels, the reservoir walls are straighter with an increase in the number of passes.

Therefore, in the above example, the following four process parameter combinations can be used

- *P* = 10 mW, *n* = 3 and *zDowns* = 3, yielding a depth of 205.93 um
- *P* = 20 mW, *n* = 3 and *zDowns* = 2, yielding a depth of 234.68 um
- *P* = 30 mW, *n* = 3 and *zDowns* = 1, yielding a depth of 228.91 um
- *P* = 40 mW, *n* = 3 and *zDowns* = 0, yielding a depth of 171.33 um

The first combination yields a depth closest to the required depth. Therefore, this combination is chosen for machining. If there are two or more combinations that are found suitable, then it is recommended that the combination with the least power is chosen so that the diameter of the reservoir is closer to the required value. A validation experiment was performed using these parameters and resulted in a reservoir of diameter 250 um and an average depth of 194 um.

2.8 Conclusions

The FLM system was introduced and machining parameters defined. Characterization of FLM focusing on the fabrication channels and reservoirs was performed using a series of experiments. Empirical equations as functions of process parameters were formulated for identifying process parameters to be used given the desired feature dimensions. The procedure for determining of the machining parameters based on the empirical equations was explained for both channels and reservoirs. The developed procedure and empirically derived parameters were employed to identify the process parameters for a channel and a reservoir of given dimensions with good results.

If the feature sizes required are out of the range of sizes for which the empirical equations are derived, then a different size focusing lens needs to be used. Similar characterization experiments need to be performed for any new focusing lens.

Using the empirical equations, features of required dimensions can be fabricated as a microdevice or master mold that can be used for hot embossing. The hot embossing characterization based on molds fabricated using this method is discussed in chapter 3.

CHAPTER 3

HOT EMBOSSING PROCESS CHARACTERIZATION

This chapter starts with providing more detailed discussion on the hot embossing process, its advantages, applications in MEMS fabrication, and available commercial hot embossing systems. The Hot Embossing Microreplication Microfabrication (HEMM) system at UTA, its sub-systems and their importance are introduced. The experimental procedure for identifying process parameters for three different polymers, PC, PMMA and PLLA, using this system is extensively discussed. Finally, the de-embossing procedure of the mold from the polymer substrate and its effect on the polymer substrate and replication quality are also discussed.

3.1 Hot Embossing Process

Microreplication using hot embossing technology is a technique of imprinting or replicating microstructures from a master (mold) onto a polymer substrate. The general steps of a traditional hot embossing process are shown in figure 3.1. The steps to be followed in the replication process are to heat the mold and substrate just above the glass transition (T_g) temperature of the substrate such that the substrate is in a soft viscous state, apply a predefined load to bring the two components together, hold the two components for a predetermined time period while holding the set temperature and load constant, then cool the two components below T_g of the substrate so that it

resolidifies, and finally release the applied load, and then separate the mold and substrate pair, thus obtaining the negative of the mold on the substrate.

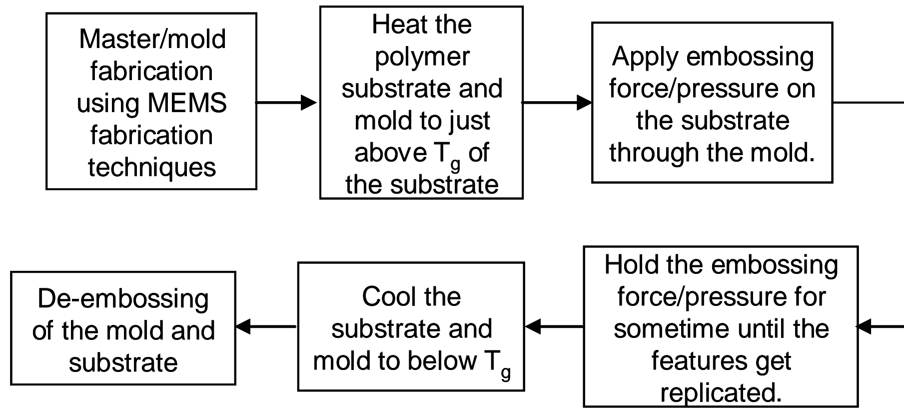

Figure 3.1 Traditional hot embossing microreplication process

The first step of HEMM requires the design and fabrication of the master mold that contains the microstructures to be replicated on the polymer. The techniques normally adopted for master mold fabrication are photolithography, LIGA and laser micromachining. Nickel and silicon are the two common materials used for the mold. The use of silicon micromachined structures as tools for fabrication of polymer microcomponents with hot embossing has several advantages over nickel embossing tools such as good de-embossing properties, no detectable wear and high replication results [26]. The mold quality starts deteriorating after about 50 to 75 embossing cycles depending on the type of mold used and the de-embossing method employed.

The design and fabrication of master mold is followed by the actual embossing process. The embossing process starts with heating of the mold and polymer above a characteristic temperature called glass transition temperature (T_g) of the polymer. The

significance of T_g is that above this particular temperature the polymer behaves as a highly viscoelastic rubbery material, which allows it to flow under pressure and fill the mold cavities thus enabling the replication of the negative of the microstructures present on the mold onto the polymer. This polymer behavior could be understood by analyzing the Young's modulus as a function of temperature as illustrated in figure 3.2 [27]. As shown in the plot, polymers undergo a tremendous loss in Young's modulus at the glass transition region. Therefore, the polymer transitions from being in a solid state to a viscous state where it starts flowing with the application of sufficient amount of pressure.

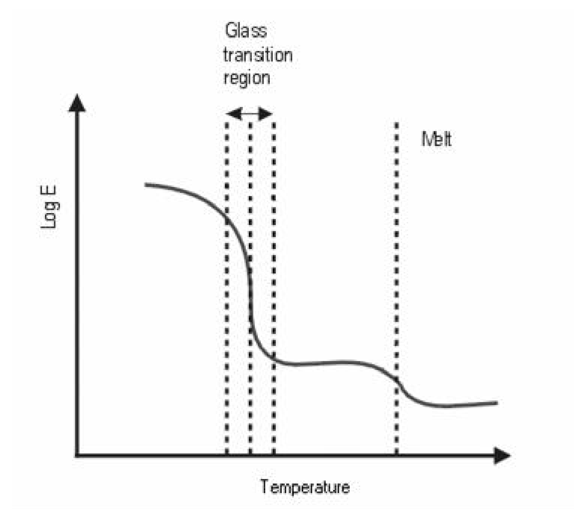

Figure 3.2 Young's modulus variation with temperature

The processing temperature should be kept slightly above T_g in order to minimize the processing time (heating and cooling time) and induced residual stresses [28]. Once the required temperature is reached, a compressive load is applied through the mold on to the viscous polymer. The load is applied until the polymer "fluid" fills

the cavities of the mold and the inverse pattern of mold is fully replicated on the polymer substrate. After the completion of this replication, the mold and polymer assembly is rapidly cooled below T_g to increase the stiffness of the polymer and retain the replicated microstructures. The molding force is maintained during the cooling process until the temperature drops well below T_g in order to prevent the polymer from flowing out of the mold. This is followed by de-embossing or demolding of the mold from the polymer. A representative embossing process temperature cycle is shown in figure 3.3.

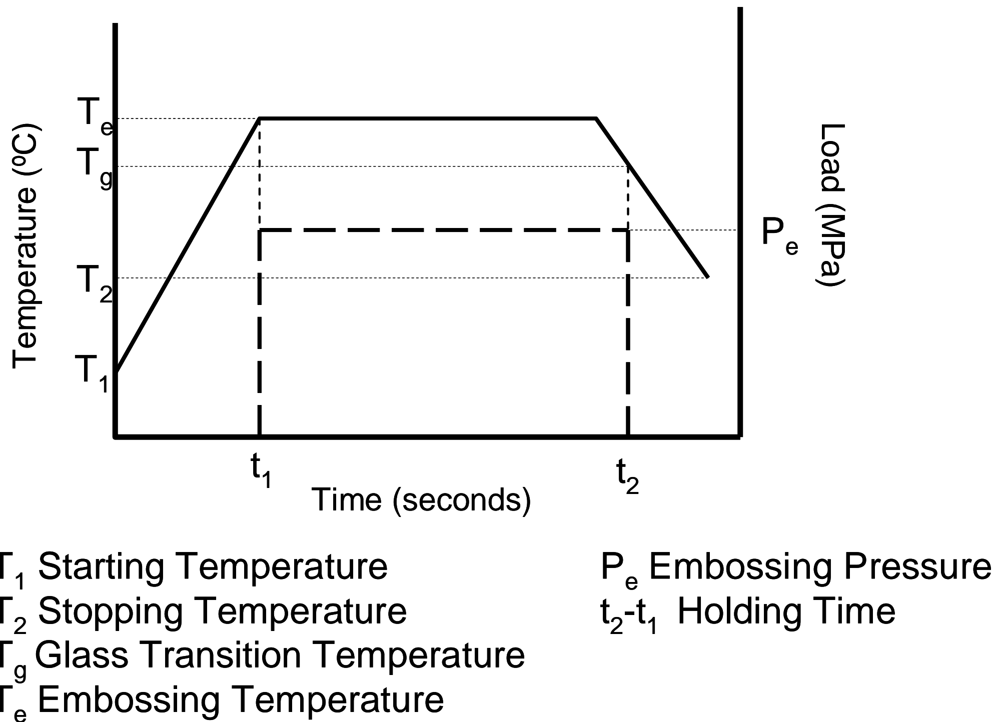

Figure 3.3 Temperature and pressure plot of hot embossing process

The heating of the mold and polymer starts at temperature T_1 which is usually room temperature. Embossing load (P_e) is applied when the polymer reaches embossing

temperature T_e and is held for the holding period $t_2 - t_1$. Cooling of the mold and embossed polymer starts after time t_2 and stops when the temperature reaches T_2, the stopping temperature. The embossing load is held until the temperature drops to just below the glass transition temperature T_g.

Usually, the hot embossing process is performed in vacuum to avoid trapping of moisture in the cavities, and to prevent reaction of polymer with the atmospheric gases at this elevated temperature. The microdevice manufacturing is completed by usually performing certain secondary processes like drilling holes, bonding, metallization, dicing, etc. on the replicated substrate.

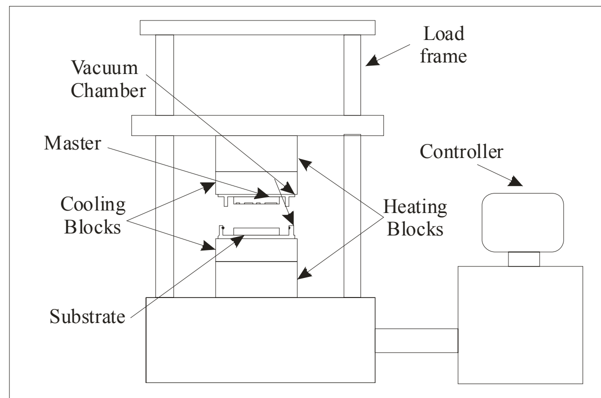

Figure 3.4 Basic schematic representation of hot embossing equipment

3.2 Basic Configuration and Subsystems of HEMM System

The embossing system shown schematically in figure 3.4 consists of top and bottom units which could be operated independently to heat and cool the mold and the polymer substrate separately. These units consist of metal heating and cooling block assemblies with the top unit attached to a moving crosshead of a forcing frame. Such a configuration enables the pressing of master mold against the polymer at an elevated

temperature as per the definition of hot embossing process. There is a controller panel for process monitoring and control.

The various subsystems and their significance in the hot embossing system are mentioned below:

- Heating subsystem: The heating subsystem should be capable of providing the required temperature gradient for both mold and substrate separately in a uniform and rapid fashion, and maintain the desired embossing temperature during the process for the desired amount of holding time.
- Cooling subsystem: A rapid and uniform cooling mechanism is required to quickly reduce the temperature of embossed mold and polymer assembly below the T_g of polymer.
- Forcing subsystem: The required embossing pressure through the mold on the heated polymer is provided and monitored by the forcing subsystem.
- Vacuum subsystem: Contact between the mold and substrate is preferable to take place in vacuum to prevent trapping of moisture in the mold cavities and avoid chemical reactions between the polymer and atmospheric gases.
- Control subsystem: This subsystem monitors and controls the overall hot embossing process.

3.3 Advantages of HEMM

The major advantages of the hot embossing process over other microfabrication techniques discussed in chapter 1 are:

- Cost effectiveness due to simplicity of the process and easy manufacturability

- Time efficiency due to low process cycle time
- Fabrication of features with high aspect ratio on the polymer substrate
- High degree of reproducibility
- Operation on a wide range of polymer substrates

3.4 Applications of HEMM

Hot embossing has been used to fabricate devices mainly for life science applications as certain polymer substrates have proved to be bio-compatible and bio-degradable. Some of the applications include sensors for biological [29] and chemical [30] analysis, actuators [31], microfluidic devices such as microreactors and micromixers [32], DNA separators and concentrators [33, 34], microoptics devices such as waveguides and switches [35], micromirrors [36], photonic pillars [37], micropyramids [38], and electrostatic comb drives [39]. Features fabricated in our laboratory on PMMA are shown in figure 3.5 below.

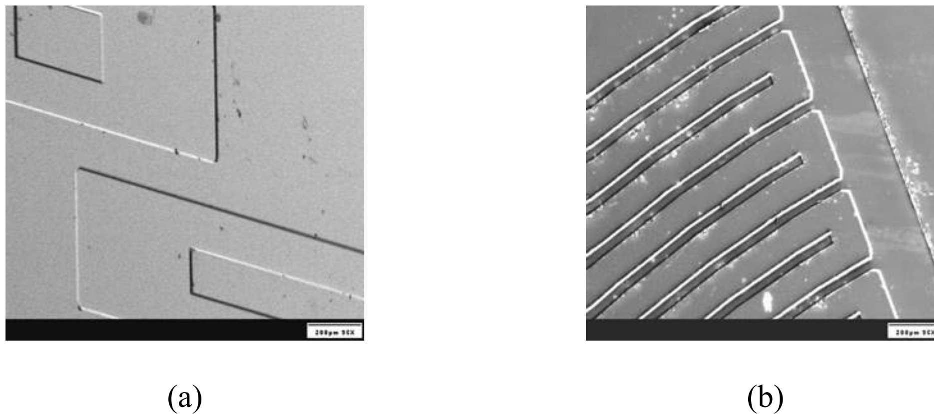

(a) (b)

Figure 3.5 PMMA embossed features
(a) Shallow channels (b) Multi-channel device

3.5 Commercial Hot Embossing Systems

Universities and companies performing research in hot embossing possibly utilize one of the commercially available systems or design their own system. Some of the commercially available hot embossing systems are:

- The hot embossing systems developed by Jenoptik-Mikrotechnik, Germany are used for series production of micro components [40]. The HEX 01 model developed by this company is shown in figure 3.6 (a) [40].

(a)

(b)

(c)

Figure 3.6 Different embossing systems (a) Jenoptik-Mikrotechnik HEX01 (b) EV 520HE (c) Obducat's NIL 4" & 6"

- The hot embossing system developed by EV Group is a semi-automated hot embossing system designed for embossing and nanoimprinting applications [41]. The EVG520HE is shown in figure 3.6 (b) [41].
- Obducat designed and developed nano imprint lithography (NIL) equipment for both laboratory and industrial use and is shown in figure 3.6 (c) [42].

A general comparison of the major design parameters of these hot embossing systems is shown in Table 3.1 [40-42].

Table 3.1 Comparison of design specifications

Process parameters	Jenoptik Mikrotechnik	EV 520HE	Obducat
Substrate size	Ø 6 inches	Ø 8 inches	Ø 6 inches
Loading capacity	< 200 kN	≤ 40 kN	40-80 bar
Heating time	< 7min	6 min	--
Cooling time	< 7min	5 min	--
Temperature gradient	--	120°C	--

3.6 HEMM System at UTA

The HEMM system used for the experiments of this research work was designed and developed in our laboratory and is shown in figure 3.7 [43, 44]. The HEMM system consists of the heating, forcing, cooling, and control subsystems.

The top and bottom heating and cooling assemblies are assembled on a dual column floor mounted frame material testing system from Instron Corporation model 5885 [45]. The substrate and the master/mold are placed one top of one another on the lower plate and then heated. Heating is accomplished though electric heating cartridges located inside the heating blocks. When the desired embossing temperature ($>T_g$) is reached, the compressive embossing force/pressure is applied by the downward motion

of the upper plates. The applied pressure is measured and controlled using a load cell. The applied pressure and temperature are kept uniform for a predetermined amount of time to allow the polymer material to flow and fill the mold cavities. Cooling takes place using a combination system; an oil temperature controller (cools the mold and substrate) and an air cooled chiller (cools the oil).

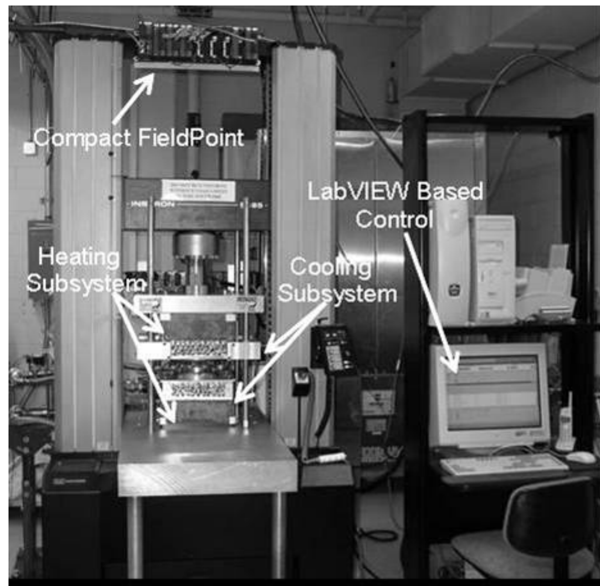

Figure 3.7 HEMM system at UTA

The selected software package for controlling, monitoring and collecting data for the HEMM system is LabVIEW by National Instruments [46]. The control interface developed is shown in figure 3.8. Temperatures at selected locations on the heating plates as well as temperatures of selected heating cartridges are monitored through this interface. It also allows the user to manually turn ON/OFF the heating cartridges and the cooling temperature controller.

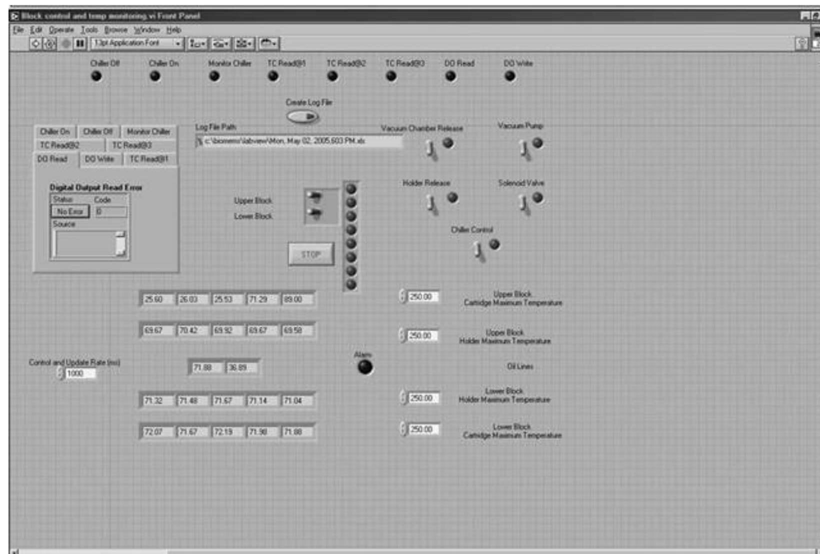

Figure 3.8 HEMM control interface

3.7 Embossing Process Parameters

The three important process parameters to be considered for hot embossing are:

- Embossing temperature: The temperature at which the polymer and substrate are heated up to. Embossing temperature can range from 5 °C to 30 °C above the glass transition temperature of the polymer. Higher embossing temperatures might sometimes reduce the thickness of the substrate which is not desirable.
- Embossing pressure: The pressure applied on the mold and substrate assembly. The usual embossing pressure ranges from 5 MPa to 20 MPa depending on the geometry of the features to be embossed and their depth. Excess embossing pressure might damage the mold.
- Holding time: The time during which the embossing pressure is applied on the mold and substrate at a constant embossing temperature. At an optimum embossing temperature and pressure, the mold and substrate can be held under

pressure for a particular holding time to allow the polymer to fill the cavities of the mold.

The above mentioned factors are highly interdependent of each other. An increase in embossing temperature can reduce the embossing pressure and holding time. An increase in embossing pressure would require lower embossing temperature and holding time. The HEMM process can be characterized by the depth/height of embossing, for a particular polymer substrate, by varying these three factors. Hence, it has been decided to vary these three parameters (factors) and measure the depth of embossing as the response parameter for these factors.

3.8 Embossing Process on the HEMM System

The general LabVIEW control interface shown in figure 3.8 is used in conjunction with another LabVIEW interface shown in figure 3.9 that is used for force control. The inputs for the force control interface include temperature at which the heating cartridges should be turned OFF (ºC), glass transition temperature of the substrate (ºC), embossing temperature (ºC), embossing load (kN), holding time (seconds), and de-embossing temperature (ºC). Experience in running and understanding the response of the heating characteristics and performance of the system are required to define the temperature value for turning OFF the heating cartridges.

The master mold and the polymer substrate are stacked on the lower heating block of the HEMM system as shown in figure 3.10. It has to be kept in mind that the polymer substrate area should be smaller than the mold as the area of the substrate increases when it is heated and subjected to pressure. This assembly is sandwiched

between two silicon wafers whose polished sides face each other. The silicon wafers are used to retain the transparency of the polymer substrate after embossing. The embossing load (kN) is calculated based on the area of the substrate (m^2) and embossing pressure (in MPa) to be used. After the stack is placed on the bottom block, the top block/assembly is moved downwards until it is just above the top silicon wafer. The temperature is raised close to the embossing temperature and the force control interface is activated. As soon as the embossing temperature is reached, the embossing load is applied by the downward motion of the top plate and controlled for the fixed amount of holding time. This load is applied until cooling starts and the temperature falls to below the glass transition of the polymer.

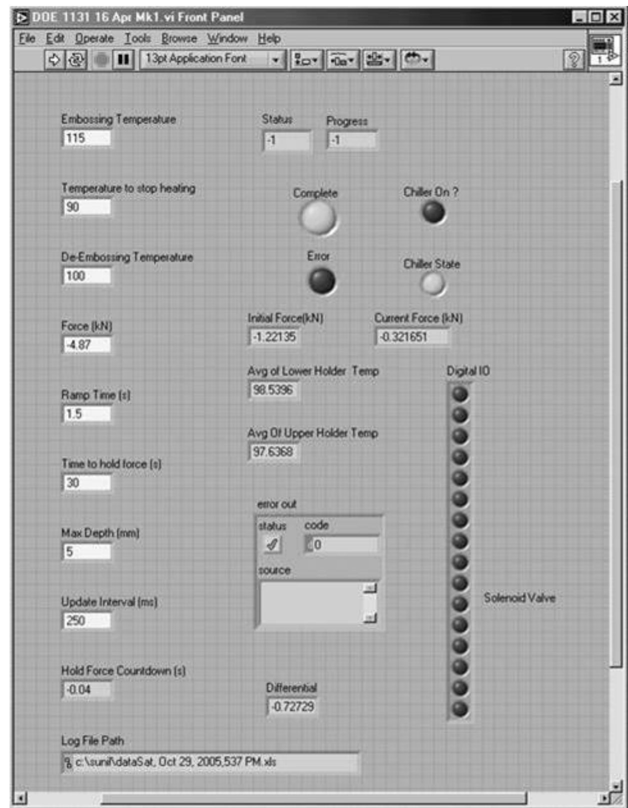

Figure 3.9 Force control LabVIEW interface

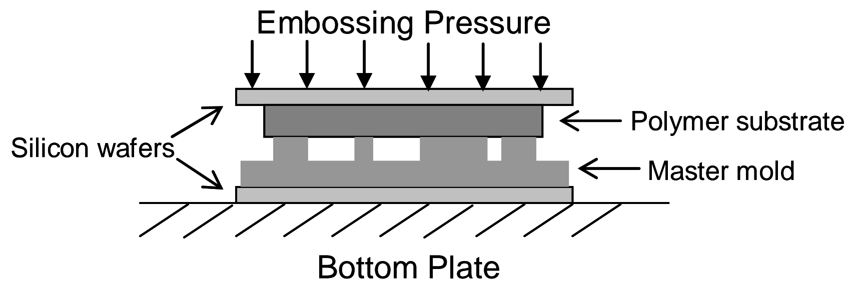

Figure 3.10 Setup of mold and substrate on the HEMM system

A characteristic temperature and load time history plot obtained from the HEMM system is shown in figure 3.11. The embossing temperature is 125 ºC, the embossing force is 5 kN and the holding time is 120 seconds. The embossing force is negative since this is a compressive load. The temperature remains almost constant at approximately 125 ºC (+2 ºC) through the holding period of 120 seconds.

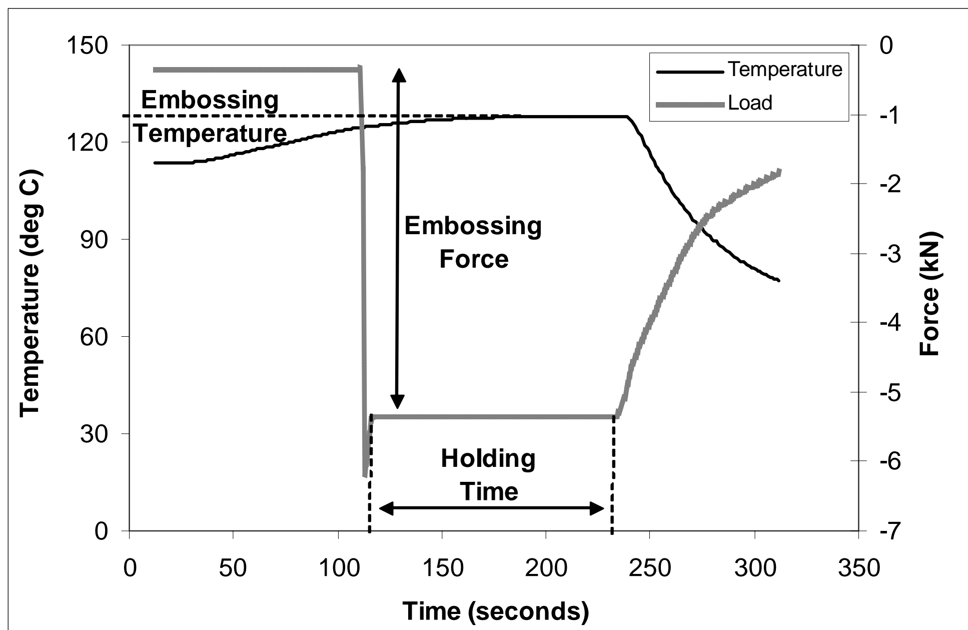

Figure 3.11 Representative temperature and pressure plot

The temperature and force profiles shown here are representative for all the embossing cycles and therefore, these plots will not be repeated for other embossing experiments mentioned in this manuscript.

3.9 De-embossing System

After the embossing cycle is completed, the mold and the substrate are separated using a process called de-embossing. This process, although not given the attention it deserves, is very important to the embossing process. In some embossing equipment, like the one from Jenoptic in figure 3.6, the mold and the substrate are held using vacuum clamps, which automatically separate each other when the top surface moves upwards after embossing. But in most cases, in the absence of a clamping system, the mold and the substrate "stick" to each other and have to be separated by peeling off the substrate from the mold leading to damaging the mold and the features on the substrate. This is due to non-uniform force exerted on the substrate and was experimentally found that damage occurs when the aspect ratio becomes greater than 0.5. In some cases, if the embossing aspect ratio is very low (< 0.5), there is easy separation. It was therefore, decided to design and fabricate a de-embossing system, as shown in figure 3.12.

The de-embossing system consists of two vacuum chucks – top and bottom. The top chuck can be moved manually using a gear system as shown. The system is designed in such a way, that the two chucks always remain parallel to each other through guide rods. The mold and the substrate are placed on the bottom vacuum chuck while the top chuck is brought down manually by turning the gears until it touches the stack. The mold and the substrate are then subjected to vacuum pressure of 20" of Hg

(508 torr) that can be monitored with the gauge attached to the vacuum pump. When the required vacuum pressure is reached, the top plate is moved upwards ensuring that the mold and the substrate are separated without damage to the features on either one.

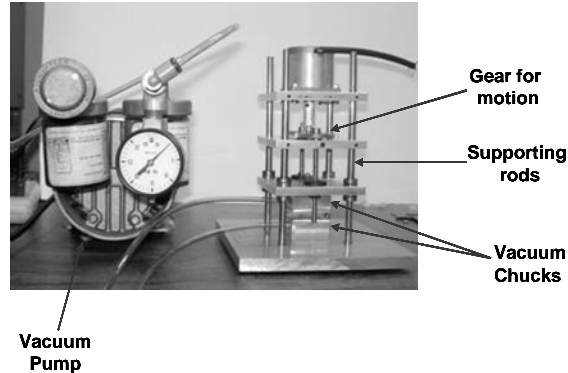

Figure 3.12 De-embossing system

3.10 Feature Measurements

The features on the mold and substrate are measured using the same procedure and equipment as discussed in section 2.4.

3.11 Polymer Characterization

The primary reason for characterizing the HEMM process for these polymers is to estimate operating parameters for embossing given as a function of the maximum feature depth on the mold and the polymer substrate on which embossing takes place. If the maximum depth of the mold and type of polymer substrate is known, the characterization plots can be consulted to estimate the three embossing parameters.

Experiments were performed on three polymers Poly Methyl Meth Acrylate (PMMA), Poly Carbonate (PC) and Poly L-Lactic Acid (PLLA). The glass transition and melting temperatures of these polymers are given in table 3.2. PMMA is the most

commonly used polymer as a substrate for microfluidic applications. PC as a substrate can also be used for microfluidic applications, but in this research work it is aimed to use PC as a secondary mold, more of which will be discussed later in chapter 4. PLLA is a biodegradable polymer that can be used for applications requiring biodegradation such as drug delivery. More about PLLA is discussed in chapter 5. Preliminary experiments were performed on all three polymers to identify the different factor levels that will be used in the characterization experiments i.e. values of these process parameters – embossing temperature, embossing pressure and holding time.

Table 3.2 Properties of polymers used for characterization

Polymer used	Glass transition temp T_g (°C)	Melting temp T_m (°C)
PC	145	250
PMMA	106	157
PLLA	75	173

The master mold for these experiments was fabricated on a silicon wafer using the Femtosecond Laser Micromachining (FLM) system. A schematic of the mold is shown in figure 3.13. The mold has 36 reservoirs arranged in a 6 by 6 matrix. There are three different nominal depths arranged on three sets of rows. These three sets of rows are fabricated with a power of 40 mW and have a nominal diameter of about 250 um. The other FLM machining parameters were identified using the empirical equations in chapter 2 and are as follows:

- Row 1 – 1 pass and 0 Z-Down, *zDist* = 23 um
- Row 2 – 2 passes and 1 Z-Down, *zDist* = 54 um
- Row 3 – 3 passes and 1 Z-Downs, *zDist* = 78 um

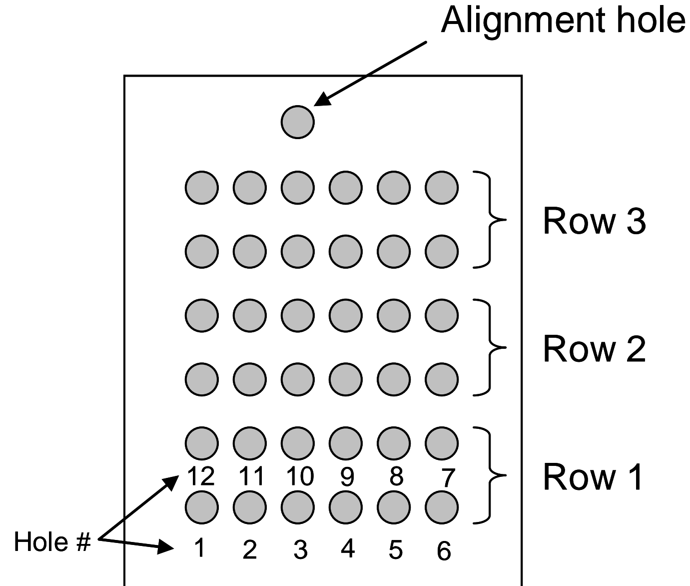

Figure 3.13 Mold used for characterization experiments

An identifier hole is also fabricated so that the reservoir # can be easily identified under the microscope. Reservoirs were chosen for the characterization experiments because they are usually deeper than channels as discussed in chapter 2.

3.12 Experimental Results and Discussion

The reservoirs on the silicon mold are embossed to fabricate pillars on the polymer substrate. The depths of three reservoirs on the mold and the corresponding pillars on the substrate are measured for each row and their average values are used for analysis.

3.12.1 Poly Carbonate (PC)

Experiments were conducted on PC substrates for the following process parameters/factors:

- Embossing temperature – 155 °C, 165 °C, 175 °C

- Embossing pressure – 14 MPa, 19 MPa
- Holding time – 30 seconds, 90 seconds

The results can be analyzed by using two different types of plots – the embossing pillar heights as a function of the temperature as shown in figures 3.14 to 3.16, and characteristic plots obtained by plotting the embossing heights as a function of different rows as shown in figures 3.17 and 3.18. The measured height values of these pillars are given in appendix E.

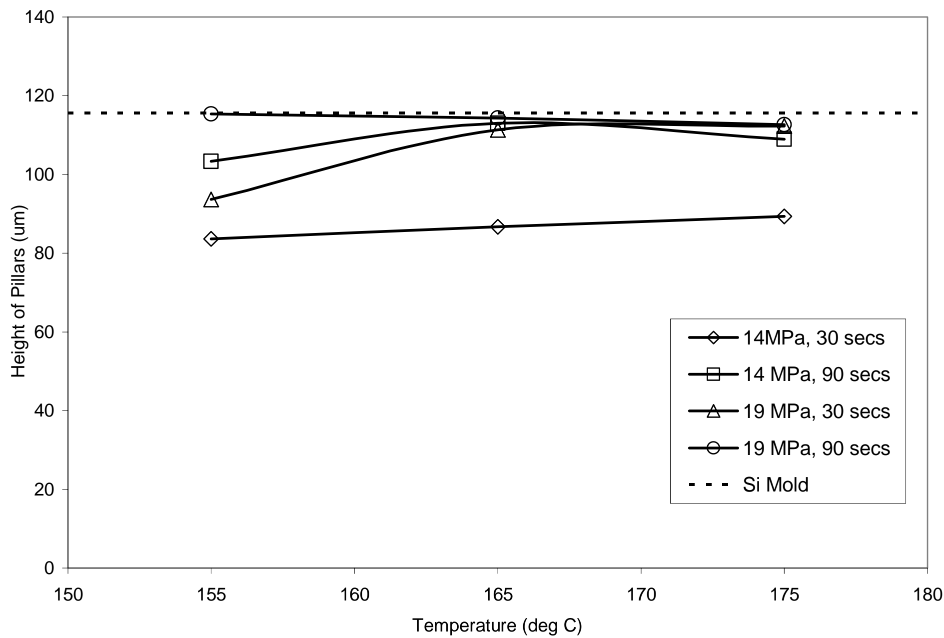

Figure 3.14 Embossing results on PC (function of temperatures) – Row 1

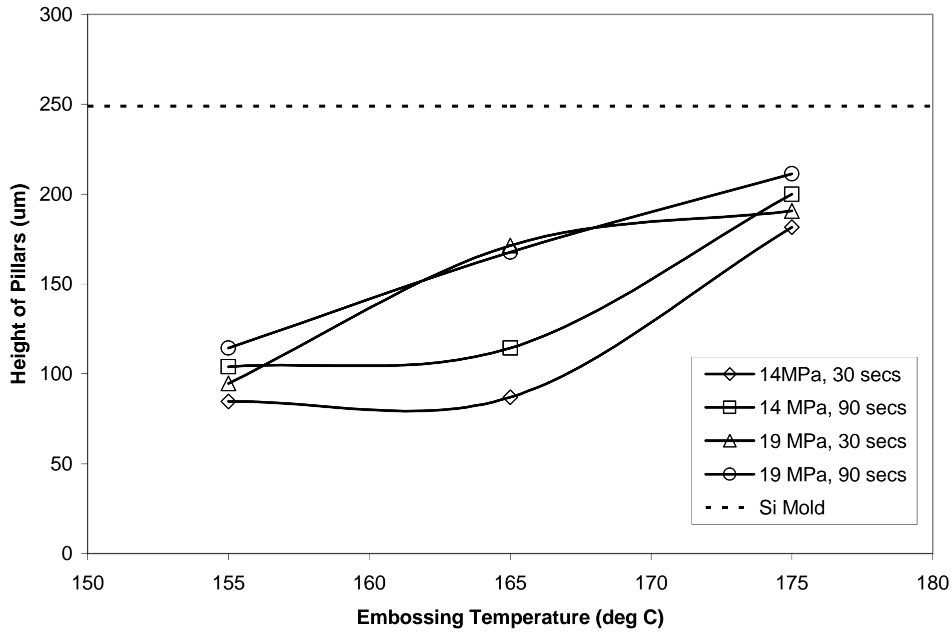

Figure 3.15 Embossing results on PC (function of temperatures) – Row 2

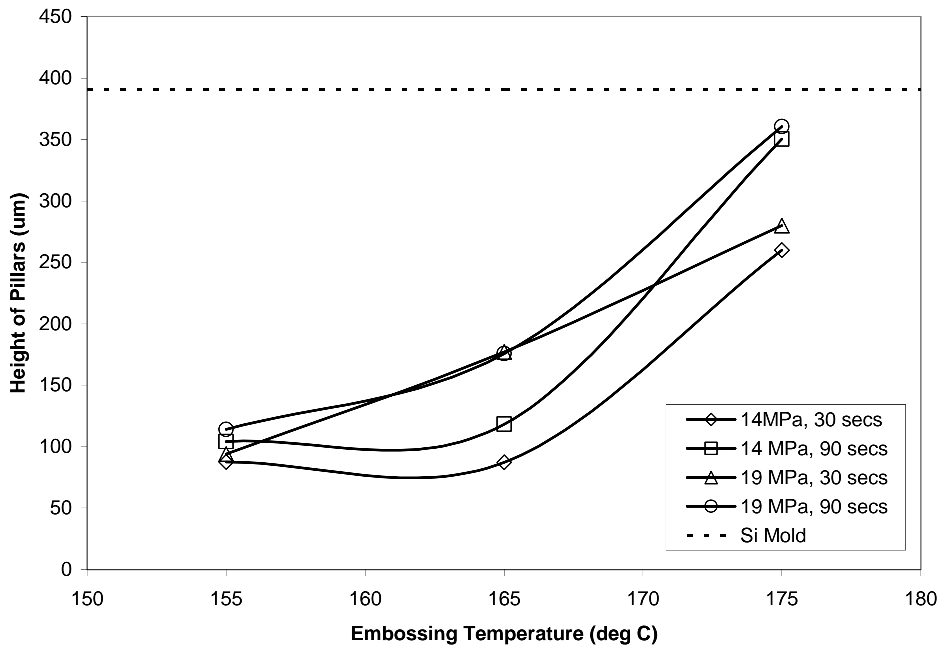

Figure 3.16 Embossing results on PC (function of temperatures) – Row 3

Row 1 completely fills up at a higher pressure (19 MPa) and higher holding time (90 seconds) even at the lowest embossing temperature used (155 °C). At temperatures greater than 165 °C, complete replication is observed even at the lower pressure (14 MPa) when the holding time is 90 seconds. In contrast, rows 2 and 3 are not filled at the higher pressure and higher holding time even at 175 °C.

The plots in figures 3.15 and 3.16 also show that better embossing is achieved through a 90 seconds holding time at the lower pressure than for a holding time of 30 seconds at the higher pressure. This is observed above 165 °C when the polymer is less viscous and flows more freely. This analysis indicates that, at higher temperatures, the holding time affects the flow of the polymer more than an increase in embossing pressure.

The characteristic plots in figure 3.17 and 3.18 are used for determining the process parameters given the maximum depth of the mold. For example, if the maximum depth of the features on the mold is 175 um, if PC is the polymer substrate used for embossing, then referring the figures, we can deduce that a process parameter combination of 165 °C, 19 MPa and 90 seconds can be used. If the maximum depth of the mold is 250 um, the process parameter combination of 175 °C, 14 MPa and 30 seconds can be used.

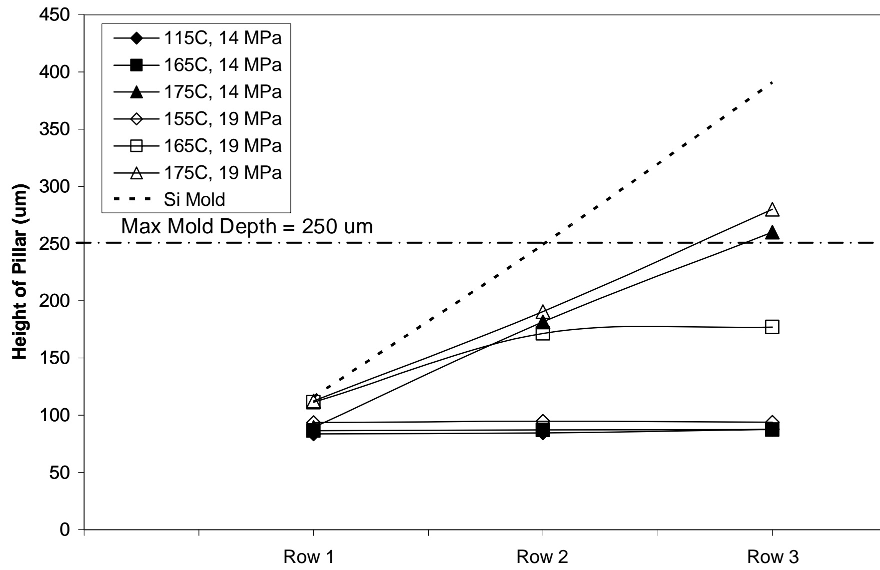

Figure 3.17 Embossing characteristic plots for PC (function of rows)
Holding time = 30 seconds

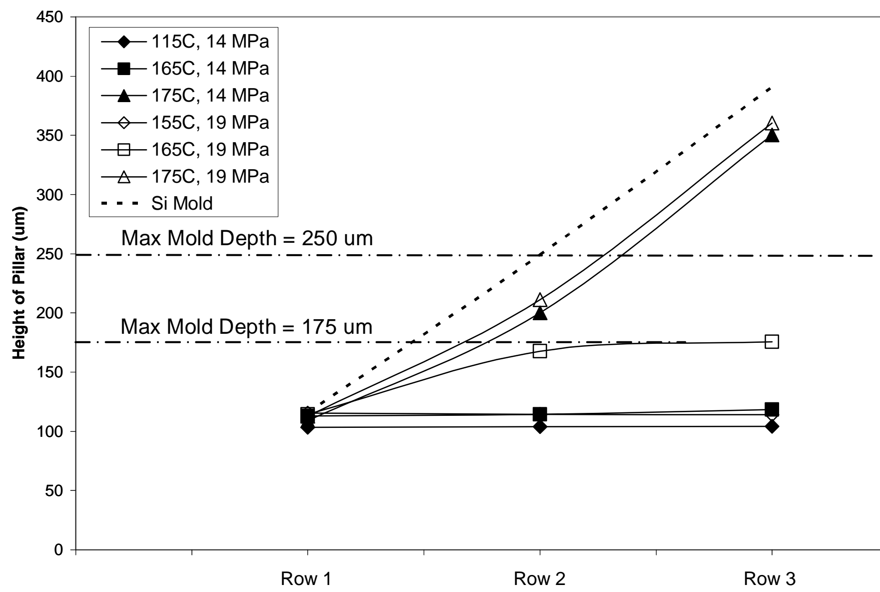

Figure 3.18 Embossing characteristic plots for PC (function of rows)
Holding time = 90 seconds

3.12.2 Poly Methyl Meth Acrylate (PMMA)

Experiments were conducted on PMMA substrates for the following parameters/factors:

- Embossing temperature – 115 °C, 120 °C, 125 °C
- Embossing pressure – 14 MPa, 19 MPa
- Holding time – 30 seconds, 90 seconds

The embossing results i.e. the measured values of height of these pillars are given in appendix E and are plotted in figures 3.19 to 3.23.

Row 1 replicates almost completely when it is held for 90 seconds even at lower pressure (14MPa). The difference between the embossed height and the mold depth is no more than 3 um and is thus attributed to measurement errors. There is complete replication of row 2 for 30 seconds holding time at the higher pressure and 125 °C, whereas complete replication is observed at 120 °C when the holding time is 90 seconds.

Similar to the behavior observed in PC, at temperatures greater than 120 °C, better embossing is achieved through a holding time of 90 seconds at lower pressure than for a time of 30 seconds at higher pressure.

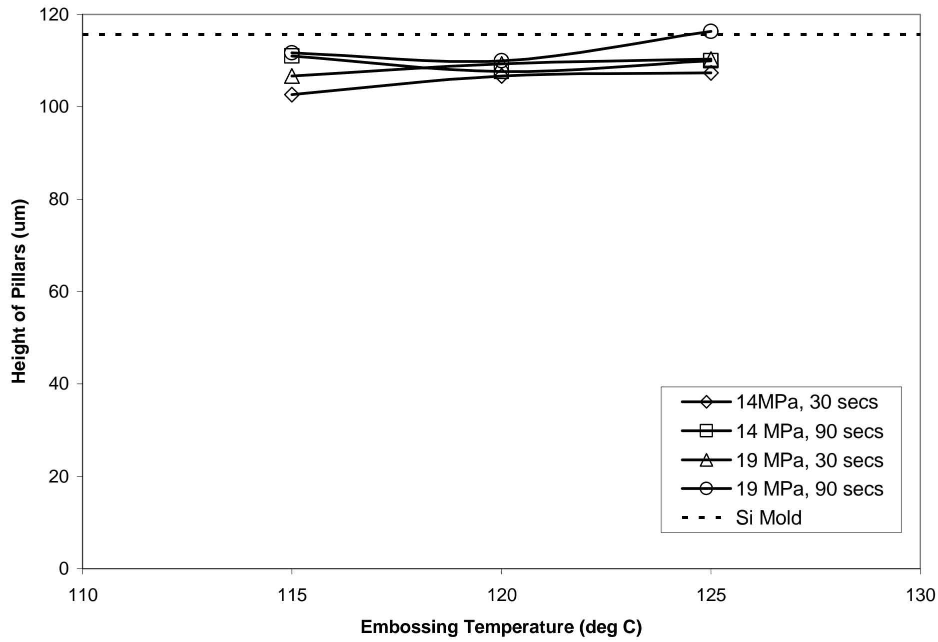

Figure 3.19 Embossing results on PMMA (function of temperatures) – Row 1

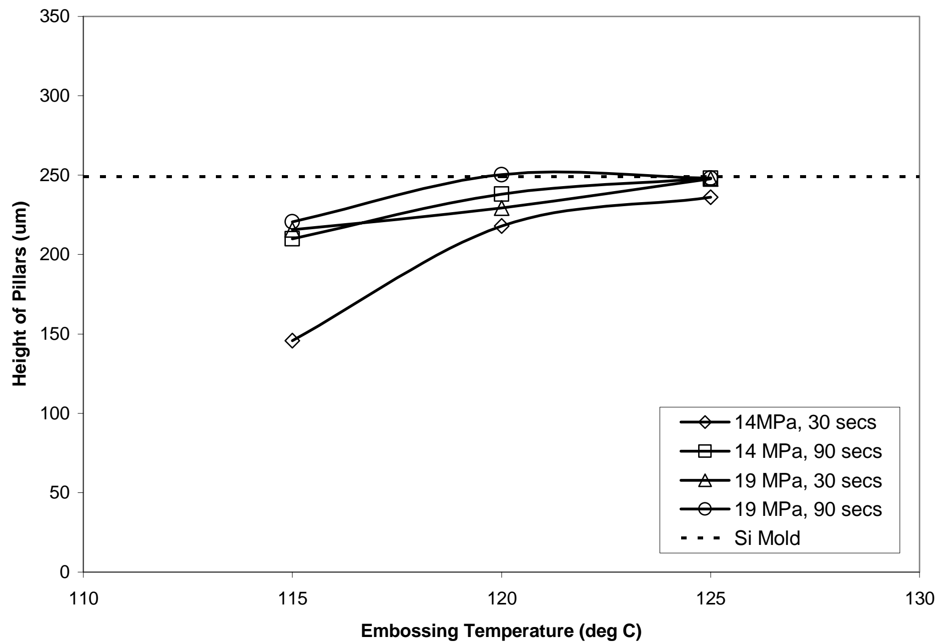

Figure 3.20 Embossing results on PMMA (function of temperatures) – Row 2

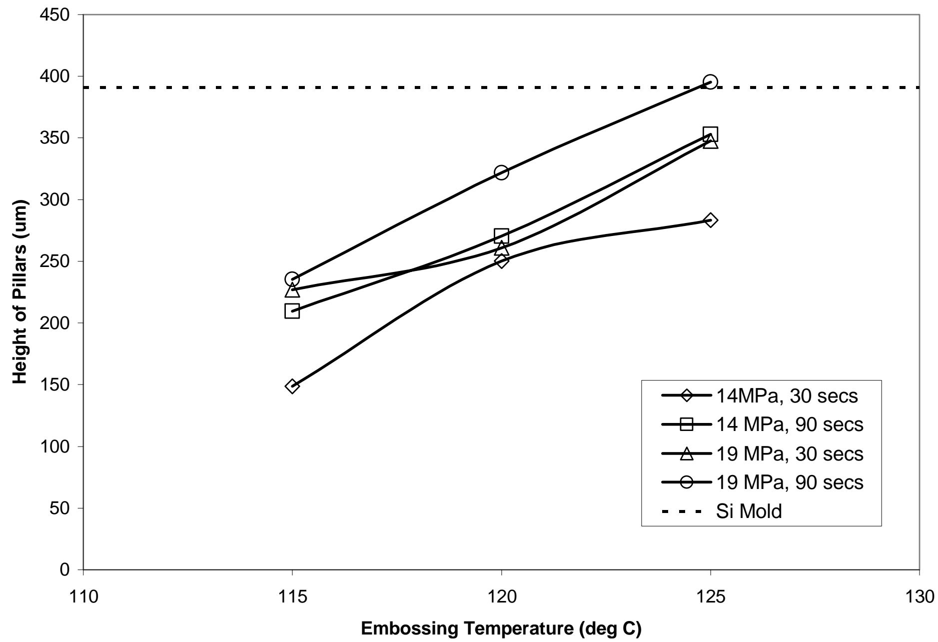

Figure 3.21 Embossing results on PMMA (function of temperatures) – Row 3

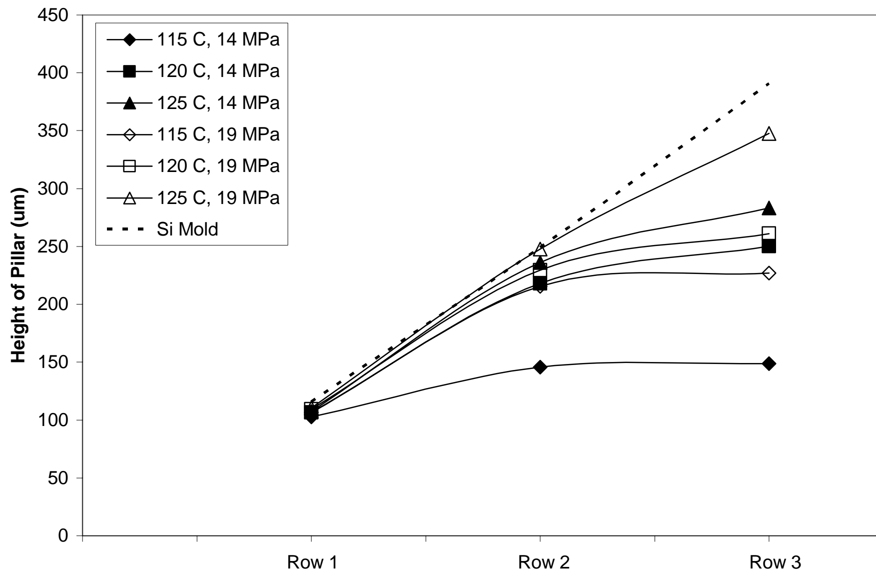

Figure 3.22 Embossing characteristic plots for PMMA (function of rows)
Holding time = 30 seconds

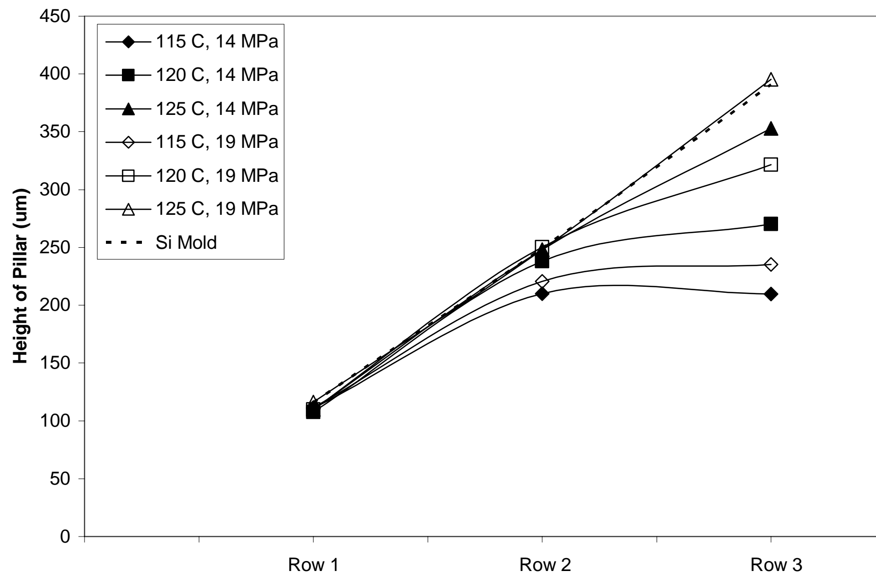

Figure 3.23 Embossing characteristic plots for PMMA (function of rows)
Holding time = 90 seconds

As explained for PC, the characteristic plots in figures 3.22 and 3.23 could be used for process parameters identification based on the deepest feature to be replicated on the PMMA substrate.

3.12.3 Poly L-Lactic Acid (PLLA)

Experiments were conducted on PLLA substrates for the following parameters/factors with the results plotted in figures 3.24 to 3.28. The measured values of height of these pillars are given in appendix E.

- Embossing temperature – 80 °C, 85 °C, 90 °C
- Embossing pressure – 14 MPa, 19 MPa
- Holding time – 30 seconds, 90 seconds

Row 1 is fully replicated at 85 °C and at higher pressure for 30 seconds holding time. At 90 °C, row 1 gets filled even at lower pressures when held for 90 seconds. Similar to PC, rows 2 and 3 are not completely replicated.

But in contrast to PC and PMMA, there is better embossing at higher pressure (19 MPa) and lower holding time (30 seconds) as compared to lower pressure (14 MPa) and higher holding time (90 seconds) at all temperatures. The reason for this behavior is explained in the section 3.13 that discusses the flow behavior as a function of normalized embossing temperatures.

As discussed for PC and PMMA, by means of characteristic plots in figures 3.27 and 3.28, determination of embossing parameters for PLLA is possible if the deepest feature of the mold is known.

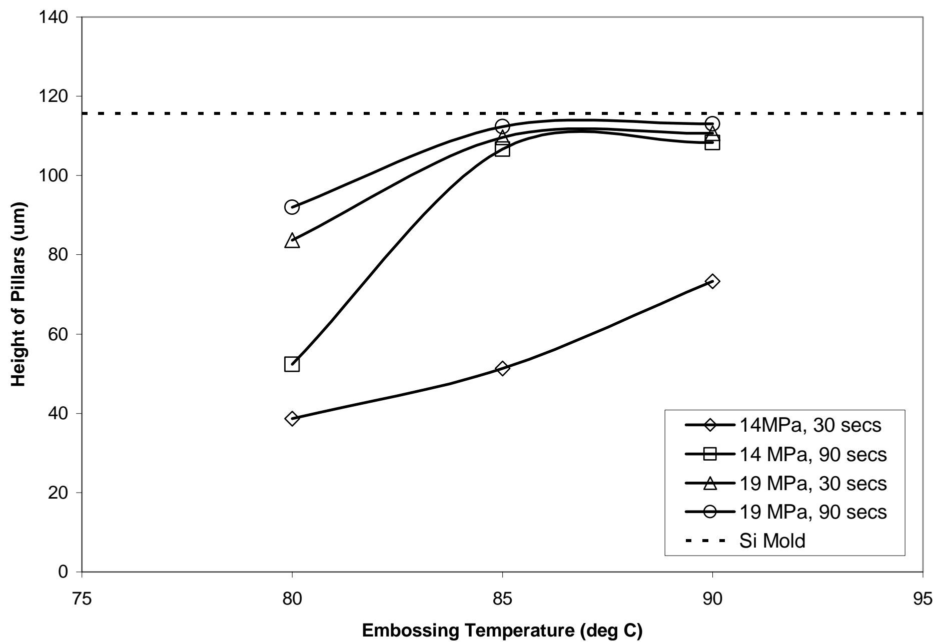

Figure 3.24 Embossing results on PLLA (function of temperatures) – Row 1

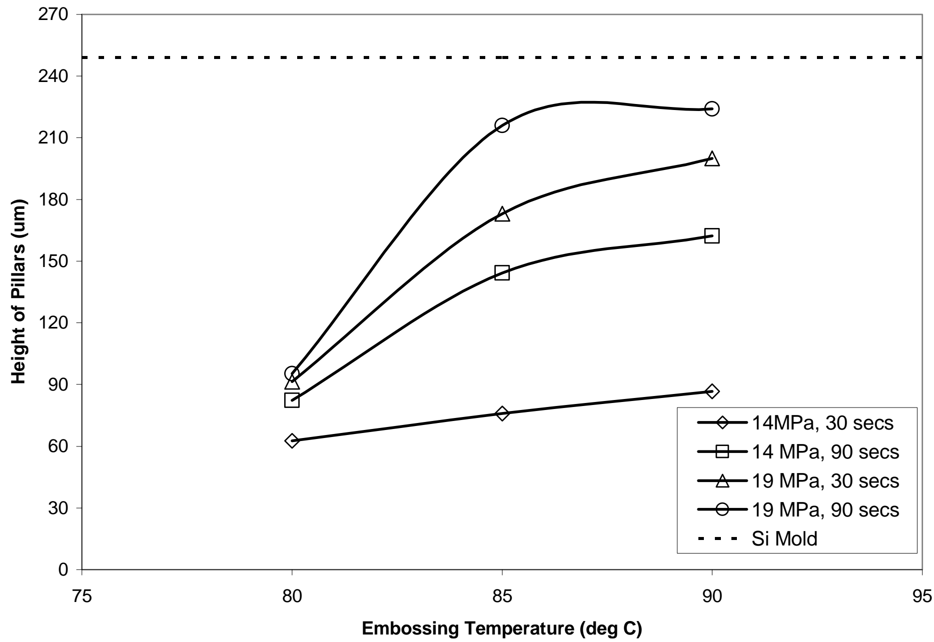

Figure 3.25 Embossing results on PLLA (function of temperatures) – Row 2

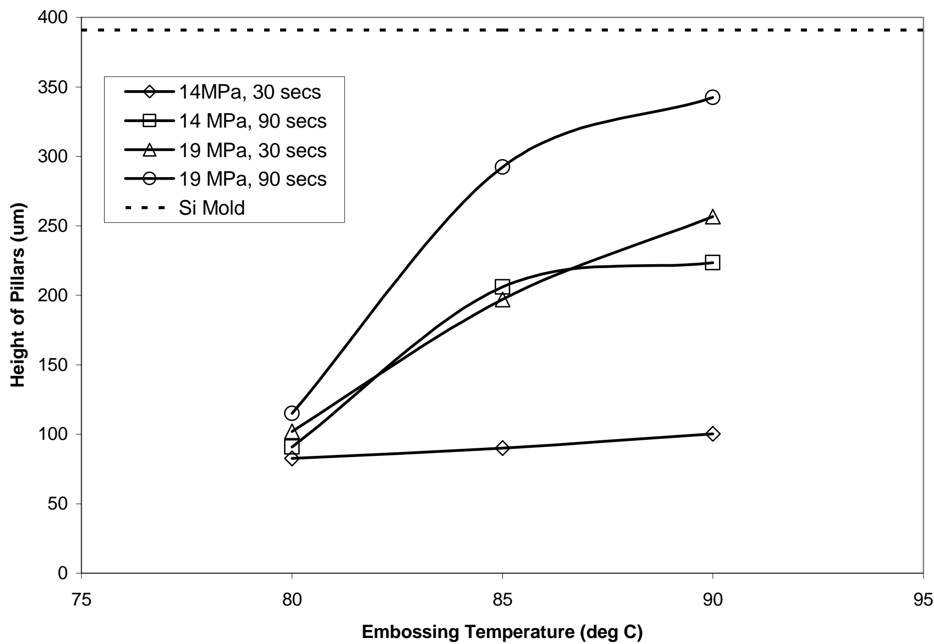

Figure 3.26 Embossing results on PLLA (function of temperatures) – Row 3

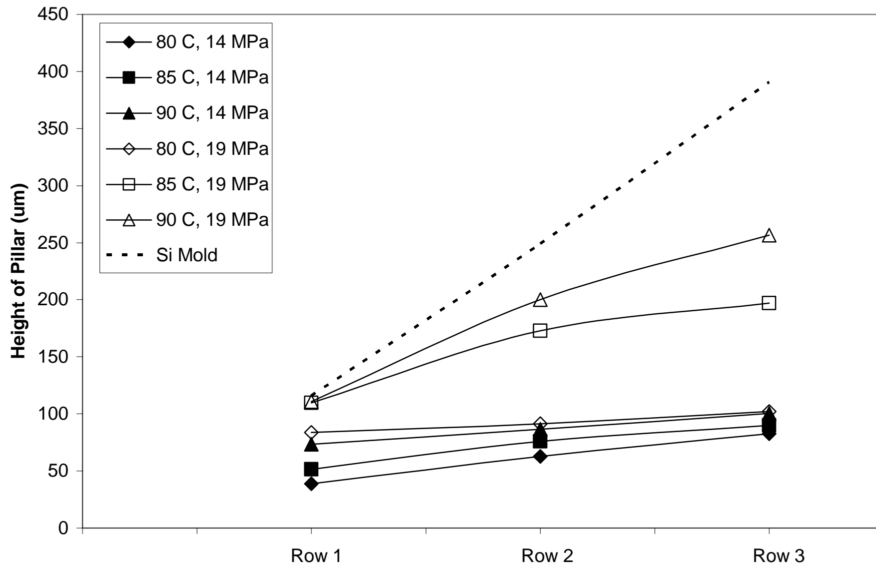

Figure 3.27 Embossing characteristic plots for PLLA (function of rows)
Holding time = 30 seconds

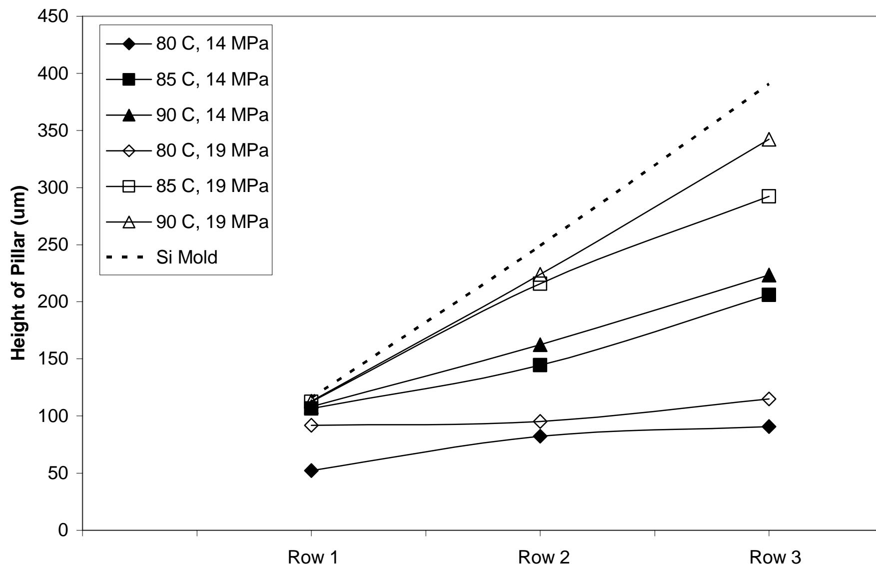

Figure 3.28 Embossing characteristic plots for PLLA (function of rows)
Holding time = 90 seconds

3.13 Normalization of Embossing Temperatures

The three polymers selected in this study have different glass transition and melting temperatures leading to different embossing temperatures. Normalization of embossing temperatures is performed to assess the HEMM process performance as a function of a normalized quantity that considers the glass transition, melting and embossing temperatures of a polymer. The performance comparison considers the flow rate or height of embossing for a given applied pressure and holding time. The temperature normalization equation is

$$\%\Delta T_i = \frac{(T_e - T_g)}{(T_m - T_g)} \times 100$$

where T_e is the embossing temperature, T_g is glass transition temperature, T_m is the melting temperature, all in °C, and ΔT_i is the % normalized temperature. ΔT_i has a scale of 0 to 100 where $\Delta T_i = 0$ at T_g and $\Delta T_i = 100$ at T_m.

The embossing results presented in section 3.12 are also used to discuss the flow behavior of the three polymers for similar embossing parameters with respect to their normalized embossing temperatures as shown in figures 3.29 and 3.30.

Summarizing the observations from section 3.12, at the lower embossing temperatures of PC and PMMA, better embossing was achieved by increasing the embossing pressure than by increasing the holding time, while at the higher embossing temperatures better embossing was achieved by increasing the holding time than by increasing the embossing pressure. The behavior of PLLA at all embossing temperatures is consistent with the lower embossing temperature behavior of PC and

PMMA. For all embossing temperatures of PLLA, better embossing was achieved by an increase in embossing pressure than by increasing the holding time. This can be explained by referring to figures 3.29 and 3.30, where PLLA has lower normalized temperatures than PC or PMMA. Therefore, it can be concluded that at low normalized temperatures the embossing pressure is a dominant parameter that dictates the embossing height while at high normalized temperature (more than 25%) the holding time becomes an dominant parameter.

After scaling the embossing temperatures, it is observed that the only relatively common range of normalized temperature at which a comparison can be made for all the three polymers is around 16% of ΔT_i. At 16% ΔT_i, referring to Row 2 results plotted in figure 3.29 (a), at low holding time and pressure, PMMA has the best embossing height, whereas PLLA and PC have the same embossing heights. At low pressures (figure 3.29 (a) and (b)), when the holding time increases, the flow rate of PLLA is better than PMMA even though PMMA has a higher embossing height. For all pressures, when the holding time is increased, the PC flow rate change is almost negligible. At high pressures, PMMA tends to approach the Si mold depth, therefore a comparison between the behavior of the three polymers at high pressures can be made by referring to figure 3.30 that presents results for Row 3 that is not completely filled even at 28% ΔT_i.

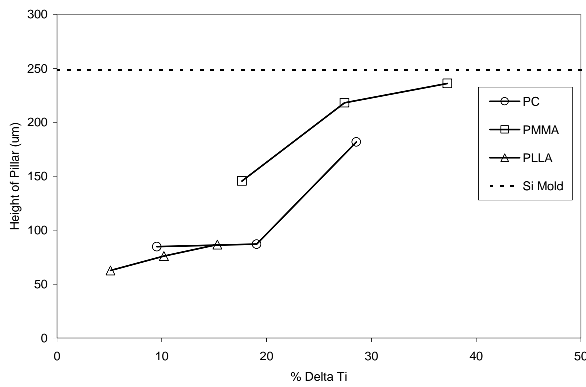

(a)

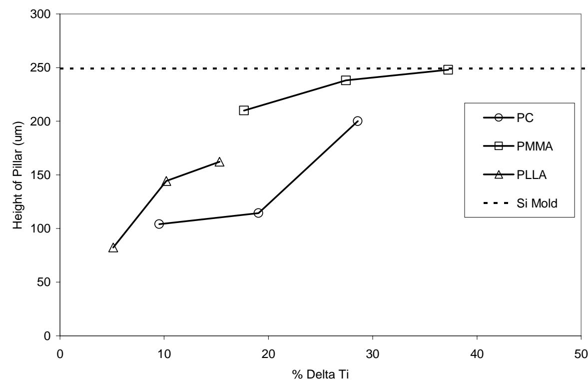

(b)

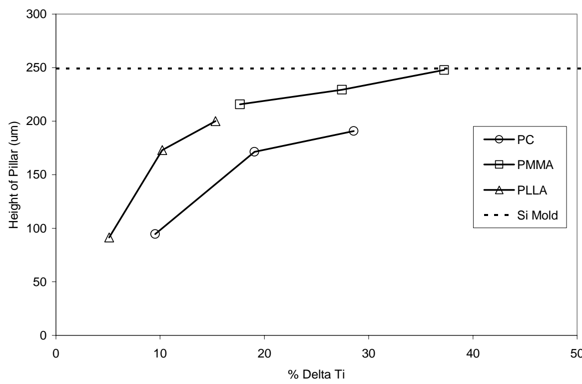

(c)

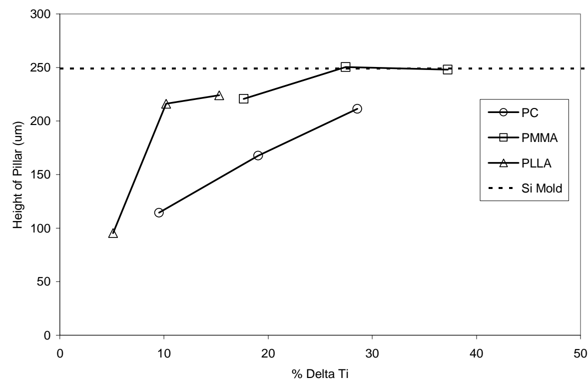

(d)

Figure 3.29 Comparison of behavior of the three polymers – Row 2
(a) 14 MPa, 30 secs (b) 14 MPa, 90 secs
(c) 19 MPa, 30 secs (d) 19 MPa, 90 secs

The flow behavior for Row 3 (figures 3.30(a) and (b)) at 16% ΔT_i also follows the same trend as that of Row 2. At lower pressures, the flow rate change of PLLA is better than that of PMMA while comparing the two holding times. At all pressures, it is observed that an increase in the holding time produces an insignificant change in the flow rate for PC. At higher ΔT_i values, only PMMA and PC can be compared. For

example, at 28% ΔT_i, PC and PMMA have the same embossing heights at the lower holding time. When the holding time is increased, the flow rate change of PC is better than that of PMMA for all pressures. This is attributed to the fact that PC flows more freely at higher normalized temperatures.

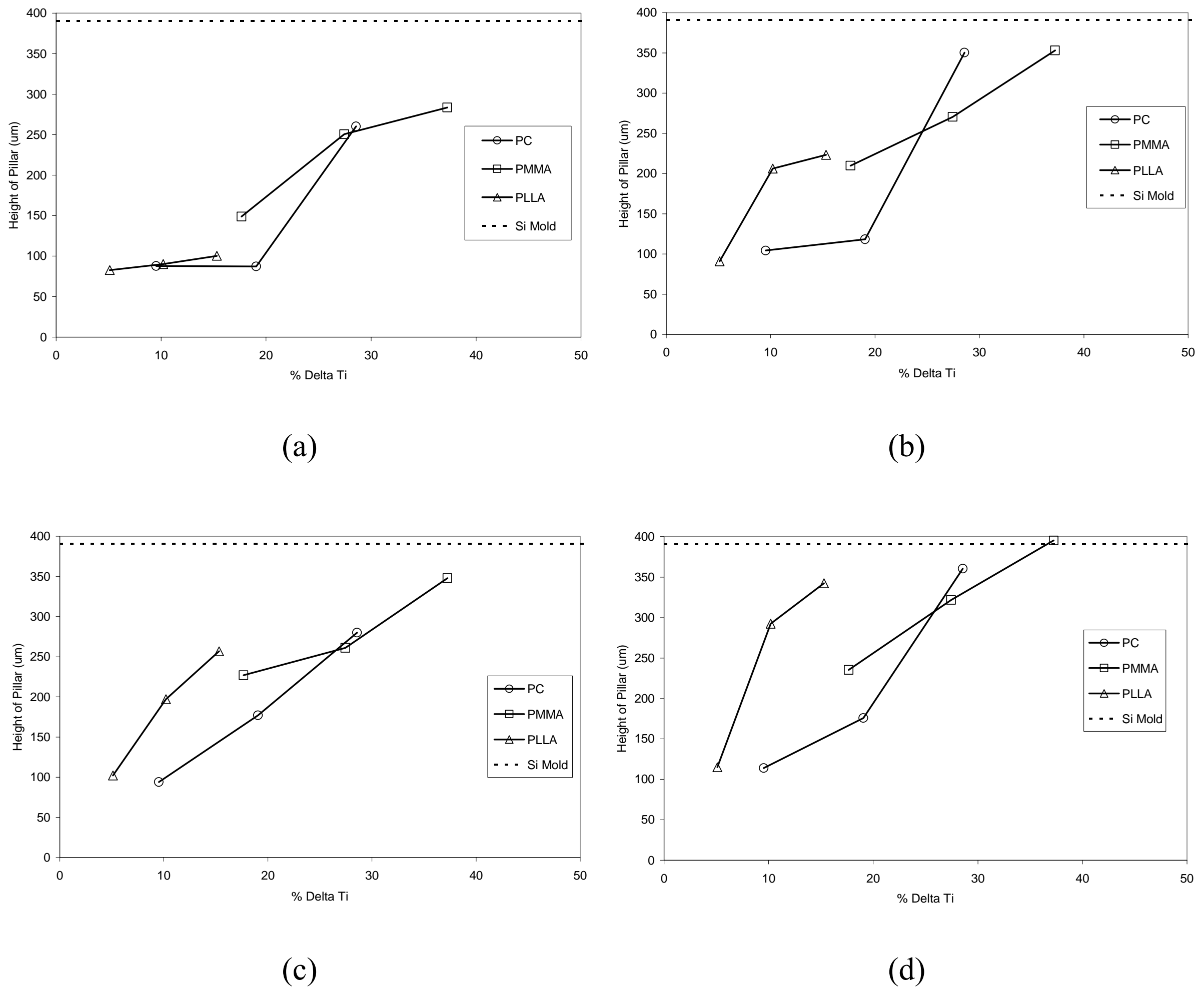

Figure 3.30 Comparison of behavior of the three polymers – Row 3
(a) 14 MPa, 30 secs (b) 14 MPa, 90 secs
(c) 19 MPa, 30 secs (d) 19 MPa, 90 secs

3.14 Conclusions

The hot embossing process using the HEMM and the de-embossing systems were introduced. Characterization of the HEMM process for three different polymers was discussed. It is observed that PMMA replicates better than PC and PLLA for the selected process parameters. This is attributed to the higher normalizing temperature for PMMA. At higher ΔT_i values, PC exhibits better flow rate change than PMMA, whereas at lower ΔT_i values, PLLA exhibits better flow rate change than PMMA and PC.

CHAPTER 4

TWO STAGE EMBOSSING

This chapter starts with the explanation for the need for two stage embossing. Introduction to the two stage embossing is presented along with its advantages and limitations. Finally, validation experiments and their results focusing on mold quality with respect to the embossing cycles of the secondary mold and the embossing quality of the substrate as compared to the primary silicon mold have been presented along with the conclusions.

4.1 Need for Two-Stage Embossing

As mentioned in chapter 2 (section 2.5), during mold making on the FLM system, a complementary of the designed device, as shown in figure 4.1, must first be modeled in the CAD system and then fabricated. This may lead to delays in prototype fabrication and also become more difficult when the device/part becomes complicated.

For example, referring to figure 4.2, when a reservoir is part of a device, figure 4.2(a), then the male mold which is a pillar, figure 4.2(b), needs to be fabricated. The same discussion is also applicable to devices with channels and reservoirs as shown in figure 4.2(c) and (d). It is easy to deduce from figure 4.1 that fabrication of the device using the FLM system would be considerably easier and faster than fabrication of the

mold. CNC programming and material removal from the mold would take a lot more time than machining the device.

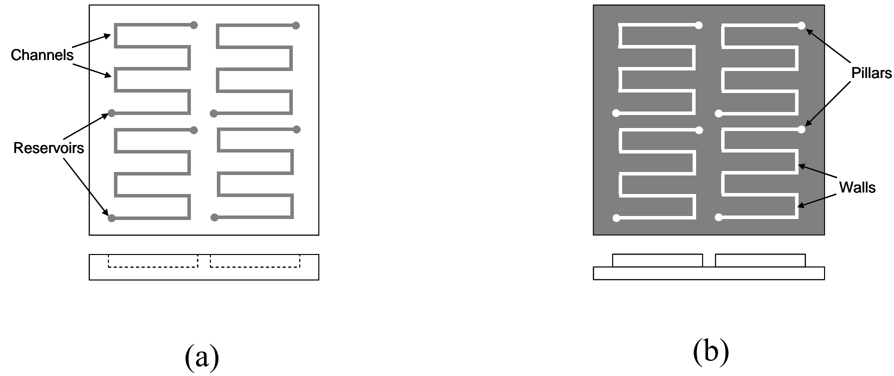

Figure 4.1 Mold making (a) Device design
(b) Mold design

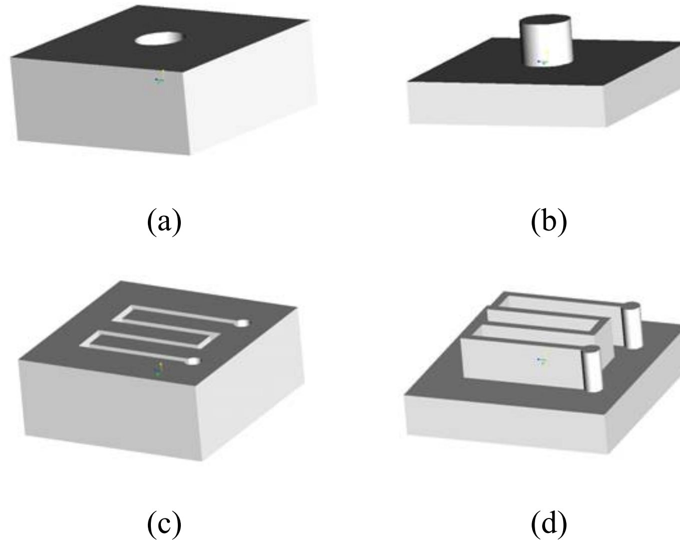

Figure 4.2 Male and female molds (a) Female mold (reservoir)
(b) Male mold (pillar) (c) Female mold (d) Male mold

4.2 Two-Stage Embossing Process

The proposed two stage hot embossing process offers certain advantages for certain cases over the traditional single stage hot embossing technology such as time reduction for mold fabrication but mainly improvement on the life expectancy of the primary mold.

It is proposed that the step for fabricating the complementary mold be by-passed and an extra step incorporated during hot embossing viz. that of fabricating a secondary mold using hot embossing. The proposed process will allow the fabrication of the silicon "primary" mold just like the way the device is designed. Subsequently, the primary mold is embossed on a polymer with a higher glass transition temperature (T_g) than that of the polymer used for the actual device. This step will generate the complementary or negative of the device on the polymer with higher T_g. Subsequently, the higher T_g polymer becomes the secondary mold that can be used to replicate the desired device features on the lower T_g polymer using HEMM technology. The two stage hot embossing procedure is schematically shown in figure 4.3. In our verification experiments, we use Polycarbonate (PC) with a T_g of 145 $^{\circ}$C for the first stage, and PolyMethylMetAcrylate (PMMA) with T_g of 106 $^{\circ}$C and Poly L-Lactic Acid (PLLA) with T_g of 75 $^{\circ}$C for the second stage. The big difference in the glass transition temperatures between the secondary mold (PC) and the two substrates (PMMA and PLLA) was one of the main reasons for the selection of these materials.

Most of the polymer molds that have been used for embossing in the past [47-51] are fabricated using polymer casting methods. If hot embossing is planned to be

used as the secondary process, then it can also be used to fabricate the secondary polymer mold. This eliminates the need of having specialized equipment and chemicals required for casting.

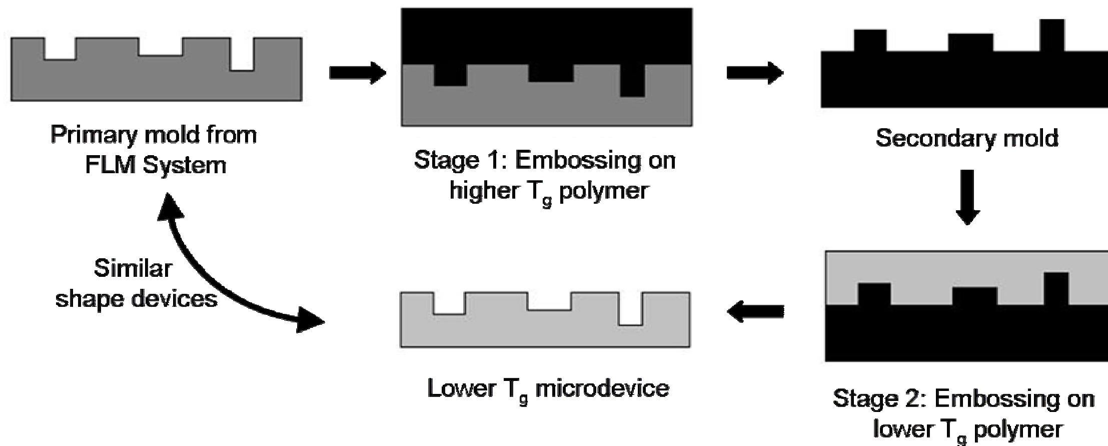

Figure 4.3 Two-stage hot embossing process

4.3 Advantages and Limitations

The advantages of the two-stage embossing process are the following:

- Less material removal from the silicon mold and consequently faster fabrication of the primary mold,
- Less material removal leads to preservation of the original surface of the silicon mold which improves the surface quality of embossed sample and helps in de-embossing/mold release,
- The silicon mold fabricated through the FLM system is not used for direct embossing thereby preserving the primary mold quality. The primary mold can be used occasionally, and therefore, one primary mold could be used for a

substantial number of embossings , thereby saving fabrication costs of molds, and

- Although, there is a small time penalty for fabricating the secondary mold using HEMM, this is offset by the elimination of the design and CAD modeling time for the complementary mold leading to faster cycle time and possible elimination of manufacturing errors.

Some of the disadvantages/limitations of this method are:

- Strict control of embossing temperature in the second stage to ensure that the temperature does not approach the glass transition temperature of the secondary mold and possibly eliminate/damage the features on the secondary mold,
- Since both the secondary mold and the secondary substrate are polymers, there might be problems during de-embossing at the second stage,
- A new secondary mold has to be made after the old one has been used for about 10-15 embossing cycles.

4.4 Experiments and Results

The proposed two stage hot embossing process was experimentally verified using three different types of silicon molds – the first prepared using wet etching, a traditional MEMS fabrication technique, and the other two fabricated using the FLM system. The first mold contains multiple channels while the other two molds (fabricated on the FLM system) contain reservoirs and channels, respectively, the two main components in microfluidic systems.

The silicon molds were first replicated using hot embossing on a PC substrate. Then, the embossed PC substrate was used as the secondary mold for hot embossing replication on PMMA and PLLA substrates. Two series of experiments were performed; the first series (experiment # 1) was performed to verify the proposed two stage embossing process while the second series (experiments # 2 and # 3) were performed to assess process parameters and replication quality.

4.4.1 Experiment # 1: Wet Etched Silicon Mold

The embossing process parameters (primary Si to PC and secondary PC to PMMA) for the two-stage embossing were identified using the characteristic plots shown in chapter 3 and are shown in Table 4.1. The secondary mold (PC substrate) was used for 10 embossing cycles and replicated on PMMA. The quality of the secondary mold and the embossed PMMA were analyzed using optical microscopy after the 1st, 2nd, 4th, 7th and 10th embossing cycles. The results at the 2ndand 10th embossings are shown in figure 4.4.

Table 4.1 Two-stage embossing process parameters – experiment # 1

Process parameters	Silicon to PC	PC to PMMA
Embossing temperature (°C)	155	115
Embossing pressure (MPa)	14	14
Holding time (seconds)	30	30
De-embossing temperature (°C)	85	80

A visual analysis of the replicated features at various embossing cycles indicates that even after 10 cycles a faithful feature reproduction is observed as shown in figure 4.4. Depth and feature measurements were not taken for this experiment as this

experiment was performed with the sole intention of validating the concept of two-stage embossing with complex features on the primary mold and identify process parameters.

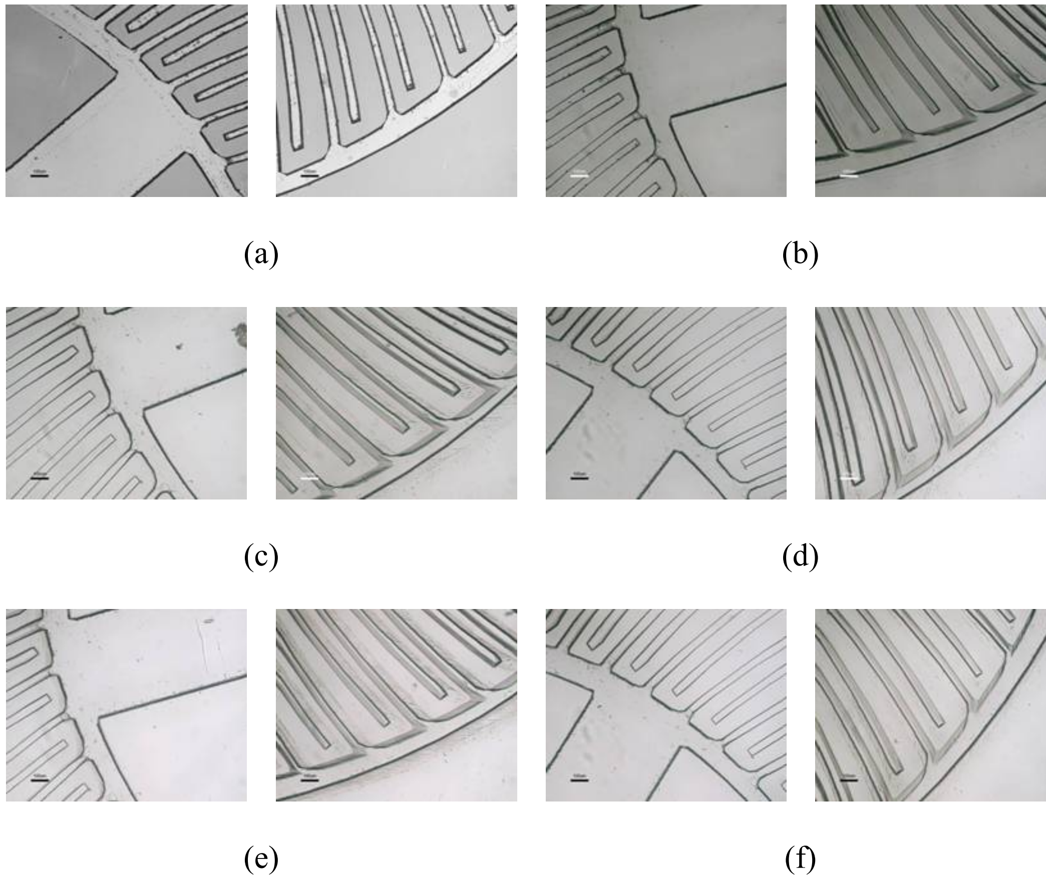

Figure 4.4 Silicon (primary) mold, PC (secondary) mold and PMMA substrate at different cycles of embossing (a) Silicon mold (b) PC (secondary mold) – before secondary embossing (c) PC (secondary mold) – after 2 secondary embossing cycles (d) PMMA substrate – after 2nd secondary embossing cycle (e) PC (secondary mold) – after 10 secondary embossing cycles (f) PMMA substrate – after 10th secondary embossing cycle

4.4.2 Experiment # 2: FLM Silicon Mold with Channels

This experiment utilized a silicon primary mold with four equally spaced channels of 10 mm length, average 89 um (microns) width and average 44 um in depth

fabricated using the FLM system. As in the first experiment, the embossing process parameters identified using characteristic plots are shown in table 4.2.

Table 4.2 Two-stage embossing process parameters – experiment # 2

Process parameters	Silicon to PC	PC to PMMA
Embossing temperature ($^{\circ}$C)	160	115
Embossing pressure (MPa)	14	14
Holding time (seconds)	30	30
De-embossing temperature ($^{\circ}$C)	85	80

The fabricated PC mold was replicated on PMMA substrates for 10 embossing cycles. The replication quality was assessed by taking width and depth measurements at the end of 1st, 2nd, 4th, 7th and 10th embossing cycles. Channels 2 and 3 of the silicon primary mold and PC secondary mold before secondary embossing, and PC secondary mold and replicated PMMA substrate at the end of 2nd and 10th secondary embossing cycles are shown in figure 4.5.

The measured width and depth of channels 2 and 3 at various embossing cycles are presented in figure 4.6. Slight decrease in the depth and increase in the width of the channels is observed. When the channels on the silicon mold and the PMMA substrate are compared, the average width of channels 2 and 3 differ by about 3 um (~ -3%) and 1 um (~ -1%) respectively as compared to the original Si mold. The average depth of channels 2 and 3 differ by an average of 2 um (~ 5%) and 2 um (~ 5%) respectively as compared to the original Si mold.

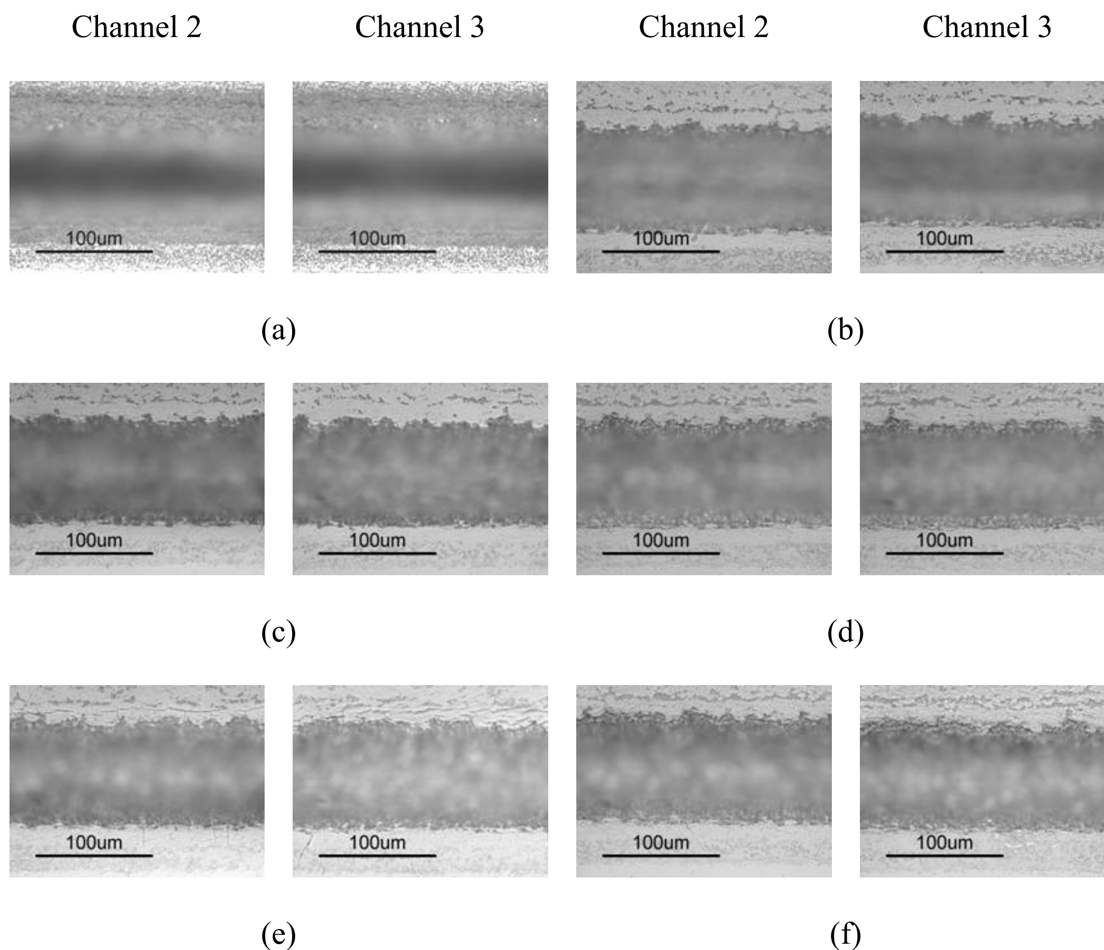

Figure 4.5 Silicon (primary) mold, PC (Secondary) mold and PMMA substrate at different cycles of embossing (a) Silicon mold (b) PC (secondary mold) – before secondary embossing (c) PC (secondary mold) – after 2 secondary embossing cycles (d) PMMA substrate – after 2nd secondary embossing cycle (e) PC (secondary mold) – after 10 secondary embossing cycles (f) PMMA substrate – after 10th secondary embossing cycle

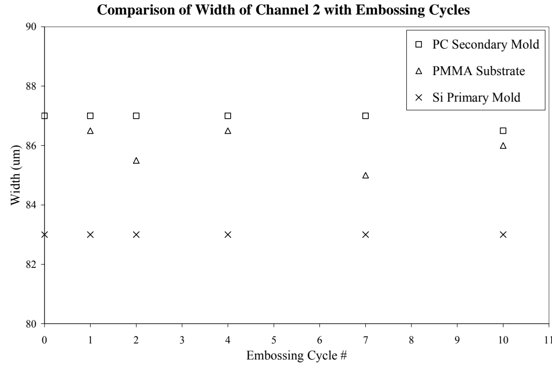

(a)

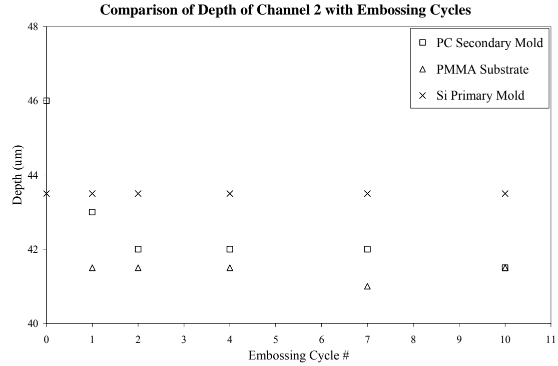

(b)

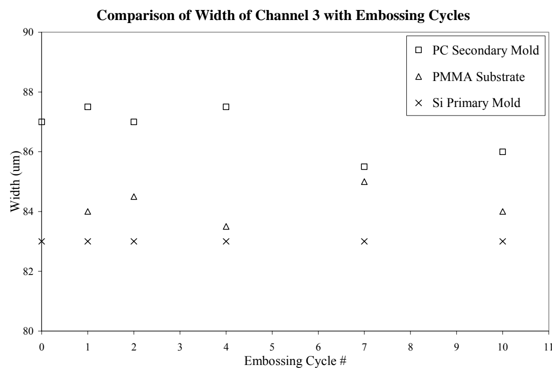

(c)

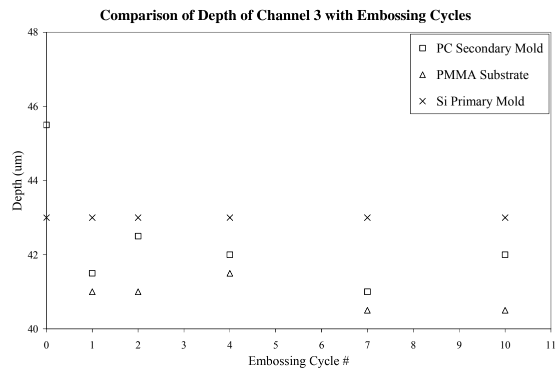

(d)

Figure 4.6 Average channel dimensions (a) Channel 2 – width
(b) Channel 2 – depth (c) Channel 3 – width (d) Channel 3 – depth

4.4.3 Experiment # 3: FLM Silicon Mold with Reservoirs

A silicon mold having a 3 by 3 matrix of reservoirs was fabricated using the FLM system. The depth and the diameter of the reservoirs were measured to be on average 230 um and 250 um respectively. The secondary substrate is the biodegradable PLLA whose T_g is much lower than that of the PC mold. The identified embossing process parameters are presented in table 4.3. An increase in the embossing parameters of PC as compared to the first two experiments is due to the fact that the depth of the

reservoir is greater than the depth of the channels in experiment 2, thus requiring lower viscosity in order to quickly replicate the Si mold features.

Table 4.3 Two-stage embossing process parameters – experiment # 3

Process parameters	Silicon to PC	PC to PLLA
Embossing temperature ($^{\circ}$C)	175	85
Embossing pressure (MPa)	19	14
Holding time (seconds)	45	45
De-embossing temperature ($^{\circ}$C)	85	60

Similar to experiment # 2, 10 embossing cycles were performed on the PC secondary mold. The quality of replication and measurements of depth and diameter of various reservoirs were performed at the end of 1st, 2nd, 4th, 7th and 10th embossing cycles. Two reservoirs, one each from rows 2 and 3 for the silicon primary mold and PC secondary mold and replicated PLLA substrate at various stages of embossing are shown in figure 4.7.

The measured diameter and depth of the selected reservoirs are plotted in figure 4.8. Comparing the silicon mold and the PLLA substrate, an increase in the diameter and decrease in the depth of the reservoirs similar to the observations in experiment 2 is observed. The depth in row 3 and row 2 differs by an average of about 7 um (~ 3%) and 5 um (~ 2%) respectively compared to the original silicon mold. The diameter of the reservoirs differs by an average of about 11 um (~ -4%) and 12 um (~ -5%) respectively compared to the original silicon mold.

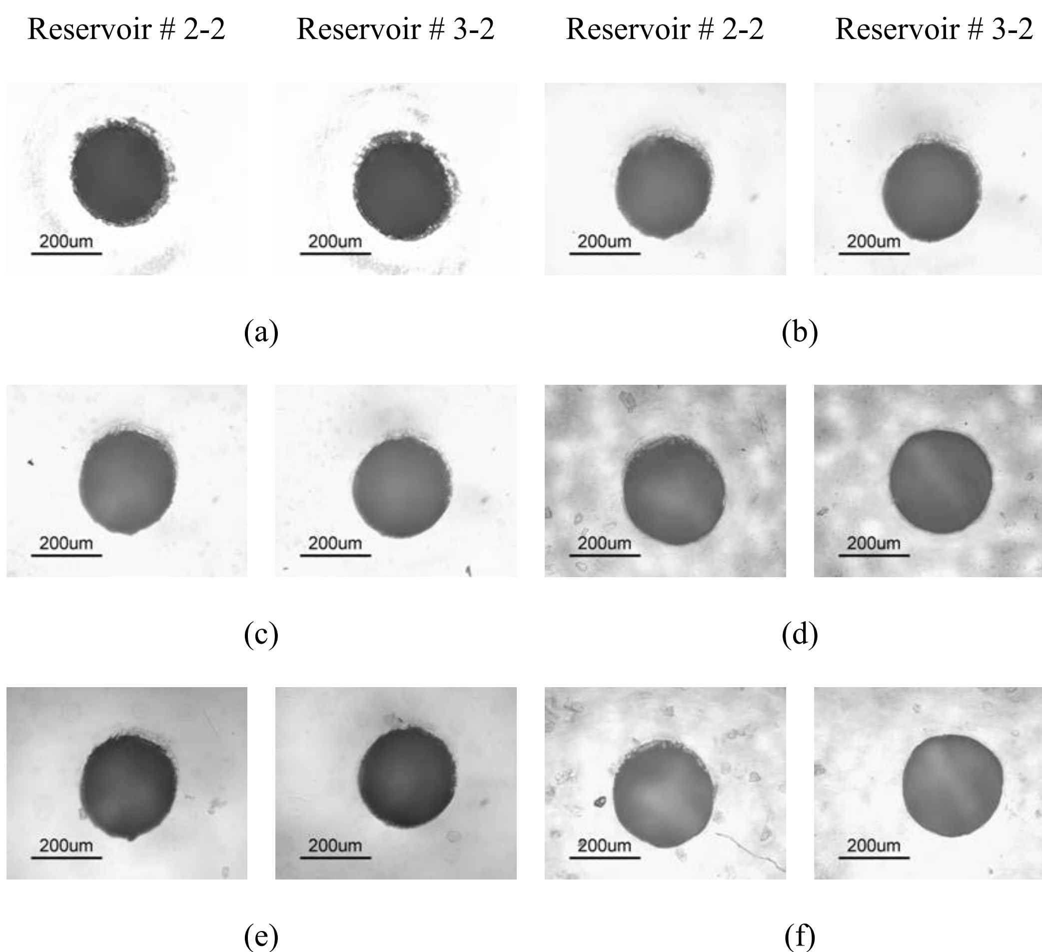

Figure 4.7 Silicon (primary) mold, PC (Secondary) mold and PLLA substrate at different cycles of embossing (a) Silicon mold (b) PC (secondary mold) – before secondary embossing (c) PC (secondary mold) – after 2 secondary embossing cycles (d) PLLA substrate – after 2nd secondary embossing cycle (e) PC (secondary mold) – after 10 secondary embossing cycles (f) PLLA substrate – after 10th secondary embossing cycle

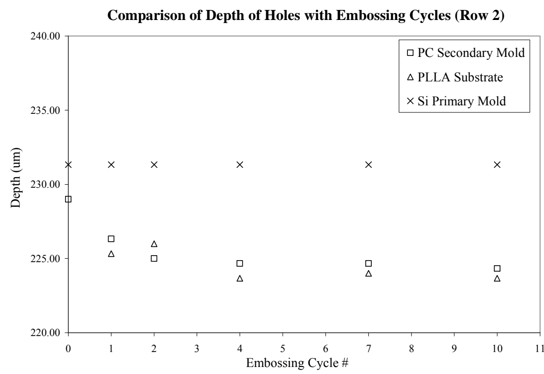

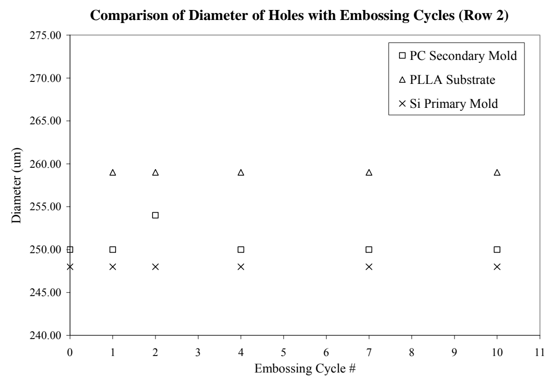

(a) (b)

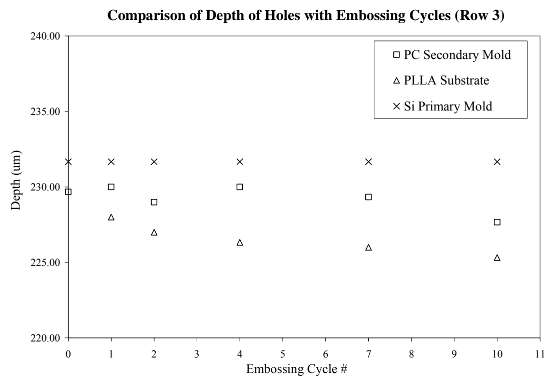

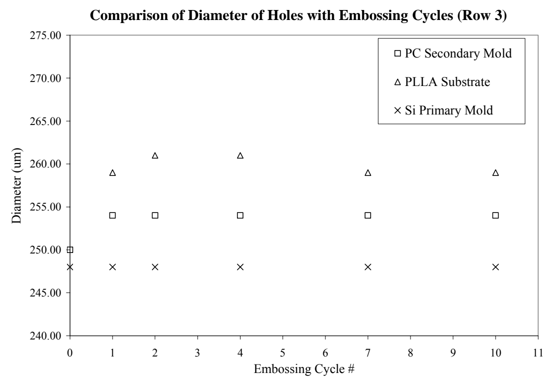

(c) (d)

Figure 4.8 Average reservoir dimensions (a) Row 2 – depth/height (b) Row 2 – diameter (c) Row 3 – depth/height (d) Row 3 – diameter

4.5 Discussions

The embossed components are characterized by surface features (width and diameter) and depth. The measurement errors using the optical microscope were ± 5 um in depth and ± 2 um in width and diameter. In the series of experiments performed and analyzed, an increase in the surface feature dimensions (width and diameter) is observed while the depth of the features experiences a decrease. This phenomenon should be expected when a polymer secondary mold is used, and attributed to the

degradation of the secondary polymer mold due to the repeated loading (both force and temperature) cycles during embossing and also partly due to errors in measurement. The experiments revealed that the error between the primary Si mold and final substrate becomes greater than 5% after 10 secondary embossing cycles. However, the replication error between the secondary mold and the final substrate is still around 2% even after 10 embossing cycles.

4.6 Conclusions

In this chapter, a novel two stage hot embossing microreplication process was introduced. The rationale behind the introduction of this process was discussed. This process was operationally verified using various types of molds and features with both surface and depth characteristics. The experiments utilized a silicon primary mold, a PC secondary mold, and PMMA and PLLA polymer substrates for the final desired features/device with reservoirs and channels. The experimental results demonstrated excellent replication quality and consistent feature sizes during consecutive embossing cycles indicating that the life of the primary silicon mold could be extended through the use of a secondary mold. The comparison of the feature sizes between the final substrate and the primary mold yields errors in width, diameter and depth of less than 5%. This research work also demonstrates that polymer to polymer embossing could be successfully and reliably performed if the proper process parameters are employed even when the secondary mold is fabricated using HEMM. The feature size on the PC secondary mold was observed to be consistent with changes of less than 5% during the consecutive embossing cycles. The consistency observed in the replication for the

embossing cycles leads to the conclusion that the feature size changes could be considered prior in the design state for a device. In closing, the proposed two stage hot embossing microreplication process is experimentally verified and should be considered both in research environments due to the ease of primary mold replication using direct subtractive techniques, and in mass-replication environments of microfeatures or devices.

CHAPTER 5

MICROMACHINING OF POLY L-LACTIC ACID

This chapter starts with a brief introduction to biodegradable polymers, its applications in drug delivery systems and various proof-of concept studies for drug release mechanisms using biodegradable polymers. Fabrication of microfeatures on PLLA using the HEMM and FLM systems are discussed in detail with emphasis on linear fill rate during embossing and determination of threshold ablation fluences for micromachining using FLM.

5.1 Introduction

A biodegradable polymer is defined as "a polymer susceptible to degradation that is accompanied by a lowering of its molar mass due to the interaction with enzymes, bacteria, or other biological systems" [52]. Biodegradable polymers have been used in the field of artificial implants [53], tissue engineering [54], drug delivery [55] and microsurgery [56]. A biodegradable device, once implanted, should maintain its mechanical properties until they are no longer needed and then be absorbed and excreted by the body, leaving no trace. Under favorable conditions, biodegradable polymers like poly-glycolic acid (PGA) and poly L-lactic acid (PLLA) break down into glycolic and lactic acids, which breakdown further into water and carbon dioxide [57]. The most common reason for using biodegradable polymers is to have a device that can

be used as an implant without the need for a second surgical intervention for its removal. Besides eliminating the need for a second surgery, the biodegradation may offer other advantages. For example, an implant prepared from biodegradable polymer can be engineered to degrade at a rate that will slowly transfer load to the fractured bone that is being fixed [58].

Another exciting application for these types of polymers is drug delivery, either as a drug delivery system alone or in conjunction to functioning as a medical device. Advantages of using biodegradable polymers for drug delivery include programmable drug delivery based on the physical activity or other medical treatment needs, localized implantation of drug delivery device reducing drug side effects, and lesser dosage quantities. Limitations of this type of implantable devices include need for implantation, higher costs as compared to traditional drug delivery methods, and the effects of by-products of degradation on the human body are still unknown [58].

Several proof-of-principle studies have been conducted on biodegradable drug delivery, including the following:

- Microchips have been fabricated from PLLA and poly (D, L,-lactic-co-glycolic acid) [59]. These microchips have 36 reservoirs that could each be filled with a different drug. The microreservoirs are covered with a sealant on one side and degradable reservoir membranes on the other side. The chemicals/drugs can be released at different times based on the material characteristic of the reservoir membranes. Compression molding was used for fabrication of the PLLA preform followed by microinjection to fabricate the reservoir members.

- Drug delivery devices with 3D microstructures on polycaprolactone (PCL) have been fabricated using micromolding [60]. The cavities on the PCL are sealed using a gold thin film. The liquid/drug inside the sealed cavity can be released by anodic dissolution of the gold film.
- A novel high aspect ratio microfabrication process of PLGA using UV-LIGA has been discussed in [61]. A prototype drug capsule has been designed that has coaxial rings and degrades in such a way that the microchambers along the concentric direction will degrade to achieve a linear rate of drug release.
- Micromolding was used to fabricate PLLA and PCL for applications including biodegradable needles for transdermal drug delivery & biodegradable ratcheting surgical ties for blood vessel surgery [62].

A review of the microfabrication techniques from the above mentioned studies and other reviews for drug delivery systems [63] and biodegradable polymers [64] show that the processes commonly used are:

- Replication techniques such as micromolding, compression molding, microinjection, and soft lithography,
- Rapid prototyping techniques such as direct deposition methods, three-dimensional printing, and laser stereolithography.

These fabrication techniques are very time consuming and complicated. Therefore, a simpler fabrication method is needed other than compression molding and microinjection for biodegradable polymers, if these devices are to be used for mass production. A method that is faster, takes place at a much lower temperature, and at the

same time fabricates features of comparable quality while fabricating a number of devices in a single cycle is needed. In this research, hot embossing using the HEMM system was investigated for precisely these reasons. A detailed literature survey has shown that hot embossing has never been used as a fabrication process for biodegradable polymers.

5.2 Hot Embossing on PLLA

Characterization experiments and two-stage embossing on PLLA in chapter 3 and 4 respectively yield good replication quality. Experiments were performed on PLLA to fabricate reservoirs of different depths that can be used for drug delivery applications. Two stage embossing was performed using a silicon mold with a 3 by 4 matrix of reservoirs as shown in figure 5.1. The nominal depth of the reservoirs in the three rows are 120 um, 260 um and 330 um respectively.

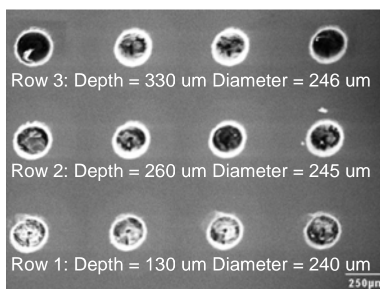

Figure 5.1 Silicon primary mold

The two stage embossing yielded interesting results for mold fill rate and hence it was decided to perform single stage embossing using the same parameters to compare the mold fill rates between these two processes. The process parameters used for single-stage and two-stage embossing are shown in tables 5.1 and 5.2 respectively.

Polycarbonate (PC) is used as a secondary mold material for the two-stage embossing process.

Table 5.1 Single-stage embossing process parameters

Process parameters	Si to PLLA
Embossing temperature (°C)	85
Embossing pressure (MPa)	18
Holding time (seconds)	30, 60, 90, 120
De-embossing temperature (°C)	60

Table 5.2 Two-stage embossing process parameters

Process parameters	Si to PC	PC to PLLA
Embossing temperature (°C)	175	85
Embossing pressure (MPa)	19	18
Holding time (seconds)	75	30, 60, 90, 120
De-embossing temperature (°C)	80	60

Comparison between the primary silicon mold and the measured embossed feature sizes on the PLLA substrates viz. pillar heights (in single-stage embossing), reservoir depths (in two-stage embossing) and the diameter of these features were measured using optical microscopy for single-stage and two-stage embossing are shown in figures 5.2 and 5.3 respectively.

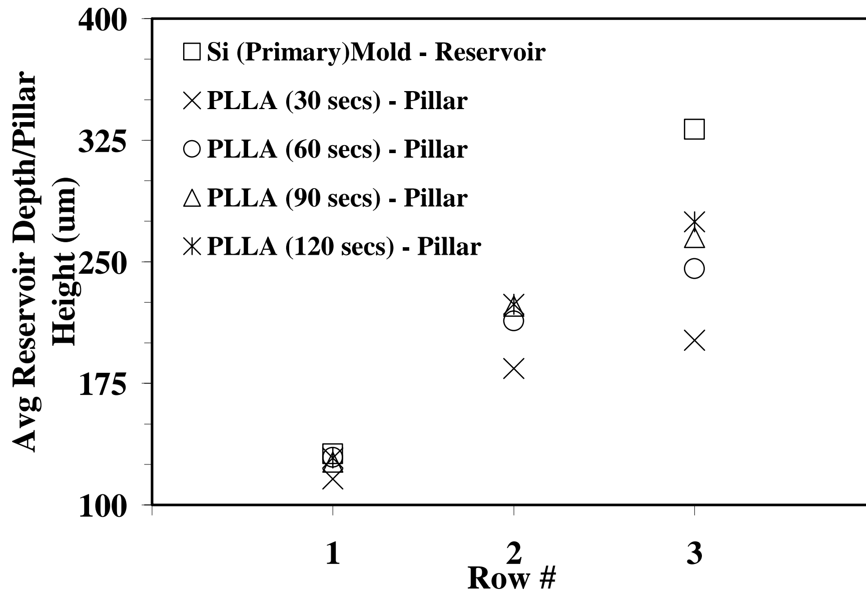

(a)

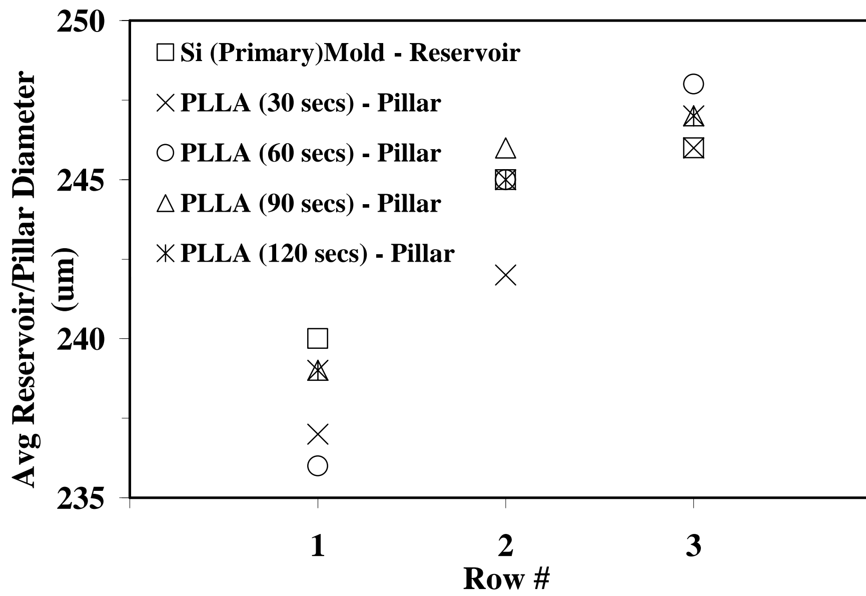

(b)

Figure 5.2 Comparison for single-stage embossing
(a) Depth/Height (b) Diameter

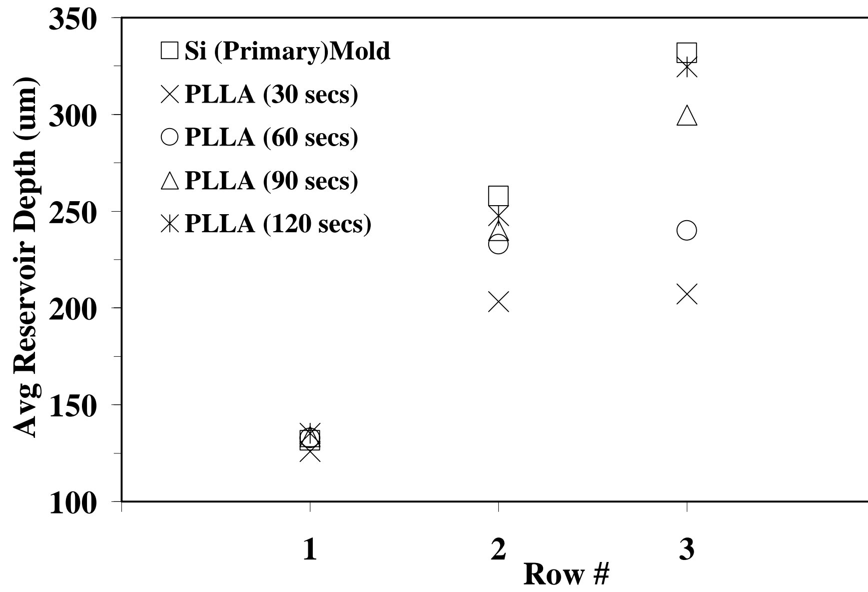

(a)

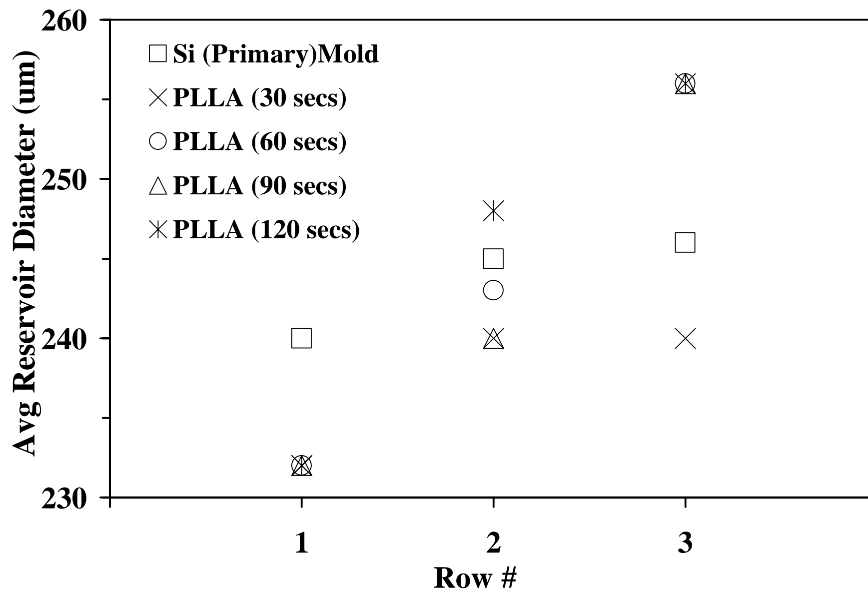

(b)

Figure 5.3 Comparison for two-stage embossing
(a) Depth (b) Diameter

It is observed that the average depth of the reservoirs and height of the pillars are directly proportional to the holding time. This is expected since by increasing the holding time the polymer is allowed more time to flow and obtain the shape of the mold. In addition, using the same process parameters, it is observed that the replication of the pillar heights into reservoir depths using two-stage embossing is better than the replication of the reservoir depths into pillar heights using single-stage embossing. This is attributed to the fact that the embossing for both processes is performed in air and the type of the features on the mold. During single-stage embossing, the air in the mold reservoirs cannot escape and is trapped to be compressed during the process, thus generating a back pressure that might prevent the material to flow freely and fill the mold cavities. In two-stage embossing, the polymer flows around the mold pillars as they are pushed into the polymer.

A comparison of the average diameters of the embossed substrates with the silicon primary mold yields a difference of ± 5 um for single-stage embossing and ± 10 um for two-stage embossing. The slight increased difference for two-stage embossing is attributed to steady increase in the diameter of the reservoirs on the PC secondary mold due to degradation caused by repeated usage.

The effect or influence of polymer flow on the embossing process could also be discussed using the average linear fill rate during the 4 time periods (0-30, 30-60, 60-90 and 90-120 seconds) for both sets of experiments. The average linear fill rate is calculated by simply dividing the increase in the height of pillars or depth of reservoirs during the corresponding time periods based on the results presented in figures 5.2 and

5.3. Note that for the two-stage embossing where reservoirs are fabricated, the average linear fill rate relates to the pillar insertion rate and not the actual fill of a cavity on the mold, but is used loosely here for both experiments. The average linear fill rates for both sets of experiments are shown in figure 5.4. For similar embossing conditions, the average linear fill rate seems to follow an exponential behavior for both single-stage and two-stage embossing.

For two-stage embossing, the linear fill rate saturates for row 1 after 60 seconds and row 2 after 90 seconds. This saturation indicates that the reservoirs in rows 1 and 2 are fabricated within 60 seconds and 90 seconds respectively. The linear fill rate for row 3 decreases and the reservoirs are fully fabricated at 120 seconds holding time.

For single-stage embossing, the linear fill rate for row 1 saturates after 60 seconds and the reservoir is completely filled generating a pillar between 60 and 90 seconds. The pillars generated from rows 2 and 3 are not fully replicated even after 120 seconds and a substantial decrease in the linear fill rate is observed. This could be attributed to the back pressure effects from air trapped in the mold reservoirs as mentioned earlier in this section. It also shows that the back pressure from trapped air reduces the linear filling rate but does not totally eliminate it. The polymer flow behavior could be improved by reducing the viscosity of the polymer thus allowing it to flow easier by either increasing the embossing temperature or pressure and by performing the embossing in a vacuum environment.

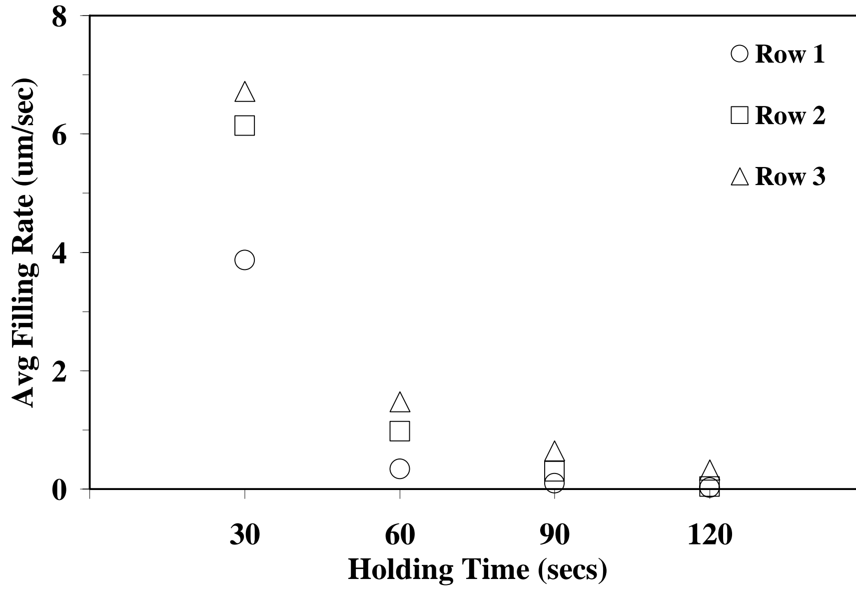

(a)

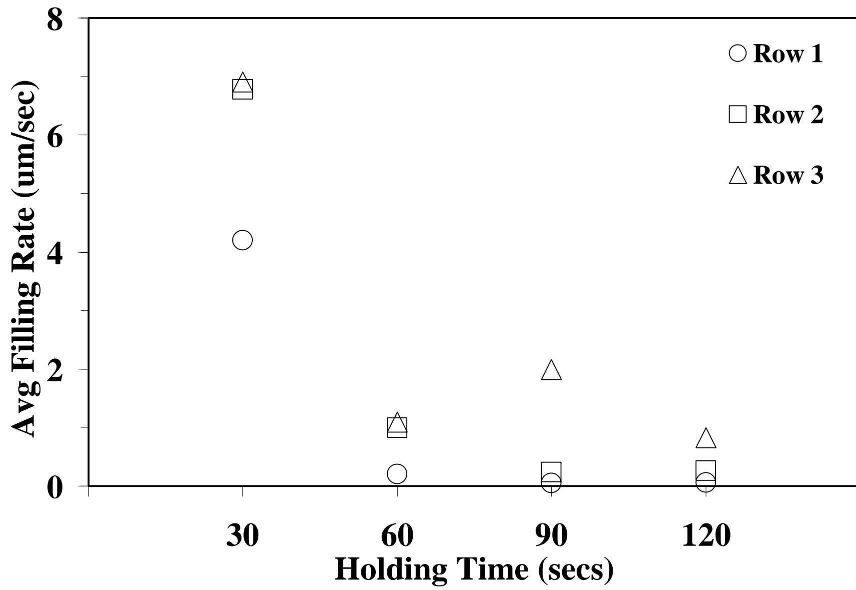

(b)

Figure 5.4 Average linear filling rates as a function of holding time (a) Single-stage embossing (b) Two-stage embossing

Further analysis of the average linear fill rates presented in figure 5.4 as functions of holding times reveal the average linear fill rate for the various time intervals during the embossing process. It can be concluded that the fill rate is highest at the beginning of the process, the first time period, then it substantially slows down in the second time period and finally saturates between the second and third or third and fourth time periods depending on the depth of the reservoirs indicating that the mold cavity has been filled. The numerical analysis yields a fill rate during the first time period of almost five times compared to the second time period and almost an order of magnitude compared to the third time period.

In two-stage embossing, similar fill rate behavior is observed as that of the single-stage embossing. The pillars in Row 2 (260 um height) and Row 3 (330 um height) exhibit a fast fill rate (insertion rate) at the first time period up to 30 seconds and then the fill rate substantially slows down in the next time period (30 to 60 seconds). At the end of the fourth time period, the fill rate does not saturate and the generated reservoirs for both Row 2 and Row 3 are almost the same depth as those of the original silicon mold indicated excellent replication. The pillars in Row 1 (130 um height) also exhibit a fast fill rate (insertion rate) at the first time period and the rate becomes almost zero at the end of the second time period indicating complete insertion at this time.

5.3 FLM on PLLA

As mentioned in chapter 2, femtosecond laser micromachining creates minimum thermal damage to the surrounding material while fabricating fine features. Lasers have been used on biodegradable materials to fabricate channels, filters and stents. Figure 5.5

(a) shows an ultrafiltration membrane on poly-vinyl alcohol (PVA) fabricated using a Nd:YAG laser [65] while 5.5 (b) shows a biodegradable stent machined using a femtosecond laser [66].

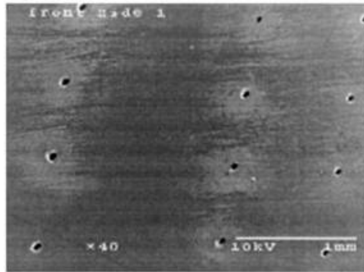

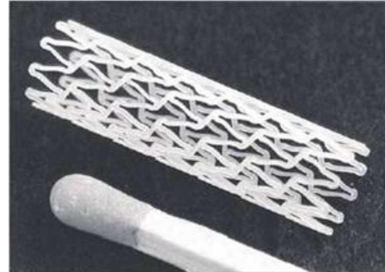

(a) (b)

Figure 5.5 Laser micromachining of biodegradable polymers
(a) Ultrafiltration membrane (b) Biodegradable stent

Fabrication of a material on FLM requires a thorough knowledge of the ablation threshold fluence of that material. The threshold fluence is the minimum amount of fluence at which the material ablates, so if the applied fluence is more than the threshold value, then material removal will occur [67]. Evaluating threshold fluence leads to

- Evaluating laser energy required to induce damage
- Understanding morphological changes on ablation
- Identifying distinct ablation regions
- Defining machining parameters for rapid prototyping
- Machining sub-micron features

Limiting the applied fluence (power level) to just above the threshold fluence will result in sub-micron machined features on PLLA because the material removal will

take place only in very limited area where the beam energy is high enough to cause ablation [67].

The applied fluence (F_i), applied pulse energy (E_{pulse}), and spot radius (ω_o) of a beam having a Gaussian profile are related by the following equation [68]:

$$F_i = \frac{2E_{pulse}}{\pi\omega_o^2}$$

The applied fluence is easily calculated if the values for E_{pulse} and ω_o are known. The threshold fluence (F_{th}), spot radius and diameter of the damaged surface (D) are related by the equation:

$$D^2 = 2\omega_o^2 \ln\left(\frac{F_i}{F_{th}}\right)$$

Detailed information on calculating threshold fluence is given in [68]. The threshold fluence for PLLA was calculated by performing experiments with 13 different power levels varying from 1 mW to 35 mW. A 25.4 mm focusing lens was used for all the experiments which were performed in air. The number of pulses fired on the substrate were 1, 10, 100, 500 and 1000 at a constant pulse repetition rate of 1 kHz.

The threshold fluence is evaluated using experimentally obtained results, the applied fluence and the ablated diameter. A plot of D^2 vs. the logarithm of applied fluence is generated from the experimental results as shown in figure 5.6. Then, a linear curve fit is performed to the experimental data. The ablation threshold fluence value is evaluated as the intersection of the linear curve fit with the abscissa (X-axis) i.e. when

$D^2 = 0$. These threshold values along with their equivalent power values are given in table 5.3 for different number of pulses.

Table 5.3 Threshold fluence values for different pulses

# of pulses	F_{th} (J/cm^2)	Power (mW)
1	7.77	3.55
10	3.85	1.76
100	2.09	0.96
500	2.00	0.91
1000	1.78	0.81

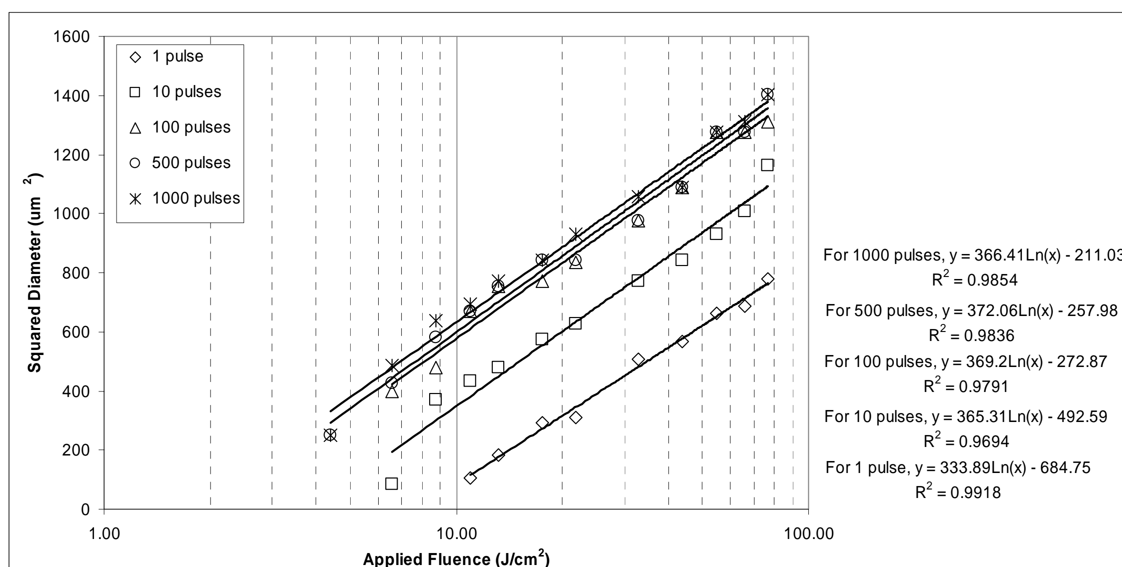

Figure 5.6 Threshold fluence value calculations

Table 5.3 shows that the threshold fluence decreases with an increase in the number of pulse at the same location. It also indicates that, even at 1 pulse, a power of less than 4 mW is needed to fabricate features on PLLA with micron and sub-micron sizes.

Using the threshold fluence values, a power of 50 mW would cause sufficient damage on PLLA to cause ablation and fabricate features on it. Channels, reservoirs and

through holes, as shown in figure 5.7, have been fabricated on a PLLA having a film thickness of 600 um using 50 mW power at speeds of 25 mm/min for channels and 10 mm/min for reservoirs and holes.

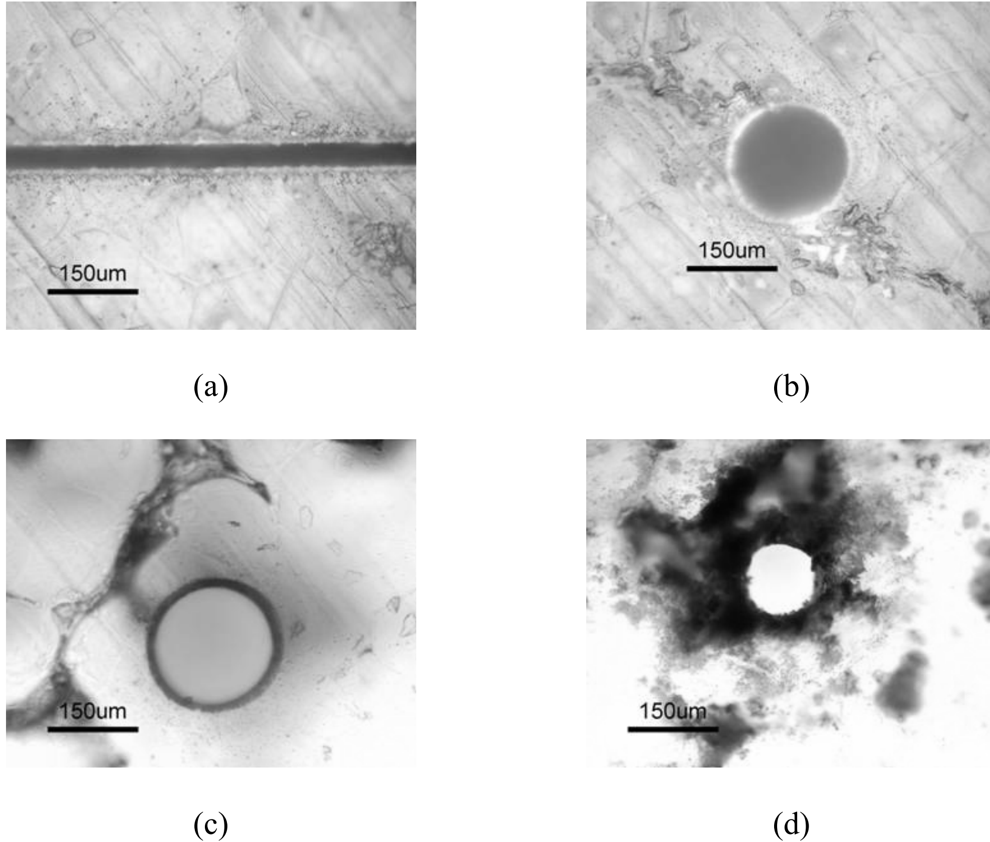

Figure 5.7 Features on PLLA using FLM (a) Channel: w_c = 40 um, h_c = 55 um (b) Reservoir: d_r = 150 um, h_r = 180 um (c) Through hole – front: d_r = 150 um (d) Through hole – back: d_r = 110 um

5.4 Conclusions

Fabrication of PLLA channels and reservoirs using the HEMM and FLM systems is performed. The linear flow rates of PLLA for single as well as two stage embossing are compared. This information can be used to fabricate reservoirs of different heights to store drugs in drug delivery devices. Micromachining of PLLA

using the FLM system is feasible and can be performed after understanding its ablation behavior for different numbers of pulses.

Studies have to be conducted on hot embossed and laser micromachined PLLA to assess any material property changes or the effects of these processes on material biodegradability.

CHAPTER 6

POLYMER BONDING USING HEMM SYSTEM

This chapter begins with an overview of different polymer bonding techniques and a literature survey on thermal bonding. Preliminary thermal bonding experiments are discussed along with results of bonding on PMMA to cover a microfabricated substrate. Finally, conclusions are drawn based on these experiments.

6.1 Different Polymer Bonding Techniques

A polymer microfluidic device is typically produced by fabricating features such as channels and reservoirs on the first substrate and subsequently bonding the second substrate/cover on the first to seal these features. In some cases, more than two substrates are bonded, with more than one substrate having features on them. Bonding should have adequate strength to withstand fluid pressures, permit leak free operation, and should cause minimum damage to the fabricated features during this process. Various polymer bonding techniques are described below:

6.1.1 Adhesives or Tapes

Adhesives have been used to bond substrates [69, 70] where a layer of adhesive is laid between the substrates and a mild force applied. UV curable adhesives are most commonly used for bonding of microfluidic devices. But adhesives may be vulnerable to unwanted reactions with chemicals used for analysis in the microfluidic system.

6.1.2 Solvent Assisted Bonding

Polymer substrates cleaned and treated with ethanol, heated to a temperature just below the glass transition temperature and pressed together with a minimum force for around 30 minutes. The estimated value of distortion is around 5 um [71], when a PMMA substrate is heated to 110 °C (T_g = 115 °C) and a force of 2 kN applied for 30 minutes.

6.1.3 Laser/plastic Welding

Localized melting due to heat generated by a laser can be used to seal and bond polymers. This has been successfully demonstrated in the fabrication of micropumps [72]. Since, the spot size of the laser tends to be in the order of tens of microns, no damage has been observed to the surrounding areas that might contain features. But, because of this same reason, thousands of spots need to be used to bond the polymer having enough strength to sustain fluidic pressures and provide proper sealing.

6.1.4 Deep X-ray Irradiation

Deep X-ray irradiation causes decrease in the molecular weight of PMMA, which in turn decreases the T_g of the polymer. Lowered T_g on the surface of two PMMA sheets makes bonding possible at low temperature. X-ray irradiation is applied at specific locations on the sheet which decreases the surface T_g to as low as 80 °C. Bonding experiments are performed using this method at pressures of 3-4 MPa with bond strength of about 0.96 MPa at a bonding temperature of 92 °C [73].

6.1.5 Lamination

Lamination is primarily used in macrofabrication processes. In this process [6], a PET foil coated with an adhesive is rolled onto a polymer substrate where the adhesive melts and bonds the foil with the substrate. When the features sizes are in the order of microns, problem of the adhesive clogging the features exists. In [74], a multi-channel chip is bonded using this process at 110 °C in a clean room.

6.1.6 Thermal Bonding

Thermal bonding has been performed extensively in microfluidic fabrication field. In thermal bonding, the two polymer substrates are heated to just below the glass transition temperature, pressurized and held for a period of time. The applied pressure forces the two substrates to get into contact with each other and the temperature helps in the bonding process. The whole process is performed with strict control of temperature and pressure to ensure minimal thermal distortion to the fabricated features. Comparable bonding strengths can be obtained by subjecting the substrates to lower pressure for a longer period of time or higher pressures for a shorter period of time. In some cases, before bonding, the polymer substrates sheets are treated with oxygen plasma in order to provide hydrophilic surfaces [75-77].

Bonding between polyethylene and PMMA cover sheet is performed at 145 °C, 0.5 kPa pressure for 1 hour [78]. Two pieces of Zeonor (T_g = 105 °C) are bonded by application of pressure (0.6 MPa to 1.4 MPa) and heat (85 °C to 104 °C) for 10 minutes [79-81] using contact aligner device.

In [31], an embossed PC sheet and membrane foils are bonded together using the same pressurized heater as for the hot embossing. The bonding was performed at 135 °C and 2000 lbs (0.4 MPa) for 1 hour. PMMA devices were bonded at 100 °C for at least 8 mins in [82]. The bonding strength of the chips was estimated to be about 1 MPa.

Two cyclic olefin copolymer (COC) substrates (layers) are heated to about 120 °C (20 °C - 40 °C below its T_g) and a pressure of 10 MPa applied [77]. Bond strength of about 20 MPa is achieved.

PMMA and Su-8 are bonded at various temperatures ranging from 50 °C to 150 °C at bonding forces of 1-2 kN on a 4" wafer. The microstructures on SU-8 are sealed with a 5 um PMMA layer spin coated on Si wafer. The sandwich is maintained at bonding temperature for 10 mins. Bonding strengths of around 4-14 MPa are obtained at these bonding conditions [83].

6.2 Preliminary Experiments Using HEMM System

Thermal bonding can be achieved using a HEMM system. Therefore, it is decided to use the HEMM system for polymer bonding experiments. Based on the literature survey, bonding experiments are performed on PMMA at 95 °C, 100 °C and 105 °C, the T_g of PMMA being 106 °C. The survey revealed two combinations of pressure and holding times – low pressure, high holding times, and high pressure, low holding times. The following two sets of bonding parameters are used:

- Set 1:

  Bonding temperature (°C) – 95, 100, 105

Bonding pressure (MPa) – 10, 15

Holding times (seconds) – 60, 120

- Set 2:

  Bonding temperature (°C) – 95, 100, 105

  Bonding pressure (MPa) – 5, 8

  Holding times (seconds) – 300, 600

For the preliminary experiments, 25 mm by 25 mm blank PMMA samples i.e. samples that do not have any features on them are used. It should be noted that the bonding temperature remains fairly constant (± 1 °C) for the first set of experiments, but varies (± 5 °C) for the second set. This is due to the fact that the HEMM system has been designed for hot embossing where the temperature remains constant for holding times not more than 120 seconds.

6.2.1 Measurement of Bonding Strength and Stack Thickness Difference

The bonding strength was measured using a material testing system. The bonded samples are then glued (with commercially available glue, Gorilla Glue) onto two aluminum plates and allowed to cure under a mild load at room temperature for a minimum of 24 hours. The plates are then held on to the holders of the testing system through two screws as shown in figure 6.1. The speed of motion of the crosshead of the testing system was 0.02 inches/min. It was noticed that the break elongation of the samples equals yield elongation. This means that the sample retains its original shape when the load is removed before the bond breaks. A sample plot of the applied tensile

force vs. elongation for experiment # 7 in set 2 is shown in figure 6.2. The breaking force is 197.284 lbs that translates into 1.36 MPa.

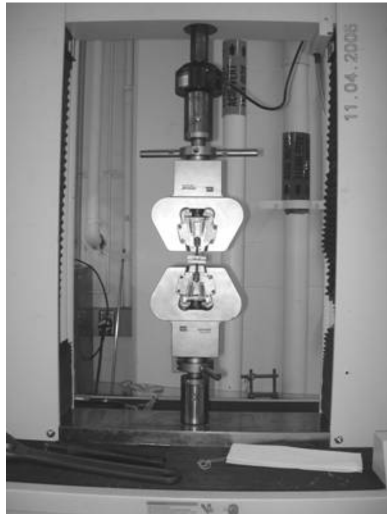

(a)

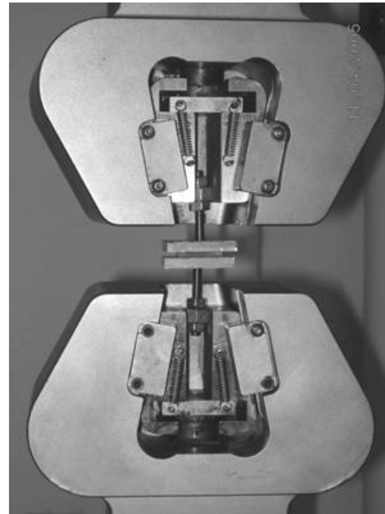

(b)

Figure 6.1 Bonding test sample (a) MTS system
(b) Sample on holders

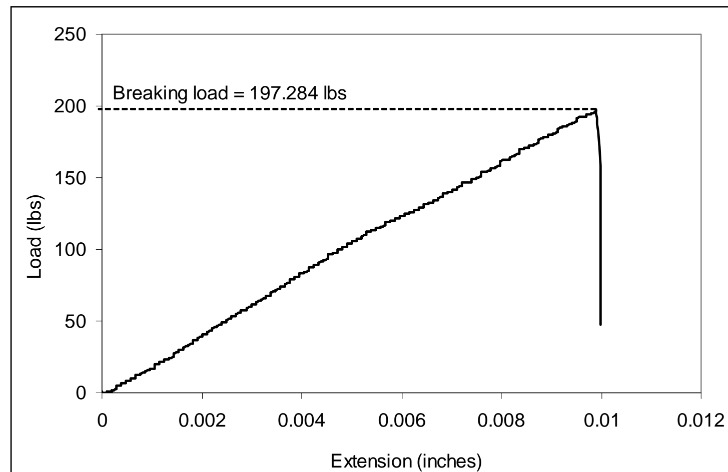

Figure 6.2 Tensile load vs. extension for expt. # 7 (Set 2)

Measurement of the thickness of the bonded polymer stack before and after bonding would provide a measure of distortion of features on the substrates. This measurement was performed using a micrometer having a resolution of 0.0001” (2.54 um). Thickness is measured at three locations and the mean value calculated for analysis.

The combinations of bonding parameters that give maximum bonding strength with minimum stack thickness reduction would be selected for additional bonding experiments using PMMA samples with microfeatures.

Table 6.1 Experimental results for Set 1

Expt No.	Pressure (MPa)	Temperature (deg C)	Time (secs)	Stack Thk Diff (um)	Break Force (lbs)	Bond Break Pressure	
						(psi)	(MPa)
1	10	105	120	311	343.431	312.571	2.155
2	15	100	120	188	265.934	226.038	1.559
3	15	105	60	123	226.996	186.038	1.283
4	10	105	60	96	130.960	124.022	0.855
5	10	100	60	108	112.108	130.556	0.900
6	15	105	120	177	321.916	265.695	1.832
7	15	95	60	49	125.023	108.669	0.749
8	10	95	60	11	87.779	75.494	0.521
9	10	95	120	33	114.972	98.611	0.680
10	15	95	120	32	139.713	124.275	0.857
11	15	100	60	31	174.084	161.966	1.117
12	10	100	120	87	119.683	113.377	0.782

Tables 6.1 and 6.2 give the stack thickness difference and bond breaking strengths for experiment Sets 1 and 2 respectively. A plot of the bond breaking pressure vs. stack thickness difference is shown in figure 6.3. The plot shows that there is an almost linear relationship between the difference in stack thickness and bond breaking

pressure which is expected. An increase in the stack thickness difference means that there is a stronger bond.

Table 6.2 Experimental results for Set 2

Expt No.	Pressure (MPa)	Temperature (deg C)	Time (secs)	Stack Thk Diff (um)	Break Force (lbs)	Bond Break Pressure (psi)	Bond Break Pressure (MPa)
1	5	105	600	143	71.352	71.352	0.492
2	8	100	600	108	130.540	130.540	0.900
3	8	105	300	180	271.703	271.703	1.873
4	5	105	300	95	176.113	176.113	1.214
5	5	100	300	43	54.927	54.927	0.379
6	8	105	600	205	359.105	359.105	2.476
7	8	95	300	35	197.284	197.284	1.360
8	5	95	300	128	68.105	68.105	0.470
9	5	95	600	19	165.978	165.978	1.144
10	8	95	600	80	162.552	162.552	1.121
11	8	100	300	61	239.361	239.361	1.650
12	5	100	600	64	228.048	228.048	1.572

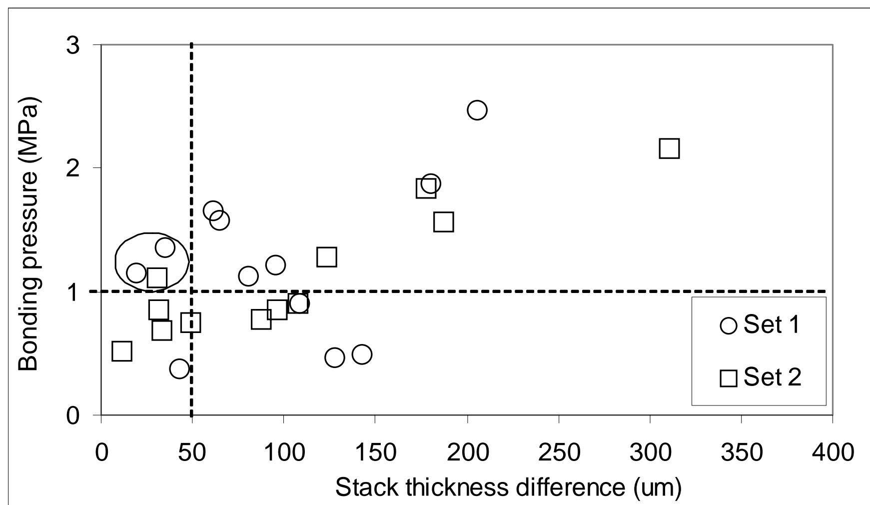

Figure 6.3 Bond pressure vs. stack thickness difference

A stack thickness difference of up to 50 um and bond strength of up to 1 MPa [73, 82] are acceptable for further experimentation. As observed in figure 6.3, there are

three bonding combinations that meet these conditions. These are experiment number 11 from Set 1 and experiment numbers 7 and 9 from Set 2.

6.3 Bonding Experiments and Discussion

The parameters for the 3 bonding experiments selected in the previous section are summarized again in table 6.3. The PMMA substrate used for these experiments is shown in figure 6.4. The substrate contains channels and reservoirs fabricated using FLM.

Table 6.3 Bonding parameters

Expt. No.	Bonding pressure (MPa)	Bonding temperature (°C)	Holding time (seconds)
1	15	100	60
2	8	95	300
3	5	95	600

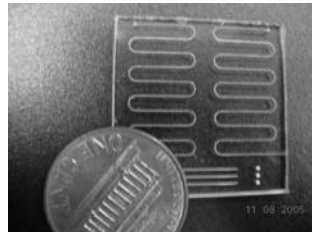

Figure 6.4 PMMA substrate for bonding

The purpose of these experiments was to analyze the dimensions of the features before and after bonding, to test if the bond is leak-proof, and to ensure fluid could flow through the channels even after bonding. Figure 6.5 and 6.6 shows similar features before and after bonding for the three experiments. As can be seen from the figure, there is a decrease in the width of the channels. The change in dimensions of the channels and reservoirs are tabulated in table 6.4.

Experiment # 2 gives the best result relative to the decrease in the feature sizes. The decrease in the width and depth of the channel are 9.5 % and 21 % respectively. It is also noticed that there is a flow of colored liquid through the channels after bonding indicating that there is no clogging of the channels after bonding. Experiment # 1 that is performed at a higher temperature yields more than 50% reduction in the depth of the channel while experiment # 3 results in a reduction of the width by almost 40%. Therefore, an increase in the bonding temperature results in a decrease in the depth of the channel where an increase in the holding time results in the decrease in the width of the channel even at lower bonding loads. Temperatures closer to the T_g of the polymer tend to soften the polymer yielding better bonding strength but at the same time reducing the size of the features.

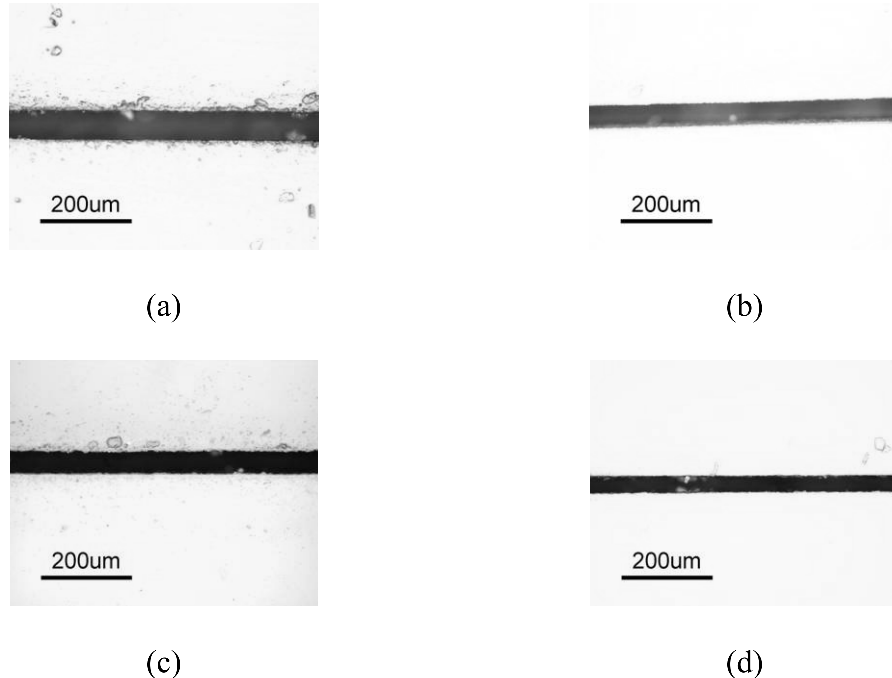

Figure 6.5 Channel on PMMA substrate (a) Before bonding (b) Expt # 1 (c) Expt # 2 (d) Expt # 3

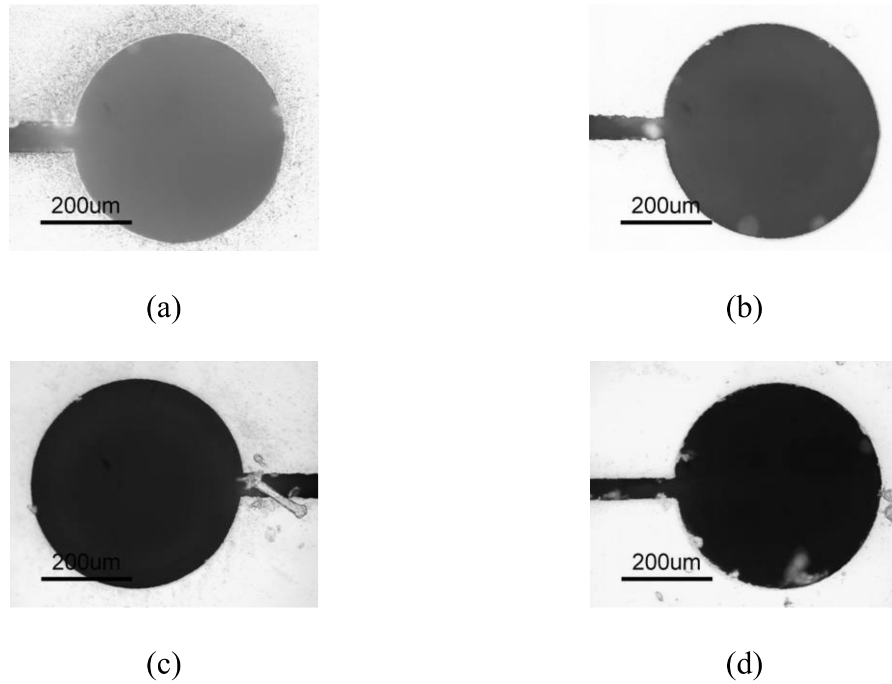

Figure 6.6 Reservoir on PMMA substrate (a) Before bonding
(b) Expt # 1 (c) Expt # 2 (d) Expt # 3

It can also be observed from figures 6.5 and 6.6 that the straightness of the channels and the circularity of the reservoirs are maintained even after bonding indicating that there is no feature shape distortion even after bonding.

Table 6.4 Feature changes after bonding

Experiment #	Channel				Reservoir Diameter (um)	
	Width (um)		Depth (um)			
	Before	After	Before	After	Before	After
1	63	54	180	75	460	468
2	63	57	180	142	460	460
3	63	38	180	120	460	460

6.4 Conclusions

Thermal bonding of PMMA was studied using the available HEMM system. Preliminary experiments were performed to identify bonding parameters. Experiments were performed using the established bonding parameters to assess if bonding takes place without distorting the features. A decrease in feature size due to thermal loading during bonding was observed. This decrease should be compensated for by taking it into account during the microdevice design phase.

The bonding experiments can be performed more effectively if the temperature could be kept constant throughout the bonding process for the longer holding times. As mentioned in the literature, treatment of the substrates with oxygen plasma to provide hydrophilic surfaces may reduce the bonding temperature requirement, probably causing less damage to the features.

CHAPTER 7

CONCLUSIONS AND RECOMMENDATIONS

This chapter concludes this report by summarizing all the conclusions drawn from the earlier chapters while suggesting recommendations that can be incorporated for future research work.

7.1 Conclusions

7.1.1 Characterization of FLM

Characterization of FLM was performed for fabricating silicon master molds for hot embossing. The machining parameters for characterization experiments were identified and experiments performed on channels and reservoirs using all combinations of these parameters. Empirical equations were derived based on experimental results. Given the feature dimensions required on a master mold, process parameters can be identified using these empirical equations. The experimental results were compared with the feature dimensions obtained through the empirical equations. Validation experiments performed with the determined process parameters for given feature dimensions establishes the legitimacy of the derived empirical equations and constants. Using these equations, features of required sizes can be machined on the FLM system to fabricate silicon master molds that will be used in hot embossing.

7.1.2 Characterization of HEMM

The hot embossing process on the developed HEMM system and the de-embossing system were presented. Process parameters for this hot embossing process were identified and experiments performed on three polymers – PC, PMMA and PLLA, using all the combinations of these process parameters. Characterization plots for the different polymers were plotted and used to establish process parameters for hot embossing given the maximum depth of the features on the mold.

The flow of different polymers into the mold cavity was compared after normalizing the embossing temperatures. It was found that at lower embossing temperature, embossing pressure is more important in achieving higher flow of the polymer than holding time while the exact opposite is true at higher temperatures.

7.1.3 Two–Stage Embossing Process

The need for two-stage embossing was explained and a novel two-stage embossing process using polymer molds was introduced. Validation experiments were performed to corroborate this process. Two-stage embossing could save mold fabrication time and at the same time preserves the silicon primary mold due to the fact that a polymer secondary mold is used to fabricate the required device during the second stage. The validation experiments showed that the secondary mold can be used for at least 10 embossing cycles. Excellent replication quality was observed during these experiments. The difference in the feature dimensions during this two-stage replication process was less than 5% and can be accommodated during the design of the master mold.

7.1.4 Micromachining of PLLA

The linear flow rates of PLLA for single and two-stage embossing were studied. Threshold ablation fluence values of PLLA for FLM were experimentally determined and used to machine channels, reservoirs and through holes on a PLLA film. The hot embossed and laser micromachined channels and reservoirs can be used for drug delivery applications.

7.1.5 Thermal Bonding of PMMA

Preliminary experiments of thermal bonding on PMMA were performed and bonding process parameters defined. The defined bonding process parameters were used to bond a microfluidic chip to study the distortion and size reduction of the features on the chip. Although there was no distortion in the feature shape, there was reduction in the size of the features. The flow of colored liquid through the bonded microfluidic chip indicates that there is no clogging of the channels even after bonding.

7.2 Recommendations for Future Research

7.2.1 Characterization of FLM for Different Lenses

Since the characterization of FLM was preformed for only one lens of focal length 25.4 mm, the same procedure can be repeated for lenses of different focal lengths. This will provide a wide array of feature sizes which can be used as a database that can be referred to while fabricating a feature using FLM. Some of the lenses that are suggested for characterization have focal lengths 6.25 mm, 12 mm and 40 mm.

7.2.2 Finite Element Analysis of Hot Embossing

Since hot embossing takes place just above T_g, the flow behavior of the polymer is substantially different from that of processes like injection molding and extrusion, two processes that take place above the melting point of the polymer. There have been some finite element simulations carried out for hot embossing [84-86] but none have been as detailed as the ones carried out for thermoforming [87, 88] and injection molding [89, 90].

The polymer at just above T_g is in a viscoelastic semi-solid state. For a viscoelastic material, when the load is applied, the elastic deformation is instantaneous while the viscous deformation occurs over time. Because of near T_g processing, the polymer tends to behave more like a solid and thus cannot relax rapidly. Due to this, higher compressive pressure is needed for embossing which may cause higher flow induced stress. High embossing pressures also cause earlier damage and wear to the mold. Even a slight increase in embossing temperature can require lower embossing pressure. It is important to find optimum values of these process parameters so that the cycle times are minimized to achieve quality embossed features. FEA software can be used in performing a study of these parameters.

Computer and finite element simulations of micromanufacturing are still in the development stage. Small scale phenomena like surface tension and mold-melt slip velocity need to be implemented in such studies. Low flow rates and embossing speeds ensure that even the smallest features are faithfully replicated. FEM simulation can give

us results such as polymer flow, pressure distribution, filling of cavities and stress concentration.

7.2.3 Temperature Control of the HEMM System

The HEMM system was primarily designed for hot embossing where the holding times do not exceed 150 seconds. But polymer bonding requires a holding time of 600 seconds in some cases. While holding the polymers at the bonding pressures for 600 seconds, it was noticed that the temperature falls by at least 8ºC. This is not desirable. Hence, the temperature control algorithm on the HEMM system has to be modified to accommodate this new requirement. The algorithm mentioned in [91] can be used as a good starting point in order to achieve this objective.

7.2.4 Nanoimprinting

NanoImprint Lithography (NIL) [92, 93] is basically a hot embossing process resulting in fabrication/replication of nano-sized features on the polymer substrate. The one major difference is that nanoimprinting (embossing) takes place at a higher temperature (30-60ºC greater than T_g) than the traditional embossing process. If a master mold having nano-sized features can be fabricated, then nanoimprinting can be attempted on the HEMM system.

7.2.5 Other Suggestions

Some of the other suggestions are as follows:

- Use of vacuum during the FLM and HEMM processes
- Rotary stage on the FLM system for machining biodegradable stents

- Oxygen plasma on polymer substrates for thermal bonding as explained in section 6.1.6.

APPENDIX A

CNC CODE FOR CHANNEL FABRICATION ON FLM

Appendix A CNC code for channel fabrication on FLM

```
; lenY = length of the channel along the Y axis (mm)
; distX = distance between 2 features along the X axis(mm)
; distZ = distance by which the Z stage moves down (mm)
; zDown = number of times the Z stage moves down (default = 0)
; pass = number of passes per zDown (default = 1)
; velFast = Fast feed rate (mm/min)
; velSlow = Slow feed rate (mm/min)
; channels = number of channels
; stepW = number of steps for channel width (default = 1)
; distW = distance by which the X stage moves to increase the channel width (mm)
; finish = number of finishing passes (default = 2)


DVAR $lenY, $distX, $distZ, $zDown, $pass, $velSlow, $velFast, $channels, $stepW,
$distW, $finish

$lenY = 10
$distX = 0.5
$distZ = 0.006
$zDown = 0
$pass = 1
$velSlow = 25
$velFast = 250
$channels = 1
$stepW = 1
$distW = 0
$finish = 2

ENABLE X Y Z

PSOCONTROL X RESET              ; reset the PSO

PSOOUTPUT X WINDOW
PSOWINDOW X 1 INPUT 0
PSOWINDOW X 1 RANGE -1400 1400 UNITS

G91
G1 Y-1.5 F 10
G1 Y1.5 F 10

REPEAT 5
```

```
REPEAT $channels
 REPEAT $stepW
  REPEAT ($zDown+1)
    REPEAT $pass
        G91
        G1 Z-5.0 F $velFast
        PSOCONTROL X ARM
        G1 Y$lenY F $velSlow
        PSOCONTROL X OFF
        G1 Z5 F $velFast
        G1 Y-$lenY
    ENDREPEAT
    G1 Z-$distZ F $velSlow
  ENDREPEAT
  G1 Z$distZ F $velSlow
  REPEAT $finish
    G1 Z-5.0 F $velFast
    PSOCONTROL X ARM
    G1 Y$lenY F $velSlow
    PSOCONTROL X OFF
    G1 Z5 F $velFast
    G1 Y-$lenY
  ENDREPEAT
  G1 Z($zDown*$distZ) F $velSlow
  G1 X-$distW F $velFast
 ENDREPEAT
 G1 X-$distX F $velFast
ENDREPEAT
$zDown = $zDown+1
ENDREPEAT
```

APPENDIX B

CHANNEL DEPTH AND WIDTH DATA

Appendix B Channel depth and width data

Table B1 Channel depth for P = 25 mW

Passes	zDowns				
	0	1	2	3	4
1	9	14	16	18	22
2	14	18	22	24	26
3	17	20	24	27	30

Table B2 Channel depth for P = 50 mW

Passes	zDowns				
	0	1	2	3	4
1	11	16	20	25	30
2	15	22	26	32	36
3	18	26	29	35	42

Table B3 Channel depth for P = 75 mW

Passes	zDowns				
	0	1	2	3	4
1	17	25	32	38	42
2	23	32	39	45	50
3	27	35	43	49	53

Table B4 Channel depth for P = 100 mW

Passes	zDowns				
	0	1	2	3	4
1	22	29	35	41	50
2	25	34	40	47	55
3	30	41	48	54	63

Table B5 Channel depth for P = 150 mW

Passes	zDowns				
	0	1	2	3	4
1	32	37	46	58	70
2	37	50	62	75	83
3	44	58	69	82	93

Table B6 Channel width for P = 25 mW

Passes	zDowns				
	0	1	2	3	4
1	61	61	61	63	63
2	60	60	61	61	63
3	62	62	62	64	64

Table B7 Channel width for P = 50 mW

Passes	zDowns				
	0	1	2	3	4
1	60	62	60	61	62
2	61	69	73	74	76
3	64	72	74	74	76

Table B8 Channel width for P = 75 mW

Passes	zDowns				
	0	1	2	3	4
1	67	70	70	72	73
2	68	72	74	76	80
3	70	74	76	78	81

Table B9 Channel width for P = 100 mW

Passes	zDowns				
	0	1	2	3	4
1	74	74	78	76	76
2	74	74	78	81	84
3	77	80	81	84	86

Table B10 Channel width for P = 150 mW

Passes	zDowns				
	0	1	2	3	4
1	101	102	102	102	102
2	101	102	102	105	106
3	103	106	106	106	110

APPENDIX C

CNC CODE FOR RESERVOIR FABRICATION ON FLM

Appendix C CNC code for reservoir fabrication on FLM

```
; spotD = spot diameter
;       = 0.022 for P=5mW
;       = 0.025 for P=10mW
;       = 0.027 for P=20mW
;       = 0.030 for P=30mW
;       = 0.030 for P=40mW
; hRatio = half the ratio between hole diameter and spot diameter
; holeD = hole diameter
; zDown = number of times the Z stage moves down (default = 0)
; pass = number of passes per zDown (default = 1)
; distZ = distance by which the Z stage moves down (mm)
; velFast = fast speed of the stages (mm/min)
; velSlow = slow speed of the stages (mm/min)
; indx = index
; numHoles = number of holes
; distHolesY = distance between two holes along Y axis (mm)
; distHolesX = distance between two holes along X axis (mm)

DVAR $spotD, $hRatio, $holeD, $indx, $pass, $zDown, $distZ, $velFast, $velSlow,
$numHoles, $distHolesY, $distHolesX

$spotD = 0.030
$hRatio = 7        ;$hRatio = 0.5*$holeD/$spotD rounded off to next whole number

$pass = 3
$distZ = 0.078


$holeD = 0.400
$zDown = 0
$velFast = 250
$velSlow = 10
$numHoles = 3
$distHolesY = 1
$distHolesX = 1

ENABLE X Y Z

PSOCONTROL X RESET

PSOOUTPUT X WINDOW
```

```
PSOWINDOW X 1 INPUT 0
PSOWINDOW X 1 RANGE -1400 1400 UNITS

G71 G91  G0

REPEAT 4
REPEAT $numHoles
 REPEAT ($zDown+1)
  REPEAT $pass
    $indx = 1
    G1 Z-5.0 F$velFast
    G17
    PSOCONTROL X ARM
    G3 I0. J$spotD/4 F$velSlow
    PSOCONTROL X OFF
    G1 Z5.0 F$velFast
    G1 Y-$spotD/4
    G1 Z-5.0 F$velFast
    REPEAT $hRatio
      PSOCONTROL X ARM
      G3 I0. J$indx*$spotD/2 F$velSlow
      PSOCONTROL X OFF
      G1 Z5.0 F$velFast
      G1 Y-$spotD/2
      G1 Z-5.0 F$velFast
      $indx = $indx + 1
    ENDREPEAT
    PSOCONTROL X ARM
    G3 I0. J$indx*$spotD/2 F$velSlow
    PSOCONTROL X OFF
    G91 G1 Z5.0 F$velFast
    G0 Y$hRatio*$spotD/2+$spotD/4
  ENDREPEAT
  G1 Z-$distZ F $velSlow
 ENDREPEAT

 G1 Z$distZ F $velSlow

 REPEAT 2     ; FINISHING PASSES
    $indx = 1
    G1 Z-5.0 F$velFast
    G17
    PSOCONTROL X ARM
    G3 I0. J$spotD/4 F$velSlow
```

```
    PSOCONTROL X OFF
    G1 Z5.0 F$velFast
    G1 Y-$spotD/4
    G1 Z-5.0 F$velFast
    REPEAT $hRatio
      PSOCONTROL X ARM
      G3 I0. J$indx*$spotD/2 F$velSlow
      PSOCONTROL X OFF
      G1 Z5.0 F$velFast
      G1 Y-$spotD/2
      G1 Z-5.0 F$velFast
      $indx = $indx + 1
    ENDREPEAT
    PSOCONTROL X ARM
    G3 I0. J$indx*$spotD/2 F$velSlow
    PSOCONTROL X OFF
    G91 G1 Z5.0 F$velFast
    G0 Y$hRatio*$spotD/2+$spotD/4
 ENDREPEAT
G1 Z(($zDown)*$distZ) F $velSlow
G1 Y-$distHolesY F $velFast
ENDREPEAT

G1 X-$distHolesX F $velFast
G1 Y($distHolesY*$numHoles) F $velFast

$zDown = $zDown+1
ENDREPEAT

G1 X-$distHolesX F$velFast
```

APPENDIX D

RESERVOIR DEPTH DATA

Appendix D Reservoir depth data

Table D1 Reservoir depth for P = 5 mW

Passes	zDown			
	0	1	2	3
1	10.00	14.33	19.67	26.33
2	17.67	25.33	35.00	46.33
3	21.00	34.00	50.67	69.00

Table D2 Reservoir depth for P = 10 mW

Passes	zDown			
	0	1	2	3
1	24.00	37.00	49.00	63.33
2	47.33	77.67	115.33	142.00
3	64.00	109.67	152.67	204.67

Table D3 Reservoir depth for P = 20 mW

Passes	zDown			
	0	1	2	3
1	57.67	83.67	104.33	130.00
2	78.67	129.33	171.00	230.00
3	95.00	164.33	223.67	304.33

Table D4 Reservoir depth for P = 30 mW

Passes	zDown			
	0	1	2	3
1	78.00	111.33	144.33	177.33
2	107.00	156.00	226.00	308.33
3	125.00	220.67	333.67	

Table D5 Reservoir depth for P = 40 mW

Passes	zDown			
	0	1	2	3
1	87.33	128.00	183.00	232.33
2	140.67	242.33	289.33	
3	171.33	304.33	375.33	

APPENDIX E

HEMM CHARACTERIZATION DATA

Appendix E HEMM characterization data

Table E1 PC – holding time = 30 seconds

Row #	Pressure = 14 MPa			Pressure = 19 MPa		
	155	165	175	155	165	175
1	83.67	86.67	89.33	93.67	111.33	112.33
2	84.67	87.00	181.67	94.67	171.33	190.67
3	87.67	87.33	260.00	94.00	177.00	280.00

Table E2 PC – holding time = 90 seconds

Row #	Pressure = 14 MPa			Pressure = 19 MPa		
	155	165	175	155	165	175
1	103.33	113.00	109.00	115.33	114.33	112.67
2	104.00	114.33	200.00	114.33	167.67	211.33
3	104.33	118.33	350.33	114.00	175.67	360.33

Table E3 PMMA – holding time = 30 seconds

Row #	Pressure = 14 MPa			Pressure = 19 MPa		
	115	120	125	115	120	125
1	102.67	106.67	107.33	106.67	109.33	110.33
2	145.67	218.00	236.00	215.67	229.33	247.67
3	148.67	250.33	283.33	227.00	261.00	347.67

Table E4 PMMA – holding time = 90 seconds

Row #	Pressure = 14 MPa			Pressure = 19 MPa		
	115	120	125	115	120	125
1	111.00	107.67	110.00	111.67	110.00	116.33
2	210.00	238.00	248.00	220.67	250.33	248.00
3	209.67	270.33	353.00	235.33	321.67	395.33

Table E5 PLLA– holding time = 30 seconds

Row #	Pressure = 14 MPa			Pressure = 19 MPa		
	80	85	90	80	85	90
1	38.67	51.33	73.33	83.67	109.67	110.67
2	62.67	76.00	86.67	91.33	173.00	200.00
3	82.67	90.00	100.33	102.00	197.00	256.67

Table E6 PLLA – holding time = 90 seconds

Row #	Pressure = 14 MPa			Pressure = 19 MPa		
	80	85	90	80	85	90
1	52.33	106.67	108.33	92.00	112.33	113.00
2	82.33	144.33	162.33	95.33	216.00	224.00
3	90.67	206.00	223.33	115.00	292.33	342.33

REFERENCES

1. http://faculty.washington.edu/yagerp/microfluidicstutorial/basicconcepts/basicconcepts.htm
2. http://www.micronit.com/
3. http://www.appliedmems.cc/htmlmems/technology.html
4. EW Becker, W Ehrfeld, P Hagmann, A Maner, D Munchmeyer, Fabrication of microstructures with high aspect ratios and great structural heights by synchrotron radiation lithography, galvanoforming, and plastic moulding (LIGA process). Microelectronic Engineering, 4, 35-56 (1986)
5. http://mems.sandia.gov/scripts/index.asp
6. H Becker, C Gärtner, Polymer microfabrication methods for microfluidic analytical applications, Electrophoresis, 21(1), 12-26 (2000)
7. http://www.cheresources.com/injectionzz.shtml
8. http://www.protron-mikrotechnik.de/technology/technology_molding_e.htm
9. M. Heckele, WK Schomburg, Review on micro molding of thermoplastic polymers, Journal of Micromechanics and Microengineering, 14, 1-14 (2004)
10. Y-C Su, L Lin, A water-powered micro drug delivery system, Journal of Microelectromechanical Systems, 13 (1), 75-82 (2004)
11. Y-C Su, L Lin, A water-powered micro drug delivery system, Journal of Microelectromechanical Systems, 13 (1), 75-82, (2004)

12. SM Metev, VP. Vieko, Laser assisted microtechnology, Springer-Verlag publications, 1998, ISBN: 354063973X
13. M Gover, Laser micromachining for manufacturing MEMS devices, Proceedings of SPIE (2003)
14. Clark-MXR Inc., http://www.cmxr.com.
15. G Keswani, Effects of process parameters on micro feature topography in femtosecond laser micromachining of silicon, Master's Thesis, August 2004
16. W Hong, H-J Woo, H-W Choi, Y-S Kim, G-D Kim, Optical property modification of PMMA by ion-beam implantation, Applied Surface Science, 169-170, 428-432 (2001)
17. BC Stuart, MD Feit, AM Rubenchik, BW Shore, MD Perry, Laser-induced damage in dielectrics with nanosecond to subpicosecond pulses, Physical Review Letters, 74(12), 2248-2251 (1995)
18. D Linde, K Sokolowski-Tinten, J Bialkowski, Laser-solid interaction in the femtosecond time regime, Applied Surface Science, 109-110, 1-10 (1997)
19. G Kovacs, Micromachined Transducers Sourcebook, WCB/McGraw-Hill, 1998
20. C Moma, BN Chichkov, S Nolte, F Alvensleben, A Tunnermann, H Welling, B Wellgehausen, Short-pulse laser ablation of solid targets. Optics Communications, 129(1-2), 134-142 (1996)
21. B Ngoi, K Venkatakrishnan, E Lim, B Tan, L Koh, Effect of above laser induced damage thresholds in micromachining of Silicon by femtosecond laser pulse, Optics and Lasers in Engineering, 35(6), 361-369 (2001)

22. Spectra-Physics Inc., http://www.spectra-physics.com.
23. Aerotech Inc., http://www.aerotech.com
24. Parametric Technologies Inc., http://www.ptc.com.
25. A Ramachandran, Automated motion planning for a femtosecond laser micromachining system, Master's Thesis, May 2004
26. H. Becker, U. Heim, Silicon as tool material for polymer hot embossing, Proc MEMS '99, 228-232 (1999)
27. DW Clegg, AA Collyer, The Structure and properties of polymer materials.
28. H Becker, U Heim, Hot embossing as a method for the fabrication of polymer high aspect ratio structures, Sensors and Actuators 83, 130-135 (2000)
29. H. Schift , LJ Heyderman, C Padeste, J Gobrecht, Chemical nano-patterning using hot embossing lithography, Microelectronic Engineering, 61-62, 423-428 (2002)
30. B Brass, A Neyer, M Johnck, D Siepe, F Eisenbeiss, G Weber, R Hergenroder, A new PMMA-microchip device for isotachophoresis with integrated conductivity detector, Sensors and Actuators B: Chemical, 72, 249-258 (2000)
31. L Klintberg, M Svedberg, F Nikolajeff, G Thornell, Fabrication of a paraffin actuator using hot embossing of polycarbonate, Sensors and Actuators A: Physical, 103,307-316, (2003)
32. W Ehrfeld, V Hessel, H Lowe, C Schulz, L Weber, Materials of LIGA technology, Microsystem Technologies, 5, 105-112 (1999)

33. G-B Lee, S-H Chen, G-R Huang, W-S Sung, Y-H Lin, Microfabricated plastic chips by hot embossing methods and their applications for DNA separation and detection, Sensors and Actuators B: Chemical, 75, 142-148 (2001)

34. P Grodzinski, RH Liu, B Chen, J Blackwell, Y Liu, D Rhine, T Smekal, D Ganser, C Romero, H Yu, T Chan, N Kroutchinina, Development of plastic microfluidic devices for sample preparation, Biomedical Microdevices, 3(4) 275-283, (2000).

35. XC Shan, R Maeda, Y Murakoshi, Development of a micro hot embossing process for fabricating micro-optical devices, Proceedings of SPIE – the international society for optical engineering, 4936, 67-75 (2002)

36. XC Shan, R Maeda, Y Murakoshi, Micro hot embossing for replication of microstructures, Japanese Journal of Applied Physics, Part 1: Regular Papers and Short Notes and Review Papers, 42(6), 3859-3862 (2003)

37. V Grigaliunas, V Kopustinskas, S Meskinis, M Margelevicius, I Mikulskas, R Tomasiunas, Replication technology for photonic band gap applications, Optical Materials, 17, 15-18 (2001)

38. L Lin, TK Shia, C-J Chiu, Silicon-processed plastic micropyramids for brightness enhancement applications, Journal of Micromechanics and Microengineering, 10, 395-400 (2000)

39. T Cui, Y Zhao, Fabrication of high-aspect-ratio polymer-based electrostatic comb drives using the hot embossing technique, Journal of Micromechanics and Microengineering, 13, 430-435 (2003)

40. Jenoptik Mikrotechnik, http://www.jo-mikrotechnik.com

41. EV Group, http://www.evgroup.com
42. Obducat, http://www.obducat.com
43. R Thanu, Design and Analysis of Hot Embossing Microfabrication System, Master's Thesis, August 2003
44. A Deshmukh, Analysis and Control of a Hot Embossing Microfabrication Microreplication System, Master's Thesis, April 2004
45. Instron Corporation, http://www.instron.com
46. National Instruments Corporation, http://www.ni.com
47. GS Fiorini, G Jeffries, D Lim, C Kuyper, D Chiu, Fabrication of thermoset polyester microfluidic devices and embossing masters using rapid prototyped polydimethylsiloxane molds, Lab on a Chip, 3(3), 158-163 (2003)
48. K Pfeiffer, M Fink, G Ahrens, G Gruetzner, F Reuther, J Seekamp, S Zankovych, C Torres, I Maximov, M Beck, M Graczyk, L Montelius, H Schulz, H-C Scheer, F Steingrueber, Polymer stamps for nanoimprinting, Microelectronic Engineering, 61-62, 393-398 (2002)
49. J Narasimhan, I Papautsky, Polymer embossing tools for rapid prototyping of plastic microfluidic devices, Journal of Micromechanics and Microengineering, 14, 96-103 (2004)
50. AP Russo, D Apoga, N Dowell, W Shain, A Turner, H Craighead, H Hoch, J Turner, Microfabricated Plastic Devices from Silicon Using Soft Intermediates, Biomedical Microdevices, 4, 277-283 (2002)

51. T Koerner, L Brown, R Xie, RD Oleschuk, Epoxy resins as stamps for hot embossing of microstructures and microfluidic channels, Sensors and Actuators B 107, 632-639 (2005)

52. IUPAC: Definitions of Terms Relating to Reactions of Polymers and to Functional Polymeric Materials, July 2001

53. MFA Goosen, YF Leung, S Chou, AM Sun, Insulin-albumin microbeads - an implantable biodegradable system, Biomaterials, Medical Devices, and Artificial Organs, 10(3), 205-218 (1982)

54. DJ Mooney, CL Mazzoni, C Breuer, K McNamara, D Hern, JP Vacanti, R Langer, Stabilized polyglycolic acid fibre-based tubes for tissue engineering, Biomaterials, 17(2), 115-124 (1996)

55. RS Shawgo, ACR Grayson, Y Li, MJ Cima, Biomems for drug delivery, Current Opinion in Solid State And Materials Science, 6(4), 329-334 (2002)

56. S Vainionpaa, P Rokkanen, P Toermaela, Surgical applications of biodegradable polymers in human tissues, Progress in Polymer Science (Oxford), 14(5), 679-716 (1989)

57. L Brannon-Peppas, Polymers in controlled drug delivery, http://www.devicelink.com/mpb/archive/97/11/003.html

58. JC Middleton, AJ Tipton, Synthetic Biodegradable Polymers as Medical Devices, Medical Plastics and Biomaterials Magazine, p 30, March 1998

59. ACR Grayson, IS Choi, BM Tyler, PP Wang, H Brem, MJ Cima, R Langer, Multi-pulse drug delivery from a resorbable polymeric microchip device, Nature Materials, 2(11), 767-772, (2003)
60. AK Deniz, C Liu, Microfabrication technology for polycaprolactone, a biodegradable polymer, Journal of Micromechanics and Microengineering, 10(1), 80-84 (2000)
61. R Yang, T Chen, H Chen, W Wang, Fabrication of biodegradable polymer (PLGA) microstructures and applications in controlled drug delivery, Proceedings of SPIE - The International Society for Optical Engineering, 5345, 130-137 (2004)
62. J-H Park, S Davis, Y-K Yoon, MR Prausnitz, MG Allen, Micromachined biodegradable microstructures, Proceedings of the IEEE Micro Electro Mechanical Systems (MEMS), 371-374 (2003)
63. Z Razzacki, PK Thwar, M Yang, VM Ugaz, MA Burns, Integrated microsystems for controlled drug delivery, Advanced Drug Delivery Reviews, 56(2), 185-198 (2004)
64. Y Lu, SC Chen, Micro and nano-fabrication of biodegradable polymers for drug delivery, Advanced Drug Delivery Reviews, 56(11), 1621-1633 (2004)
65. VV Kancharla, S Chen, Fabrication of biodegradable polymeric micro-device using laser micromachining, Biomedical Microdevices, 4(2), 105-109 (2002)
66. NH Rizvi, Femtosecond laser micromachining: Current status and applications, RIKEN Review focused on Laser Precision Microfabrication, 50, 107-112 (2003)

67. N Uppal, Femtosecond laser micromachining of engineering ,materials: process parameters study and microrapid prototyping, Master's thesis, May 2005

68. S Baudach, J Bonse, J Kruger, W Kautek, Ultrashort pulse laser ablation of polycarbonate and polymethylmethacrylate, Applied Surface Science, 154-155, 555-560 (2000)

69. Y Lin, DW Matson, DE Kurath, J Wen, F Xiang, WD Bennett, PM Martin, RD Smith, Microfluidic devices on polymer substrates for bioanalytical applications, IMRET3, 3rd International Conference on Microreaction Technology, (1999)

70. J-H Tsai, L Lin, Micro-to-macro fluidic interconnectors with an integrated polymer sealant, Journal of Micromechanics and Microengineering, 11, 577–581 (2001)

71. D Gomez, I Goenaga, I Lizuain, M Ozaita, Femtosecond laser ablation for microfluidics, Optical Engineering, 44(5), 051105 (2005)

72. KP Kampar, J Dopper, A self-filling low-cost membrane micropump, Proc. MEMS'98, 432-437 (1998)

73. HS Lee, DS Kim, TH Kwon, A novel low temperature bonding technique for plastic substrates using X-ray irradiation, TRANSDUCERS '03, The 12th International Conference on Solid-State Sensors, Actuators and Microsystems, 1331-1334 (2003)

74. A Paulus, SJ Williams, AP Sassi, PH Kao, H Tan, HH Hooper, Integrated capillary electrophoresis using glass and plastic chips for multiplexed DNA analysis, Proc. SPIE Microfluidic Devices and Systems, 3515, 94-103 (1998)

75. V Studer, A Pepin, Y Chen, A Ajdari, Fabrication of microfluidic devices for AC electrokinetic fluid pumping, Microelectronic Engineering, 61-62, 915-920 (2002)

76. V Studer, A Pepin, Y Chen, Nanoembossing of thermoplastic polymers for microfluidic applications, Applied Physics Letters, 80, 3614-3616 (2002)

77. CH Ahn, JW Choi, G Beaucage, J Nevin, JB Lee, Disposable Smart Lab on a Chip for Point-of-Care Clinical Diagnostics, Proceedings of the IEEE, 92(1), 154-173 (2004)

78. A Han, O Wang, SK Mohanty, M Graff, B Frazier, A multi-layer plastic packaging technology for miniaturized bio analysis systems containing integrated electrical and mechanical functionality, Proceedings of the Second Annual International IEEE-EMB, (2002)

79. A Tan, S Benetton, JD Henion, Chip-based solid-phase extraction pretreatment for direct electrospray mass spectrometry analysis using an array of monolithic columns in a polymeric substrate, Anal Chem., 5(20), 5504-5511 (2003)

80. J Kameoka, HG Craighead, H Zhang, J Henion, A polymeric microfluidic chip for CE/MS determination of small molecules, Anal Chem., 73(9), 1935-1941 (2001)

81. C Li, Y Yang, HG Craighead, KH Lee, Isoelectric focusing in cyclic olefin copolymer microfluidic channels coated by polyacrylamide using a UV photografting method, Electrophoresis, 26, 1800-1806 (2005)

82. S-H Chen, W-C Sung, G-B Lee, Z-Y Lin, P-W Chen, P-C Liao, A disposable poly(methylmethacrylate)-based microfluidic module for protein identification by nanoelectrospray ionization-tandem mass spectrometry, Electrophoresis, 22(18), 3972-3977 (2001)

83. B Bilenberg, T Nielsen, B Clausen, A Kristensen, PMMA to SU-8 bonding for polymer based lab-on-a-chip systems with integrated optics, Journal of Micromechanics and Microengineering, 14, 814-818 (2004)

84. YJ Juang, LJ Lee, KW Koelling, Hot embossing in microfabrication. Part II: Rheological characterization and process analysis, Polymer Engineering and Science, 42(3), 551-566 (2002)

85. C-R Lin, C Hung, Finite element analysis of hot embossing of polymer optical sheet, Materials Science Forum, 437-438, 379-382 (2003)

86. C-R Lin, C Hung, The characterization and finite-element analysis of a polymer under hot pressing, International Journal of Advanced Manufacturing Technology, 20(3), 230-235 (2002)

87. G Sala, D Cassago, A numerical and experimental approach to optimize sheet stamping technologies: Polymers thermoforming, Materials and Design, 23(1), 21-39 (2002)

88. M Bellet, J-F Agasaant ,B Monasse , A Rodriguez-Villa, D Lebouvier, P Wouters, Finite element simulation of thermoforming and extrusion blow molding processes, Numisheet ’99, 555-560 (1999)

89. WH Yang, A Peng, L Liu, DC Hsu, R-Y Chang, Integrated numerical simulation of injection molding using true 3D approach, ANTEC 2004 – Annual Technical Conference Proceedings, Society of Plastics Engineers (2004)

90. AW Mcfarland, JS Colton, Production and analysis of injection molded micro-optic components, Polymer Engineering and Science, 44(3), 564-479 (2004)

91. AS Deodhar, Intelligent Heat Control for a Hot Embossing Micro Replication System, Master's Thesis, May 2005

92. K Pfeiffer, M Fink, G Ahrens, G Gruetzner, F Reuther, J Seekamp, S Zankovych, CM Torres, I Maximov, M Beck, M Graczyk, L Montelius, H Schulz, H-C Scheer, F Steingrueber, Polymer stamps for nanoimprinting, Microelectronic Engineering 61–62, 393–398 (2002)

93. H Schulz, D Lyebyedyev, H-C Scheer, K Pfeiffer, G Bleidiessel, G Grutzner, J Ahopelto, Master replication into thermosetting polymers for nanoimprinting, Microelectronics and Nanometer Structures, 18(6), 3582-3585 (2000)

BIOGRAPHICAL INFORMATION

Sunil Belligundu received his Bachelor of Engineering in Mechanical Engineering at University of Mumbai, India in 1998. After his bachelor's degree, he worked in Godrej-GE Appliances Ltd. for a year before coming to The University of Texas at Arlington in Fall 1999. He received his Master of Science in Mechanical Engineering in August 2001. He continued his Ph.D. studies in the same university while working for Aerospace Technologies Inc. in Fort Worth, Texas. He returned to The University of Texas at Arlington in Fall 2002 to pursue full-time Ph.D. studies. He is a graduate research assistant in the MARS and BioMEMS laboratories and will receive his doctorate in Mechanical Engineering in December 2005.

His research interests include microfluidics, BioMEMS, robotics, micromanufacturing of polymers, and micromachining of metals and non-metals using femtosecond laser.